KINETIC CAPILLARY ELECTROPHORESIS

AND ITS APPLICATIONS

MAXIM BEREZOVSKI

A DISSERTATION SUBMITTED TO THE FACULTY OF GRADUATE STUDIES

IN PARTIAL FULFILMENT OF THE REQUIREMENTS

FOR THE DEGREE OF

DOCTOR OF PHILOSOPHY

GRADUATE PROGRAM IN HIGHER EDUCATION

YORK UNIVERSITY,

TORONTO, ONTARIO

JULY 2005

KINETIC CAPILLARY ELECTROPHORESIS

AND ITS APPLICATIONS

by Maxim Berezovski

a dissertation submitted to the faculty of graduate Studies of York University in partial fulfillment of the requirements for the degree of

DOCTOR OF PHILOSOPHY

The Dissertation Committee for Maxim Berezovski Certifies that this is the approved version of the following dissertation:

KINETIC CAPILLARY ELECTROPHORESIS AND ITS APPLICATIONS

Committee:

Dr. Sergey Krylov
Supervisor

Dr. Michael Siu

Dr. Philip Johnson

Dr. Katalin Hudak

Dr. Rene Fournier
Dean Representative

Dr. X. Chris Le
External Examiner

ABSTRACT

Non-covalent molecular interactions play crucial role in regulatory biological processes, such as gene expression, DNA replication, signal transduction, cell-to-cell interaction, and immune response. The molecular mechanisms of the action of many drugs are based on forming non-covalent molecular complexes with therapeutic targets. The formation of non-covalent molecular complexes is pivotal to many analytical techniques and devices used in research and disease diagnostics.

Capillary electrophoresis (CE) has been one of rapidly growing analytical techniques to study affinity interactions in recent years. Since CE features quick analysis, high efficiency, high resolving power, low sample consumption and wide range of possible analytes, it is beneficial for analysis of biomolecules and their interactions.

In my dissertation I propose kinetic capillary electrophoresis (KCE) as a conceptual platform for the development of kinetic homogeneous affinity methods and their application to selection of binding ligands to specific targets and characterizing their binding parameters. KCE is defined as the CE separation of species, which interact under equilibrium or non-equilibrium conditions during electrophoresis. Depending on how the interaction is arranged, different KCE methods can be designed. In this proof-of-principle work, I present two KCE methods: Non-Equilibrium Capillary Electrophoresis of Equilibrium Mixtures (NECEEM), and Sweeping Capillary Electrophoresis (SweepCE), mathematical models of the methods, and demonstration of their applications. The spectrum of their applications includes: (i) measuring equilibrium and rate constants from

a single experiment, (ii) quantitative affinity analyses of proteins, (iii) measuring temperature in capillary electrophoresis, (iv) studying thermochemistry of affinity interactions, and (v) kinetic selection of ligands from combinatorial libraries.

I used NECEEM to select and characterize DNA aptamers for protein farnesyltransferase (PFTase). A single round of NECEEM-based selection was sufficient to obtain an aptamer with an equilibrium dissociation constant equals 0.5 nM. The entire selection procedure (excluding cloning and sequencing) took less than 5 hours and consumed only 10^{-16} moles (1 picogram) of the target protein. The NECEEM-based selection can be easily automated to facilitate mass production of aptamers, and used for discovery and characterization of drug candidates and the development of new diagnostic methods.

DEDICATION

For my mother

&

my father

ACKNOWLEDGEMENTS

I want to say thank-you to my supervisor Dr. Sergey N. Krylov, for sharing his great passion, enthusiasm, and dedication to science; for teaching me how to find and develop brilliant scientific ideas; for showing me the art of writing clever scientific articles; for helping me in solving many big and small problems in everyday life. Truly, I have never had a dull moment over the last four years. Every morning I wake up with a strong desire to come in a lab and do my exciting research. I am very proud to be his first Ph.D. student.

Thanks to the lab members: Michael Musheev, Alex Petrov, Andrei Drabovich, Julia Jitkova, Sergey Arhipov, Kang Hu, Dr. Lana Krylova, Dmitry Rosenberg for all their help, sanity, sympathy, and friendship.

I am also forever indebted to Dr. Victor Okhonin for his great mind and ability to solve almost any mathematics problem. His extra time and help has been greatly appreciated.

Special thanks to Dr. Michel Siu and Dr. Philip Johnson for taking the time to serve as research evaluation committee members and providing me with valuable scientific suggestions and recommendations.

To York University and Ontario Graduate Scholarship for financial support.

TABLE OF CONTENTS

ABSTRACT iv

DEDICATION vi

ACKNOWLEDGEMENTS vii

TABLE OF FIGURES xii

LIST OF ABBREVIATIONS xiv

CHAPTER 1
KINETIC CAPILLARY ELECTROPHORESIS

1.1. INTRODUCTION 1

1.1.1. Non –Covalent Molecular Complexes 1

1.1.2. Methods for Measurement of Equilibrium and Rate Constants 2

1.2. KINETIC CAPILLARY ELECTROPHORESIS (KCE) 5

1.2.1. Overview of Capillary Electrophoresis 5

1.2.2. Existing KCE Methods 9

1.2.2.1. Calculation from Change in Peak Area or Plateau Height 12

1.2.2.2. Calculation from Change in Electrophoretic Mobility 12

1.2.2.3. Capillary Zone Electrophoresis (CZE) 14

1.2.2.4. Affinity Capillary Electrophoresis (ACE) 15

1.2.2.5. Hummel-Dreyer method (HD) 17

1.2.2.6. Frontal Analysis (FA) 17

1.2.2.7. Vacancy Peak Method (VP) and Vacancy Affinity Electrochromatography (VACE) 18

1.2.3. New KCE Methods 19

1.3. CONCLUSION 19

CHAPTER 2
NON-EQULIBRIUM CAPILLARY ELECTROPHORESIS OF EQULIBRIUM MIXTURE (NECEEM)

2.1. INTRODUCTION 21

2.2. RESULTS AND DISCUSSION 23

2.2.1. Principle of NECEEM 23

2.2.2. Determination of K_d 27

2.2.3. Determination of Relative Quantum Yield 29

2.2.4. Determination of k_{off} and k_{on} 32

2.3. CONCLUSION 34

2.4. EXPERIMENTAL METHODS 34

2.4.1. Chemicals and Materials 34

2.4.2. Capillary Electrophoresis 35

2.4.2. Equilibrium Mixtures 36

CHAPTER 3
MATHEMATICAL MODEL OF NECEEM

3.1. INTRODUCTION 37

3.2. RESULTS AND DISCUSSION 38

3.2.1. Major Assumptions 38

3.2.2. Solution for C 40

3.2.3. Solutions for A and B 40

3.2.4. Simulated Electropherograms 42

3.2.5. Determination of K_d and k_{off} 46

3.3. CONCLUSION 50

3.4. EXPERIMENTAL METHODS 50

3.4.1. Chemicals and Materials 50

3.4.2. Capillary Electrophoresis 51

3.4.3. Equilibrium Mixtures 51

3.4.4. Calculations....52

3.6. APPENDIXES....52

Appendix 3.6.1. Green's Function....52

Appendix 3.6.2. Integral of Multiplication Product of Two Gauss Functions....52

Appendix 3.6.3. Double Integral of Gauss Function in Finite Limits....53

CHAPTER 4
AFFINITY-MEDIATED NECEEM

4.1. INTRODUCTION....54

4.2. RESULTS AND DISCUSSION....57

4.2.1. Affinity-Mediated NECEEM....57

4.2.2. Determination of K_d....60

4.2.3. Determination of Migration Time of Apt•Thr Complex....62

4.2.4. Determination of k_{off}....63

4.2.5. Determination of Unknown Protein Concentration by NECEEM....64

4.2.6. Using ssDNA Binding Protein for Hybridization Analysis....65

4.3. CONCLUSION....71

4.4. EXPERIMENTAL METHODS....71

4.4.1. Chemicals and Materials....71

4.4.2. Capillary Electrophoresis....72

4.4.3. Aptamer and Probe Design....73

4.4.4. Equilibrium Mixtures....74

CHAPTER 5
TEMPERATURE-CONTROLLED NECEEM

5.1. INTRODUCTION....76

5.2. RESULTS AND DISCUSSION....78

5.2.1. Temperature-Controlled NECEEM....78

5.2.2. *Taq* DNA Polymerase/Aptamer System....80

5.2.3. SSB/ssDNA System....81

5.2.4. Determination of Thermodynamic Parameters 84
5.2.5. Using NECEEM for Determination of Temperature in CE 85
5.3. CONCLUSION 92
5.4. EXPERIMENTAL METHODS 93
5.4.1. Chemicals and Materials 93
5.4.2. NECEEM 94
5.4.3. Equilibrium Mixtures 95

CHAPTER 6
SweepCE

6.1. INTRODUCTION 96
6.2. RESULTS AND DISCUSSION 97
6.2.1. SweepCE 97
6.2.2. Mathematical Model of SweepCE 99
6.2.2. Determination of k_{on} 103
6.3. CONCLUSION 106
6.4. EXPERIMENTAL METHODS 107
6.4.1. Chemicals and Materials 107
6.4.2. SweepCE 107

CHAPTER 7
NECEEM – COMREHENSIVE KCE METHOD FOR SELECTION OF APTAMERS

7.1. INTRODUCTION 109
7.2. RESULTS AND DISCUSSION 111
7.2.1. Concept of NECEEM-Based Selection 111
7.2.2. Efficiency of NECEEM-Based Selection 115
7.2.3. One-Step Selection of Aptamers for PFTase 119
7.2.4. Influence of Aptamer on PFTase Activity 127

7.3. CONCLUSION....127

7.4. EXPERIMENTAL METHODS....130

7.4.1. Chemicals and Materials....130

7.4.2. DNA Library and Primers....130

7.4.3. Capillary Electrophoresis....131

7.4.4. Selection of Aptamers....132

7.4.5. Finding Binding Parameters....134

7.4.6. Finding Dissociation Constants of Aptamers with Ultra-Filtration and Fluorescence Detection....135

7.4.7. Background of NECEEM-Based Partitioning....136

7.4.8. Measuring PFTase Activity in Presence of Aptamer....136

7.4.9. Influence of Substrates on Aptamer Binding....137

CONCLUDING REMARKS....139

REFERENCES....140

CURRICULUM VITAE....151

TABLE OF FIGURES

Figure 1.1. Methods for Measurement of Binding Parameters.... 3

Figure 1.2. Principle of SPR Spectroscopy.... 4

Figure 1.3. Diagram of CE System.... 6

Figure 2.1. NECEEM of SSB and fDNA.... 25

Figure 2.2. NECEEM of SSB and fDNA with Shortened Separation Time.... 26

Figure 2.3. Determination of Areas in NECEEM.... 28

Figure 2.4. Determination of Relative Quantum Yield.... 30

Figure 2.5. Influence of Separation Time on NECEEM Electropherograms.... 31

Figure 2.6. Determination of k_{off}.... 33

Figure 3.1. Simulated NECEEM electropherograms.... 44

Figure 3.2. Simulated NECEEM Electropherograms for Different Rate Constants..... 45
Figure 3.3. Fitting Experimental NECEEM Electropherograms with Simulated Ones ... 49
Figure 4.1. Structure of Thrombin Aptamer 57
Figure 4.2. Affinity-Mediated NECEEM of Thrombin and Its Aptamer 59
Figure 4.3. Determination of K_d and k_{off} for Thrombin and Its Aptamer 61
Figure 4.4. Structure of Hybridization Probe and Complex with Target..... 67
Figure 4.5. SSB-Mediated DNA Hybridization Analysis in Gel-Free CE 69
Figure 4.6. SSB-Mediated Hybridization Analysis. 70
Figure 4.7. Structure of Extended Aptamer with Probe..... 74
Figure 5.1. NECEEM for Two Protein-DNA Systems..... 79
Figure 5.2. Temperature Dependences for Equilibrium and Kinetic Binding parameters 83
Figure 5.3. Van't Hoff plots..... 84
Figure 5.4. Dependence of Dissociation Kinetics of Protein-DNA Complex on Temperature of Capillary..... 88
Figure 5.5. Temperature Dependence of Dissociation Rate Constant 89
Figure 5.6. Temperature Dependence of Electric Field in CE..... 90
Figure 5.7. DNA Aptamer for Taq Polymerase 93
Figure 6.1. Sweeping of DNA by DNA-Binding Protein in CE..... 98
Figure 6.2. Fitting Experimental SweepCE Electropherograms with Simulated SweepCE Electropherograms 104
Figure 6.3. Fitting Experimental Data with k_{on} Value Different from Correct One..... 105
Figure 7.1. Schematic Representation of NECEEM-Based Selection of DNA Aptamers 114
Figure 7.2. Efficiency of NECEEM-Based Partitioning..... 118
Figure 7.3. One-Step Selection of Aptamers for Protein Farnesyltransferase (PFTase) 123
Figure 7.4. Scheme of NECEEM-SELEX of DNA Aptamers 126
Figure 7.5. PFTase-Catalyzed Farnesylation of Cysteine Residue in dff-GCVIA Peptide..... 129
Figure 7.6. CE-LIF Separation of Product from Substrate in Farnesylation Reaction... 138

LIST OF ABBREVIATIONS

μ	electrophoretic mobility
ν	velocity
μM	micromolar
A	adenosine
ACE	affinity capillary electrophoresis
Ar	argon
C	complex
CD	cyclodextrine
CE	capillary electrophoresis
CEMSA	capillary electrophoresis mobility shift assay
CZE	capillary zone electrophoresis
DNA	deoxyribonucleic acid
dNTP	deoxyribonucleoside triphosphate
ds	double stranded
E_a	activation energy
EMSA	electrophoresis mobility shift assay
EOF	electroosmotic flow
exp	exponential function
FA	frontal analysis
fDNA	fluorescently labelled DNA
FTIR	Fourier transform infrared spectroscopy
G	guanine
HCl	hydrochloric acid
HD	Hummel-Dreyer
HPLC	high pressure liquid chromatography
I	intensity
I.D.	inner diameter
IgE	immunoglobulin E
K_b	equilibrium binding constant
KCE	kinetic capillary electrophoresis
K_d	equilibrium dissociation constant
k_{off}	rate constant of complex decay
k_{on}	rate constant of complex formation
L	ligand
L•T	ligand-target complex
LIF	laser induced fluorescence
M	moles/litre (molar)
Mg	magnesium
min	minute
mM	millimolar
MS	mass spectrometry

NaOH	sodium hydroxide
NECEEM	non-equilibrium capillary electrophoresis of equilibrium mixtures
nm	nanometre
nM	nanomolar
NMR	nuclear magnetic resonance
O.D.	outer diameter
P	protein
P•DNA	protein-DNA complex
PCR	polymerase chain reaction
PFTase	protein farnesyltransferase
R	gas constant
RNA	ribonucleic acid
RT-PCR	reverse transcriptase
s	second
SDS	sodium dodecyl sulphate
SELEX	selection of ligands by exponential enrichment
SPR	surface plasmon resonance
ss	single stranded
SSB	*E. coli* single-stranded DNA binding protein
SweepCE	sweeping capillary electrophoresis
T	target
t	time
Taq	*Thermus Aquaticus*
TEAA	triethylammonium acetate
Thr	thrombin
VACE	vacancy peak capillary electrophoresis
VP	vacancy peak

CHAPTER 1

KINETIC CAPILLARY ELECTROPHORESIS

1.1. INTRODUCTION

1.1.1. Non –Covalent Molecular Complexes

Non-covalent molecular complexes play a crucial role in regulatory biological processes, such as gene expression, DNA replication, signal transduction, cell-to-cell interaction, and immune response [1-3]. The molecular mechanisms of the action of many drugs are based on drugs forming non-covalent molecular complexes with therapeutic targets. In addition, the formation of the non-covalent molecular complexes is pivotal to many analytical techniques and devices used in research and disease diagnostics, such as immunoassay, biosensors, and DNA hybridization analyses.

The formation and the dissociation of a non-covalent complex, L•T, between molecules L (a ligand) and T (a target), are characterized by a bimolecular rate constant k_{on}, and a monomolecular rate constant, k_{off}, respectively:

$$L + T \underset{k_{off}}{\overset{k_{on}}{\rightleftharpoons}} L\bullet T \qquad (1.1)$$

The stability of the complex is often described in terms of the equilibrium dissociation constant (K_d) or the equilibrium binding constant ($K_b = 1/K_d$). The three constants, k_{on}, k_{off}, and K_d, are interconnected through the equation:

$$K_d = \frac{k_{off}}{k_{on}} \qquad (1.2)$$

Knowledge of k_{on}, k_{off}, K_d, and their dependence on certain factors such as buffer composition, buffer pH, buffer ionic strength, and temperature can assist in: (i) understanding the dynamics of biological processes, (ii) determination of pharmacokinetics of receptor-binding drugs, and (iii) design of quantitative affinity analyses. In practical terms the determination of k_{on}, k_{off}, K_d can assist in developing and/or selecting drug candidates with desired kinetic parameters. It may also help in developing suitable dosage regimes.

1.1.2. Methods for Measurement of Equilibrium and Rate Constants

Methods for the measurement of equilibrium and rate constants can be classified into two categories: mixture-based and separation-based (**Figure 1.1**). The first category includes light absorption, fluorescence spectroscopy, nuclear magnetic resonance (NMR), Fourier transform infrared spectroscopy (FTIR), mass spectrometry (MS), Raman spectroscopy, potentiometry, calorimetry, Surface Plasmon Resonance (SPR). The separation-based methods include dialysis, ultrafiltration, ultracentrifugation, chromatography (liquid chromatography and thin-layer chromatography), and electrophoresis (planar and capillary electrophoresis). Separation-based methods can provide signals of individual interacting components and/or complexes, thus avoiding the interference of other components. Though some conventional methods, such as dialysis, ultrafiltration, ultracentrifugation, chromatography, and planar electrophoresis, are widely used to study ligand-target interactions, they are constrained by a number of factors, such as volume shift, Donnan effect, nonspecific adsorption, leakage of bound

molecules through membrane, excessive analysis time, large sample size as well as errors due to sedimentation, back diffusion, and viscosity.

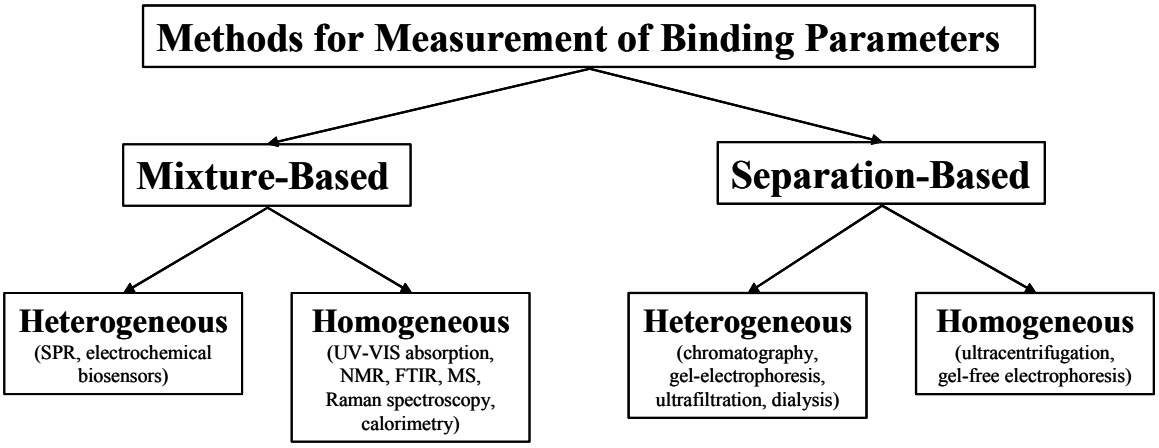

Figure 1.1. Methods for Measurement of Binding Parameters

Mixture-based and separation-based methods can be subdivided into two broad categories: heterogeneous and homogeneous binding assays. In heterogeneous assays, T is affixed to a solid substrate, while L is dissolved in a solution and can bind T affixed to the surface. In advanced heterogeneous binding assays such as SPR, T is affixed to a sensor that can change its optical or electrical signal upon L binding to T [4-6]. In the method, K_d can be found in a series of equilibrium experiments. The concentration of L in the solution is varied and L and T are allowed to reach equilibrium. The signal from the sensor versus the concentration of L has a characteristic sigmoidal shape and K_d can be found from the curve by identifying the concentration of L at which the signal is equal to half of its maximum amplitude. The k_{off} value can be determined by SPR in a single non-equilibrium experiment in which the equilibrium is disturbed by rapidly replacing the solution of L with a buffer devoid of L. The complex on the surface decays in the

absence of L in the solution, and the complex decay generates an exponential signal on the sensor (**Figure 1.2**).

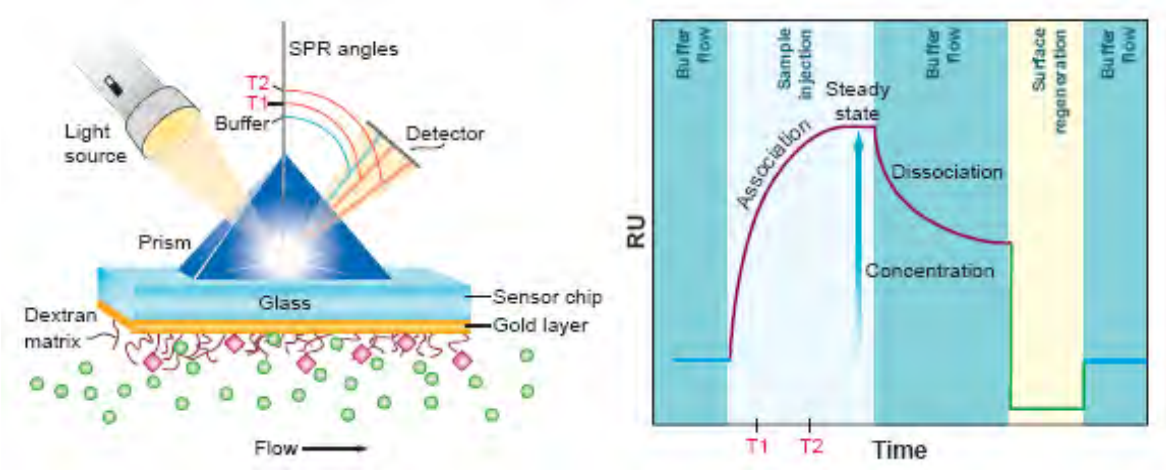

Figure 1.2. Principle of SPR Spectroscopy

At left, an SPR optical unit and a sensor chip detect the L molecules (green spheres) in the flow solution, which passes by the T (pink diamonds) linked to the dextran matrix. The blue SPR angle defines the position of the reduced-intensity beam. Time points T1 and T2, shown in the schematic sensorgram (right) correspond to the two red SPR angles, which shift as L binds to T over time. As the concentration of bound L increases (arrow), the RU response approaches saturation. The complex dissociates upon reintroduction of the buffer. As shown, the response to the injection solution will fall below the baseline if its refractive index is lower than that of the buffer [6].

Heterogeneous binding assays have certain advantages and drawbacks. The most serious drawback is that affixing T to the surface changes the structure of T. The extent of such change will depend on the method of immobilization. The change in the structure can potentially affect the binding parameters of L to T. This problem is especially severe when L binds to T through interaction with a large part of T. In addition, the immobilization of T on the surface may be time-consuming and expensive. Moreover, non-specific interactions with the surface are always a concern.

In homogeneous binding assays T and L are mixed and allowed to form a complex in solution; neither of the molecules are affixed to the surface. Complex formation is followed by either monitoring the changing physical-chemical properties of L or T upon binding. Such properties can be optical (absorption, fluorescence, polarization) or separation-related (chromatographic or electrophoretic mobility). Equilibrium experiments with varying concentrations of L can be used similarly to heterogeneous analyses to find K_d. Non-equilibrium stopped flow-experiments, in which L and T are mixed rapidly and the change in spectral properties is monitored, can be used to find k_{on}.

1.2. KINETIC CAPILLARY ELECTROPHORESIS (KCE)

1.2.1. Overview of Capillary Electrophoresis

Capillary Electrophoresis (CE) is a relatively new analytical separation technique which is becoming more and more popular among analytical chemists. CE is a family of related techniques that employ narrow-bore (10-200 μm inner diameter) capillaries to perform high efficiency separations of both large and small molecules. Sample introduction is accomplished by immersing the end of the capillary into a sample vial and applying differential pressure or voltage. Various CE techniques perform separations based on several mechanisms, such as molecular size (sieving), isoelectric focusing and hydrophobicity. High voltages are used to separate molecules based on differences in charge and size. In free-zone CE, separation results from the combination of electrophoretic migration (the movement of charged molecules towards an electrode of

opposite polarity) and electroosmotic flow (the bulk of electrolyte flow caused by a charged inner capillary wall and an applied potential). As illustrated in **Figure 1.3**, positive, neutral and negatively charged molecules are shown migrating toward the negative electrode. The electroosmotic flow carries negatively charged molecules as well as neutral ones, towards the negative electrode. The electroosmotic flow is dependent upon field strength, electrolyte pH, buffer composition and ionic strength, viscosity and capillary surface characteristics; all of which can be used singly or in combination to enhance separations. Detection is achieved by monitoring light absorption directly on-column through a window in the capillary or off-column using a sheath-flow cuvette. Other detection options include Laser-Induced Fluorescence, Diode Array, Conductivity, and Mass Spectrometry.

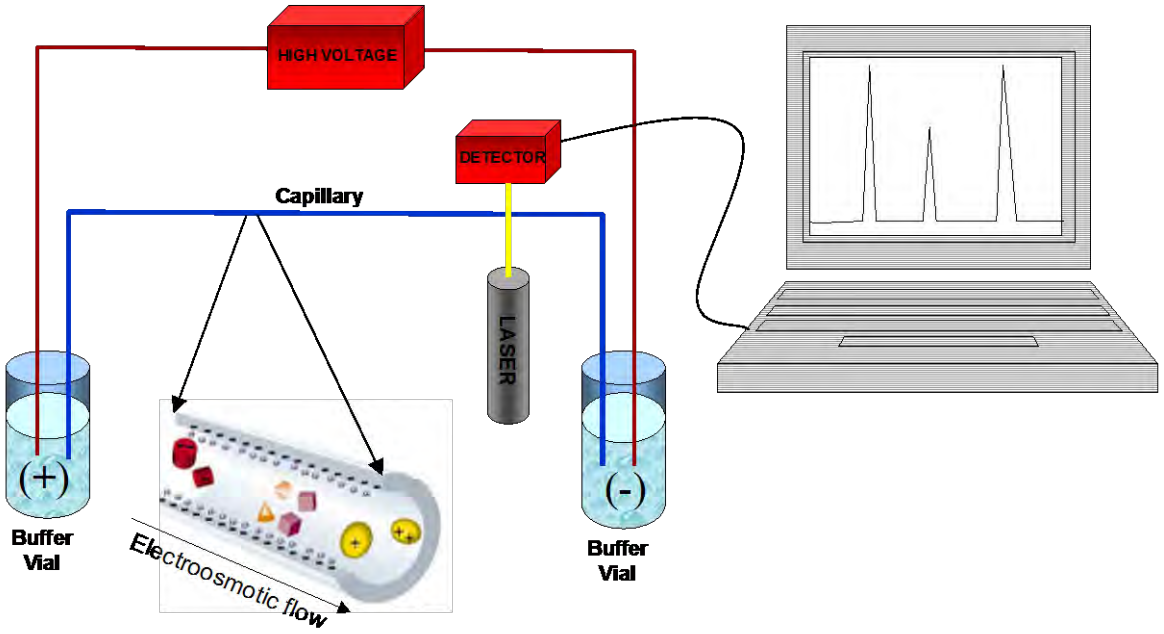

Figure 1.3. Diagram of CE System

Although CE technology may be applied to many different types of research, it has gained its reputation from the study of molecules that have traditionally been difficult to separate. In general, CE should be considered first when dealing with highly polar, charged analytes. CE excels in the analysis of ions when rapid results are desired, and has become the predominant technique for the analysis of both basic and chiral pharmaceuticals. This technology is making its mark in biotechnology, replacing traditional electrophoresis for the characterization and analysis of macromolecules such as proteins and carbohydrates, and promises to be a valuable tool in tackling the characterization challenges posed by proteomics analysis. CE technology has also served to accelerate the accumulation of genome-level knowledge by automating DNA sequencing and genotyping. The homogeneous approach, which is a key feature of this technique, is also ideal for creating environments in which molecular interactions may be detected and studied.

Valuable applications of CE include:

- Genetic analysis.
- Analysis of drugs and pharmaceuticals with chiral centers (enantiomers).
- Protein characterization.
- Carbohydrate analysis for the determination of posttranslational modifications.
- Investigation of DNA-Protein, DNA-DNA/RNA, DNA-Small Molecule, Protein-Protein, Protein-Peptide, Protein–Small Molecule interactions.
- Analysis of products of enzymatic reactions.

Here, I want to list several advantages of CE:

- CE can be operated under physiological or near-physiological buffer conditions in the analysis of biomolecules.
- Low surface-to-volume ratio gives less heating and higher voltage than in convenient slab gel electrophoresis.
- High-performance separation produces high plate numbers of more than 10^6 and up to 10^9, and the analysis time is usually within 10 min or comparable to that of high-performance liquid chromatography (HPLC).
- Minimum sample amount requirement is usually less than pg or μL.
- Rinsing of the capillary is easy because in most techniques an open tubular fused silica capillary is used.
- Running cost is low because almost no organic solvent is used but aqueous buffer solutions of small volumes (few mL) are required.
- The automated instrumental version of CE is available.

There are a few limitations of practical CE applications:

- The concentration detection limit is low (in a range of 10^{-6} M), although the mass detection limit is very high (~10^{-15} moles) because of small volume of an injected sample. An exception is capillary electrophoresis with laser-induced fluorescence detection where the concentration limit can reach 10^{-12} M.
- The reproducibility of migration time and peak heights (areas) are slightly poorer compared to HPLC, owing to slightly unstable electroosmotic velocity.
- CE applications are difficult to adjust to preparative purposes.

CE is an attractive alternative to other separation-based techniques for evaluating binding parameters. The application of CE to study target-ligand interactions was first reported in 1992 [7, 8]. From then on, CE has been widely used to study molecular interactions and has become a powerful tool for the determination of binding parameters of various bioaffinity interactions. In CE, the electrophoretic mobility of an analyte is mainly determined by three factors: (i) the charge of the analyte, (ii) its size, and (iii) the chemical additives present in the background electrolyte interacting with the analyte.

1.2.2. Existing KCE Methods

Capillary electrophoresis where there is interaction of separated species can be called Kinetic Capillary Electrophoresis (KCE). Therefore, all affinity CE methods are classified as kinetic methods. Existing kinetic CE methods can be used for: (i) quantitative affinity analyses with strong binding (low k_{off}), (ii) measuring equilibrium dissociation or binding constants K_d or K_b, (iii) determination of thermodynamic parameters ΔH and ΔS, and (iv) calculation of binding stoichiometry.

Prior to our work, several KCE methods were available to measure equilibrium binding constants, e.g. capillary zone electrophoresis (CZE) [9, 10], affinity capillary electrophoresis (ACE) [11], Hummel–Dreyer method (HD) [12], frontal analysis (FA) [13], vacancy peak method (VP) [14], and vacancy affinity capillary electrophoresis (VACE) [15]. With the exception of ACE and VACE, they were primarily developed in high-performance liquid chromatography (HPLC) and transferred to CE. CE methods for

the estimation of binding constants and their experimental setups are summarized in **Table 1.1.**

In order to estimate equilibrium constants, a series of experiments, where the concentration of one component is varied while keeping that of the other component constant, should commonly be performed. The equilibrium constants are calculated from the dependence of either the electrophoretic mobility or the concentration ratio of unbound (free) and bound analytes. Various affinity interactions, such as drug–protein, protein–protein, protein–DNA, protein–carbohydrate, peptide–antibiotic, enzyme–cofactors, lectin–sugar, antigen–antibody and cyclodextrins (CDs)–enantiomer have been investigated by CE [16, 17]. All these methods assume that equilibrium (1.1) is established very quickly, the reversible binding between L and T is expressed by the following equation:

$$r = \frac{[L \bullet T]}{[T]_{total}} = \sum_{i=1}^{m} n_i \frac{K_i[L]}{1+K_i[L]} \tag{1.3}$$

where r is the ratio of number of bound target (a ligand–target complex) molecules to total target molecules; [T], [L•T] and $[T]_{total}$ are the concentrations of a free target, a ligand–target complex and a total target, respectively; n_i is the number of sites of class i and K_i is the corresponding equilibrium binding constant.

Table 1.1. Existing KCE Methods and Their Experimental Setups for Estimation of Binding Constants

KCE method	Schematic representation of initial conditions	Initial conditions	Simulated electropherogram	Quantitative foundation	Applicability	Applications
CZE	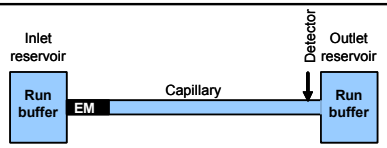	•Capillary filled with Run buffer •Injection of the equilibrium mixture of L+T	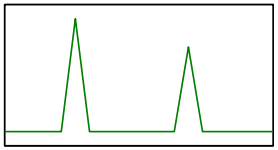	Area or height vs. [L]	Fast k_{on} and slow k_{off}	•Determination of K_b, ΔH and ΔS
ACE	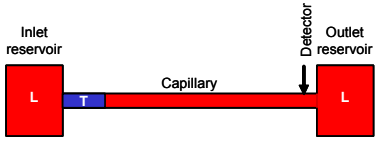	•Capillary filled with Run buffer+ L • Injection of a small plug of T	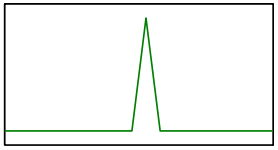	Mobility vs. [L]	Fast k_{on} and k_{off}	•Determination of K_b, ΔH and ΔS •Determination of the binding stoichiometry
HD	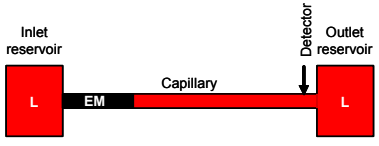	•Capillary filled with Run buffer+L •Injection of a long plug of the equilibrium mixture of L+T	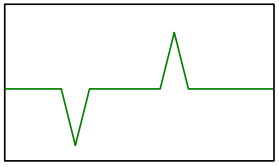	Area or height vs. injected [L]	Fast k_{on} and k_{off}	•Determination of K_b •Determination of the binding stoichiometry
FA	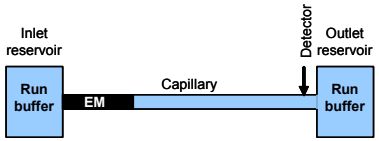	•Capillary filled with Run buffer •Injection of a long plug of the equilibrium mixture of L+T	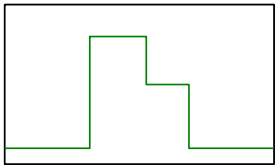	Height vs. [L]	Fast k_{on} and slow k_{off}	•Determination of K_b •Determination of the binding stoichiometry
VP (VACE)	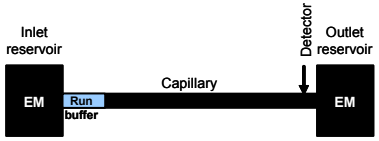	•Capillary filled with the equilibrium mixture of L+T •Injection of a plug of Run buffer	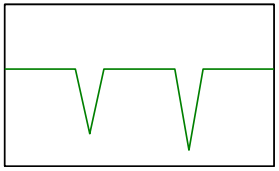	Area or height (for VP), mobility (for VACE) vs. [L]	Fast k_{on} and k_{off}	•Determination of K_b •Determination of the binding stoichiometry

1.2.2.1. Calculation from Change in Peak Area or Plateau Height

In CZE, HD, VP and FA, a peak area or a plateau of a complex linearly depends on the concentration of analytes. Assuming that the stoichiometry of the binding between L and T is 1:1, the reversible reaction between L and T is expressed by (1.1) and the binding constant (K_b) is given by:

$$K_b = \frac{[L \bullet T]}{[L][T]} \tag{1.4}$$

where [T] is the concentration of free target. To have a linear function, (1.4) can be traditionally rearranged as below [18, 19]:

$$\frac{1}{r} = 1 + \frac{1}{K_b} \times \frac{1}{[L]} \tag{1.5}$$

Consequently, the binding constant is calculated from the slope ($1/K_b$). On the contrary, a non-linear plot is observed when multiple binding sites with different binding constants exist on T. Although each binding constant can be calculated from each linear slope in some cases, it is usually considered a non-linear regression curve fitting of acquired experimental data with equation (1.3).

1.2.2.2. Calculation from Change in Electrophoretic Mobility

In ACE and VACE, the K_b value is calculated from the dependence of the electrophoretic mobility on the free and bound analyte concentrations. When it's assumed that the stoichiometry of binding between L and T is 1:1 and that the analyte is T, the apparent electrophoretic mobility of T, μ_i, is expressed by the following expression:

$$\mu_i = \frac{[T]}{[T] + [L\bullet T]}\ \mu_{free} + \frac{[L\bullet T]}{[T] + [L\bullet T]}\ \mu_c \tag{1.6}$$

where μ_{free} and μ_c are the electrophoretic mobilities of free T and L•T, respectively. Equation (1.6) is further rearranged as below:

$$\frac{[L\bullet T]}{[T]} = K_b[L] = \frac{\mu_{free} - \mu_i}{\mu_i - \mu_c} \tag{1.7}$$

Equation (1.7) has been traditionally used for the calculation of binding constants with ACE [20]; however, the mobilities of T and L•T, μ_{free} and μ_c, respectively, must be experimentally measured. To know the real mobility of L•T complex, μ_c, is challenging. A non-linear curve fitting of acquired experimental data, therefore, should be employed with (1.7). In this case, the measurement of μ_c is not required. From (1.4) and (1.6), the following equations are obtained:

$$\mu_i = \frac{\mu_{free} + \mu_c K_b[L]}{1 + K_b[L]} \tag{1.8}$$

$$(\mu_i - \mu_{free}) = \frac{(\mu_c - \mu_{free})\, K_b[L]}{1 + K_b[L]} \tag{1.9}$$

Equation (1.9) can be further rearranged into different forms:

$$\frac{1}{(\mu_i - \mu_{free})} = \frac{1}{(\mu_c - \mu_{free})\, K_b} \times \frac{1}{[L]} + \frac{1}{(\mu_c - \mu_{free})} \tag{1.10}$$

$$\frac{[L]}{(\mu_i - \mu_{free})} = \frac{1}{(\mu_c - \mu_{free})}\ [L] + \frac{1}{(\mu_c - \mu_{free})\, K_b} \tag{1.11}$$

Equations (1.10) and (1.11) are called the double reciprocal and x-reciprocal forms, respectively. They have appeared in publications with different names. The

double-reciprocal plot is known as the Benesi–Hildebrand binding curve in spectrophotometry and the Lineweaver–Burk plot in enzymology, while the x-reciprocal plot is called the Eadie plot in enzyme kinetics or the Scatchard plot in protein binding studies [21].

The above equations assume a 1:1 binding stoichiometry. The assumption may be supported by the linearity of the plots. However, two or multiple binding sites may exist on the receptors; for drug–human serum albumin and antibody–antigen binding, multiple stoichiometry is well documented [22, 23]. In these cases, the binding constants cannot be calculated from the plots according to (1.10) and (1.11) because some plots are non-linear. Different studies, such as NMR, UV-spectra and Mass Spectrometry, have been also practically useful to obtain further information on stoichiometry for the affinity interactions of the complexes.

1.2.2.3. Capillary Zone Electrophoresis (CZE)

In this method, the target and the ligand are pre-equilibrated together before injecting onto the CE column where the free target is separated from the complexed target and ligand. The free target concentration can be calculated using an external calibration curve. The binding constant is then calculated from equation (1.5) using a Scatchard plot. This method is applicable to systems having suitably stable complexes where the dissociation rate constants are slow compared to the separation timescale. In order to use this technique, it should be demonstrated that the observed peaks are due to the uncomplexed target, the uncomplexed ligand, and the complex. It should also be

demonstrated that changes in peak quantitation (either peak area or height) are a result of complexation, and not due to other phenomena (quenching, decomposition, etc.).

1.2.2.4. Affinity Capillary Electrophoresis (ACE)

ACE is the most popular method for measuring equilibrium binding constants in CE. The capillary is filled with a buffer containing L with varying concentration and a small amount of T is injected. Since the equilibrium between L and T is established in the capillary, the apparent mobility of T depends on the binding constant and the difference between μ_{free} and μ_c. The binding constant is calculated from the change in the electrophoretic mobility of T. On the contrary, T can be added to the buffer instead of L. In this case, a small amount of L is injected as the sample. ACE has several potential advantages as follows: (1) only a small amount of T is required, (2) the injected sample does not have to be purified, and (3) binding constants of several samples can be simultaneously determined. For instance, plasma binding of racemic drugs is potentially stereoselective. Each drug enantiomer frequently exhibits different pharmacological activities and/or different side effects. The estimation of each binding constant is essential for stereoselective drug developments. For this purpose, ACE can be performed by injecting the racemic mixture directly. The enantiomer separations are performed by dissolving plasma proteins in the running buffer [24].

As compared to the other methods such as HPLC and non-chromatographic methods, approximate equilibrium binding constants can be estimated with ACE. However, it should be done carefully when attempting the estimation of accurate

equilibrium binding constants due to several disadvantages of ACE. First, the fluctuation of the electroosmotic mobility may influence the observed electrophoretic mobility. Although the effect of the electroosmosic flow on the velocity of the complex is mostly compensated for the effective mobility of the complex, change on the electroosmotic flow during a single run will affect the measurement of the effective mobility. The conditioning of the capillary surface is important to obtain reproducibility of the electroosmotic mobility. Second, changes in the magnitudes of both electrophoretic and electroosmotic mobilities are observed due to the viscosity variation with increasing concentration of the buffer additive. Third, some components such as proteins, peptides and basic analytes, may adsorb on the inner wall of the capillary. This causes peak broadening and inaccurate mobility measurements. In order to avoid the adsorption, the ionic strength and pH of the running buffer must be carefully selected. Alternatively, a neutral coated capillary, e.g. a linear polyacrylamide-coated capillary or a polyvinylalcohol-coated one, is frequently useful for this purpose [25]. By using the neutral coated capillary, the change in the electroosmotic mobility can also be avoided due to the almost complete suppression of the electroosmotic flow. Fourth, the concentration of unbound L, [L], in the above equations is not equal to the concentration of L dissolved in the running buffer. In order to calculate K_b values, however, one usually needs to substitute the total ligand concentration, $[L]_{total}$, for [L] in the equations. When $[L]_{total}$ is much higher than the total target concentration or the equilibrium binding constants are not large, it does not significantly affect the K_b value because [L] can be approximated by $[L]_{total}$.

1.2.2.5. Hummel-Dreyer method (HD)

In the Hummel-Dreyer method, the ligand is dissolved in the run buffer at varying concentrations, creating a high detector background response. The target is dissolved in the run buffer containing the ligand before being injected into the capillary. The complexed ligand and target migrate out of the injection plug, leaving a zone of reduced ligand concentration behind. This zone is detected as a negative peak, and the area is related to the concentration of bound ligand. A positive peak corresponding to the ligand-target complex is also observed. The concentration of the complexed target can be determined from a plot of detector response *versus* the concentration of the excess ligand in the injection plug [14]. The equilibrium binding constant can be obtained using non-linear regression of equation (1.5).

1.2.2.6. Frontal Analysis (FA)

In frontal analysis (FA), the equilibrium between L and T is obtained in a sample vial. After the hydrodynamic injection of a long plug of the equilibrated sample into the capillary filled with a run buffer, the free and bound components are separated in a capillary [24]. In FA, the electrophoretic mobility of the free target must be different from the mobility of the ligand and the ligand-target complex. The separation produces a broadened plateau of the free target that migrates away from the ligand and ligand-target complex. The equilibrium concentration of the free target is calculated from the height of the resulting plateau. The binding constant is calculated from the free target concentration using a Scatchard-type plot. Frontal analysis can be applied to the estimation of K_d below

1 mM. For weak interactions, where K_d is higher than 1 mM, it is experimentally difficult to measure accurately the height difference between the frontal zones of the free target and the complex.

1.2.2.7. Vacancy Peak Method (VP) and Vacancy Affinity Electrochromatography (VACE)

In the vacancy peak method, the equilibrium mixture of a target and a ligand is dissolved in a run buffer, resulting in a high background signal at a detector. The run buffer without L or T is injected, producing two negative peaks. One peak arises from the free T and the other peak arises from the complex. The free T concentration is calculated from the peak areas (or heights) at varying the concentration of L in the buffer. The equilibrium binding constant is calculated from the free T concentration as a function of the L concentration. Vacancy affinity capillary electrochromatography (VACE) is performed in a similar manner [25]. L and T are dissolved in the run buffer, and then the buffer without L or T is injected. Two negative peaks result, corresponding to free and complexed T. By varying the concentration of L in the buffer, the mobilities of the negative peaks can be correlated to the fraction of free and complexed T. Binding constants can be calculated using equation (1.9). For the vacancy peak methods, as for any method using inverse detection, the concentration of the absorbing species in the run buffer should be optimized in order to obtain good sensitivity. Too little background absorbance results in poor dynamic range while excessive background absorbance saturates the detector, again resulting in poor sensitivity.

1.2.3. New KCE Methods

In this thesis, I propose kinetic capillary electrophoresis (KCE) as a conceptual platform for the development of kinetic homogeneous affinity methods and their application to screening and selection of binding ligands for specific targets. KCE is defined as CE separation of species, which interact during electrophoresis. Depending on how the interactions are arranged, different KCE methods can be designed. All KCE methods are described by the same mathematics – the same system of partial differential equations with only initial and boundary conditions being different (see Chapter 3 "Mathematical Model of NECEEM" and Chapter 6 "SweepCE"). Every qualitatively unique set of initial and boundary conditions define a unique KCE method. In this proof-of-principle work, I present two new KCE methods: Non-Equilibrium Capillary Electrophoresis of Equilibrium Mixtures (NECEEM), and Sweeping Capillary Electrophoresis (SweepCE), mathematical modeling of the methods, and demonstration of their applications. The spectrum of their applications includes: (i) measuring K_d, k_{off}, and k_{on}, (ii) quantitative affinity analyses of proteins, (iii) measuring temperature in capillary electrophoresis, (iv) studying thermochemistry of affinity interactions, and (v) kinetic selection of ligands from combinatorial libraries.

1.3. CONCLUSION

Capillary electrophoresis has been one of the most rapidly growing analytical technique to study affinity interactions in recent years and the analytical methodology progresses continuously. Since CE features quick analysis, high efficiency, high

resolving power, low sample consumption and wide range of possible analytes, it contributes an indispensable tool for the estimation of equilibrium binding constants, stoichiometry, and thermodynamic parameters of complex formation. In this chapter, the existing kinetic methods and their mathematical equations for the estimation of equilibrium binding constants are described. The concept of Kinetic Capillary Electrophoresis allows for creating an expanding toolset of powerful kinetic homogeneous affinity methods, which will find their applications in studies of biomolecular interactions, quantitative analyses, and screening of complex mixtures for affinity probes and drug candidates.

CHAPTER 2

NON-EQULIBRIUM CAPILLARY ELECTROPHORESIS OF EQULIBRIUM MIXTURE (NECEEM)

2.1. INTRODUCTION

Non-covalent protein-DNA complexes participate in gene expression, DNA replication, DNA integrity control, and DNA damage repair. In order to understand the dynamics of these biological processes it is important to know the kinetic parameters of the formation and the decay of relevant protein-DNA complexes. The knowledge of these parameters is also essential for the development and the optimization of analytical methods and molecular biology techniques based on protein-DNA interactions. The formation and the decay of a protein-DNA complex, P•DNA, are characterized by a bimolecular rate constant k_{on}, and a monomolecular rate constant, k_{off}, respectively:

$$P + DNA \underset{k_{off}}{\overset{k_{on}}{\rightleftharpoons}} P\bullet DNA \tag{2.1}$$

The stability of the complex is often described in terms of the equilibrium dissociation constant:

$$K_d = \frac{k_{off}}{k_{on}} \tag{2.2}$$

Since k_{on}, k_{off}, and K_d are related through the last expression, obtaining any pair of the three constants is sufficient to calculate the third one. For a protein-DNA complex, it is more practical to determine K_d and k_{off} in experiment and then calculate k_{on} from

expression (2.2). Classically, K_d of a protein-DNA complex is obtained by electrophoresis mobility shift assay (EMSA) on slab gels [26]. EMSA has been also used to estimate the values of k_{off} [27], although the accuracy of this method is low and the dynamic range is limited. More recently, surface plasmon resonance (SPR) has been successfully applied to measurements of K_d and k_{off} for protein-DNA complexes [4, 5]. Both EMSA on slab gels and SPR experiments require relatively large amounts of a protein, and they are heterogeneous methods.

When the quantity of a protein is a limiting factor, capillary electrophoresis (CE) has proved to be a technique of choice for studies of protein-DNA interactions. A CE analogue of slab-gel EMSA (CEMSA) has been developed and applied to the determination of K_d for protein-DNA complexes [28-31]. For rapidly decaying protein-DNA complexes, affinity capillary electrophoresis (ACE) of the complex can be used to prevent complex decay during the separation [32, 33]. In ACE, the run buffer is supplemented with one of the components of the complex to maintain the equilibrium during separation. The assumption of equilibrium in CEMSA and ACE allows for the determination of K_d but makes finding k_{off} difficult. Here I propose non-equilibrium capillary electrophoresis of the equilibrium mixtures (NECEEM) of a protein, DNA, and a protein-DNA complex as a fast method to find both K_d and k_{off} in a single experiment. I used the new method to study the interaction between an *E. coli* single-stranded DNA binding protein (SSB) and a fluorescently labeled 15-mer oligonucleotide (fDNA).

2.2. RESULTS AND DISCUSSION

2.2.1. Principle of NECEEM

Equilibrium mixtures contain three components: free SSB, free fDNA and the SSB•fDNA complex. The fDNA was labeled by fluorescein and was detectable with laser-induced fluorescence (LIF). NECEEM of such mixtures generated electropherograms with three essential features: peaks 1 and 2 and curved line 3 (**Figure 2.1**). The sole peak 1 was observed when SSB was not present in the equilibrium mixture, indicating that peak 1 represents fDNA (**Figure 2.1A**). When, the concentration of SSB was intermediate, all three features where observed (**Figure 2.1B**). The height of peak 1 decreased with increasing concentration of SSB. When the concentration of SSB was saturating, peak 1 was not observed (**Figure 2.1C**). Curve 3 was shown to be perfectly fitted by a single exponential line and therefore will be called an "exponential part" of the electropherogram. To reveal the identities of the three features in the electropherograms it's needed to consider the fate of the three components (free SSB, free fDNA, and the SSB•fDNA complex) while being separated by NECEEM. Both SSB and fDNA were negatively charged under the conditions resulting in negative electrophoretic mobilities for both free SSB and free fDNA. However, the negative charge to size ratio was lower for SSB; therefore, the electrophoretic mobility of free SSB was higher than that of free fDNA. The SSB•fDNA complex had an intermediate value of electrophoretic mobility. Because of these differences in the electrophoretic

mobilities, the equilibrium fractions of free fDNA and free SSB were removed from the electrophoretic zone of the SSB•fDNA

The equilibrium fraction of free fDNA migrated as a single electrophoretic zone and resulted in peak 1 with the longest migration time, as was confirmed by sampling pure fDNA. The equilibrium fraction of free SSB also migrated as a single zone, but due to the lack of a fluorescent label, free SSB did not contribute to the electropherograms. The equilibrium fraction of the SSB•fDNA complex could not generate a single electrophoretic peak since the equilibrium of the complex was not maintained in NECEEM. The complex continuously decayed during the separation resulting in the non-equilibrium production of free fDNA and free SSB. According to reaction (2.1), the rate of fDNA production reduced exponentially following the monomolecular decay of the complex during NECEEM separation:

$$\frac{d[\mathrm{fDNA}]}{d\mathrm{t}} = -\frac{d[\mathrm{SSB} \bullet \mathrm{fDNA}]}{d\mathrm{t}} = [\mathrm{SSB} \bullet \mathrm{fDNA}]_{\mathrm{eq}} \exp(-\mathrm{k}_{\mathrm{off}}\mathrm{t}) \quad (2.3)$$

Here $[SSB•fDNA]_{eq}$ is the equilibrium concentration of the complex in the equilibrium mixture, k_{off} is the monomolecular rate of complex decay and t is time passed from the beginning of the separation. The exponential part 3 of the electrophoregrams reflects the production of free fDNA, or in other words, the decay of the SSB•fDNA complex. Peak 2 corresponds to the SSB•fDNA complex that remained intact at the time of its elution from the capillary. This was confirmed by increasing peak 2 with decreasing separation time (**Figure 2.2A**). During a shorter separation time a lesser fraction of the complex decayed and a larger fraction of the complex exited the capillary intact.

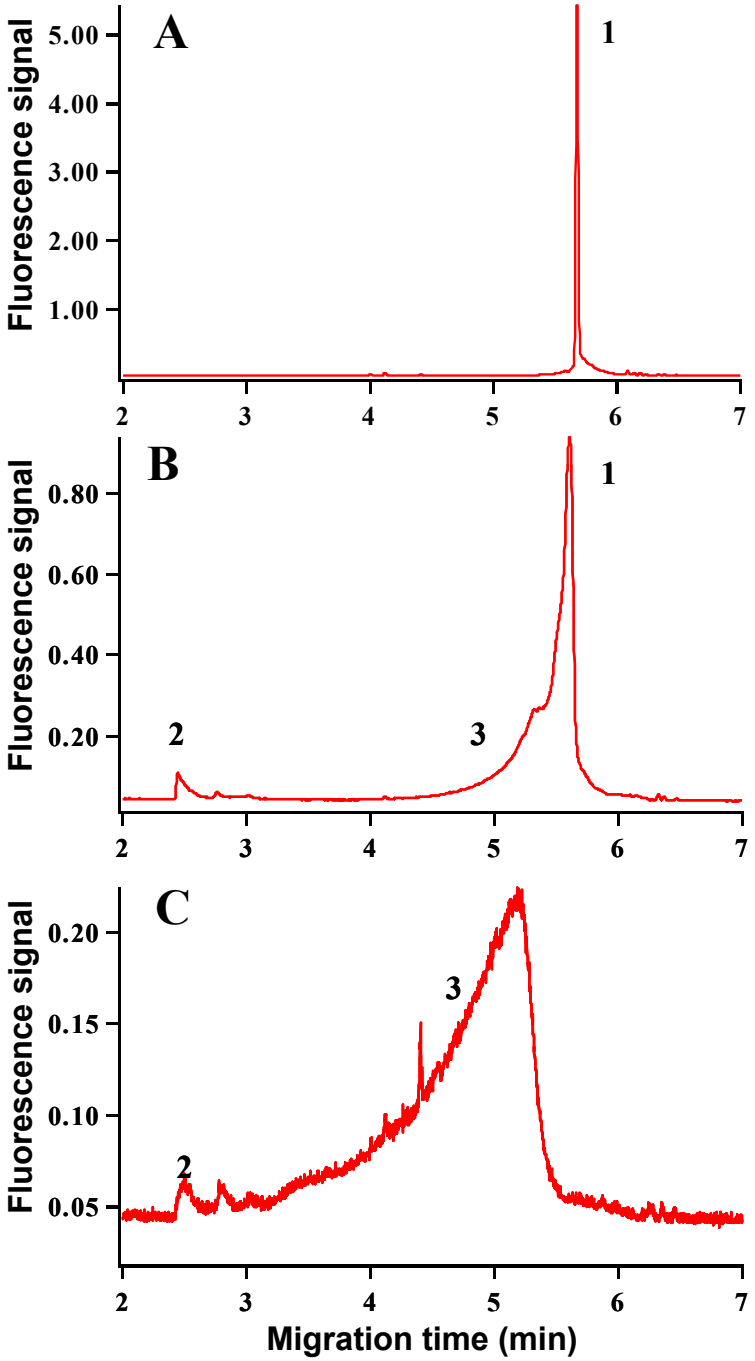

Figure 2.1. NECEEM of SSB and fDNA

The total concentrations of SSB and fDNA in the mixtures were: (A) $[SSB]_0 = 0$, $[fDNA]_0 = 0.20$ μM; (B) $[SSB]_0 = 0.32$ μM, $[fDNA]_0 = 0.16$ μM; (C) $[SSB]_0 = 0.80$ μM, $[fDNA]_0 = 0.10$ μM. The run buffer was 25.0 mM tetraborate at pH 9.4.

The identities of the features in the electropherograms were also confirmed by measuring the fluorescence anisotropy of fDNA in the two peaks and the exponential part (**Figure 2.2B**). The fDNA molecule is much smaller than the SSB•fDNA complex; therefore the anisotropy of free fDNA is lower than that of the complex. Peak 1 and exponential part 3 had identical small anisotropy, r_{fDNA} = 0.03, corresponding to free fDNA, while peak 2 had a higher anisotropy, $r_{SSB•fDNA}$ = 0.11, corresponding to the SSB•fDNA complex. It should be emphasized that NECEEM provides a unique way of directly measuring the fluorescence anisotropy of the complex. I used the values of r_{fDNA} and $r_{SSB•fDNA}$ in our determination of the relative quantum yield of SSB-bound fDNA.

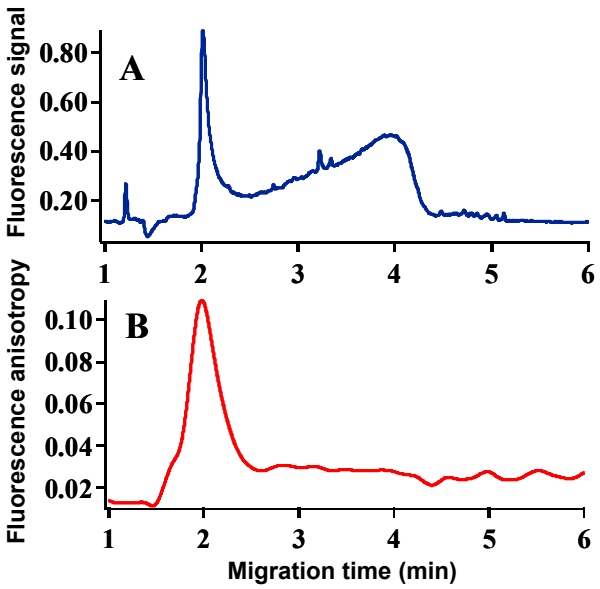

Figure 2.2. NECEEM of SSB and fDNA with Shortened Separation Time

Shortening of the separation time (compare to **Figure 2.1**) was achieved by increasing the velocity of electroosmotic flow; the velocity was increased through decreasing the ionic strength of the run buffer. Panel A shows the total fluorescence intensity while panel B demonstrates the corresponding fluorescence anisotropy. The total concentrations of the protein and fDNA in the mixture were: $[SSB]_0$ = 1.30 μM and $[fDNA]_0$ = 0.13 μM. The run buffer was 12.5 mM tetraborate at pH 9.4.

2.2.2. Determination of K_d

The assignment of peak 1 to the equilibrium fraction of free fDNA and both peak 2 and exponential part 3 to the equilibrium fraction of the SSB•fDNA complex allowed me to calculate the equilibrium dissociation constant K_d. The equilibrium fraction of free fDNA is proportional to the area of peak 1, A_1:

$$[\text{fDNA}]_{eq} = A_1 \frac{a}{\varphi_{\text{fDNA}}} \tag{2.4}$$

where "a" is a constant, and φ_{fDNA} is the quantum yield of fluorescence of free fDNA. The equilibrium fraction of the complex is dependent on the areas of peak 2, A_2, and exponential part 3, A_3:

$$[\text{SSB} \bullet \text{fDNA}]_{eq} = A_2 \frac{a}{\varphi_{\text{SSB}\bullet\text{fDNA}}} + A_3 \frac{a}{\varphi_{\text{fDNA}}} \tag{2.5}$$

where $\varphi_{\text{SSB}\bullet\text{fDNA}}$ is the quantum yield of fluorescence of the complex. Constant "a" is responsible for transferring an area unit to a concentration unit in equations (2.4) and (2.5). The constant depends on chemical properties of a fluorescent tag and does not change during the complex formation. Using expressions (2.4) and (2.5) on can find the ratio, R, of the two equilibrium fractions:

$$R = \frac{[\text{fDNA}]_{eq}}{[\text{SSB} \bullet \text{fDNA}]_{eq}} = \frac{A_1}{A_2 \varphi_{\text{fDNA}} / \varphi_{\text{SSB}\bullet\text{fDNA}} + A_3} \tag{2.6}$$

On the other hand the knowledge of this ratio is sufficient for the determination of K_d:

$$K_d = \frac{[\text{SSB}]_0 (1+R) - [\text{fDNA}]_0}{1 + 1/R} \tag{2.7}$$

To determine R we need to find the relative quantum yield, $\varphi_{fDNA}/\varphi_{SSB\bullet fDNA}$, and the three areas, A_1, A_2, and A_3. The relative quantum yield was found to be 0.95 ± 0.03 (see the next section). The areas A_1, A_2, and A_3 were calculated as demonstrated in **Figure 2.3**. Expressions (2.6) and (2.7) were then used to calculate the value of K_d equals to 282 ± 51 nM based on six experiments with different concentrations of SSB and fDNA mixed. This value is in agreement with those obtained by other methods: 227 nM and 200 nM for binding of SSB with an 11-mer oligonucleotide measured by ACE and fluorescence anisotropy, respectively [32, 33], and 714 nM for binding of SSB with a 16-mer oligonucleotide measured by the fluorescence quenching method [34]. Insignificant differences between the K_d values can be ascribed to differences in oligonucleotide length and to the use of different buffers.

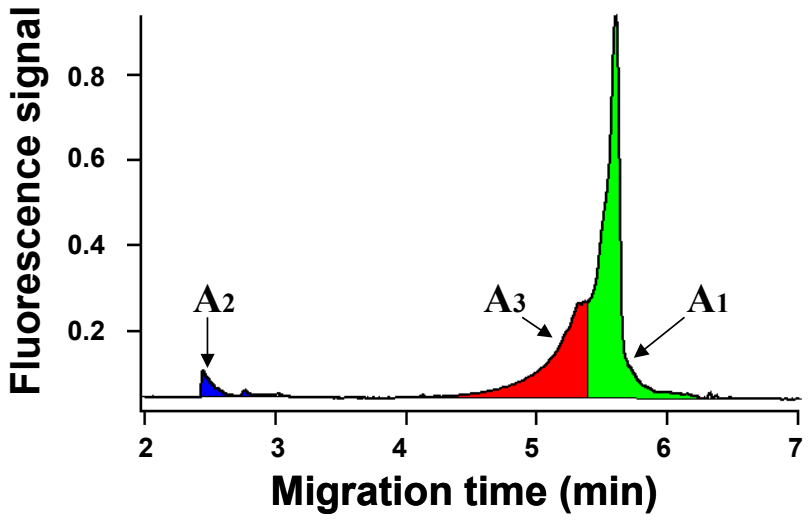

Figure 2.3. Determination of Areas in NECEEM

Determination of areas A_1 and $A_2 + A_3$ required for finding the equilibrium dissociation constant K_d of the SSB•fDNA complex from a single NECEEM experiment.

2.2.3. Determination of Relative Quantum Yield

The value of the relative quantum yield of fluorescence of fDNA, $\varphi_{fDNA}/\varphi_{SSB\bullet fDNA}$, was found by comparing peak areas generated by free fDNA and SSB-bound fDNA. Fluorescence of free fDNA was measured in a CE experiment with no SSB in the sample or in the running buffer (**Figure 2.4A**). Fluorescence of SSB-bound fDNA was measured in an ACE experiment with the running buffer containing SSB (**Figure 2.4B**). Fluorescein, which does not interact with SSB, was used as an internal marker in both experiments to normalize the fluorescence intensities of fDNA. The presence of SSB in the running buffer maintained the equilibrium between free fDNA and SSB-bound fDNA during the ACE separation. The relative quantum yield of SSB-bound fDNA was calculated using the following expression:

$$\frac{\varphi_{fDNA}}{\varphi_{SSB\bullet fDNA}} = \frac{1 - (r_{SSB\bullet fDNA} - r_{ACE})/(r_{SSB\bullet fDNA} - r_{fDNA})}{A_{ACE}/A_{CE} - (r_{SSB\bullet fDNA} - r_{ACE})/(r_{SSB\bullet fDNA} - r_{fDNA})} \qquad (2.8)$$

where A_{ACE} and A_{CE} are peak areas generated by the same amount of fDNA in the ACE and CE experiments, respectively; r_{ACE} is the fluorescence anisotropy in the ACE experiment; the values of fluorescence anisotropy of free fDNA, r_{fDNA}, and SSB-bound fDNA, $r_{SSB\bullet fDNA}$, were determined in NECEEM experiments (see above). The relative quantum yield of fluorescence, $\varphi_{fDNA}/\varphi_{SSB\bullet fDNA}$, was found to be equal to 0.95 ± 0.03. I expected that this value would be close to unity since the fluorescein moiety is not involved directly into SSB-fDNA interactions. Thus, in general the $\varphi_{fDNA}/\varphi_{SSB\bullet fDNA}$ ratio in expression (2.6) can be assumed to be equal to 1 unless fDNA is labeled with a fluorophore whose fluorescence can be quenched by a protein [34].

Whether or not the quantum yield of fDNA changes upon binding to SSB can be examined in a fast fashion in NECEEM experiments with varying separation time. If the separation time shortens then more of the intact SSB•fDNA complex reaches the detection end of the capillary. Thus, area A_2, which corresponds to the complex, increases, while areas A_1 and A_3 decrease.

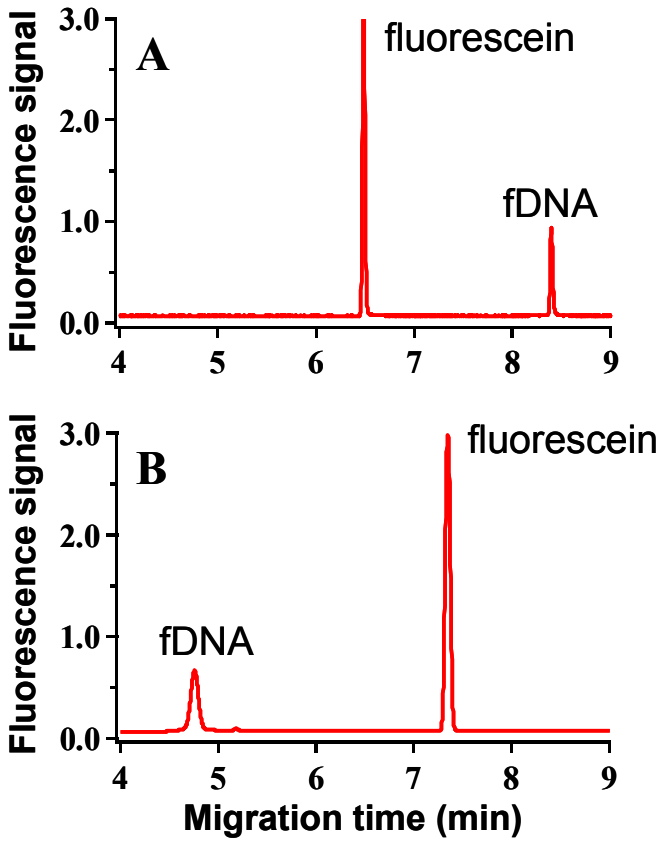

Figure 2.4. Determination of Relative Quantum Yield

Analysis of the same amount of fDNA (0.10 μM) by CE (panel A) and by ACE (panel B). In both experiments, the solution of fDNA contained 0.25 μM fluorescein used as an internal marker. In CE, the run buffer was 25.0 mM tetraborate at pH 9.4; in ACE, the run buffer was 25.0 mM tetraborate supplemented with 1.0 μM SSB. The areas of the peaks were identical in the two experiments confirming that the quantum yield of fDNA did not change upon binding to SSB.

If the total area $A_1 + A_2 + A_3$ does not change then the quantum yield of fDNA fluorescence is not affected upon binding to SSB. I decreased the separation time by using running buffers with decreasing ionic strengths. **Figure 2.5** shows the observed changes in the electrophoretic features. The total area, $A_1 + A_2 + A_3$, did not change confirming that the quantum yield of fDNA was not affected by binding to SSB.

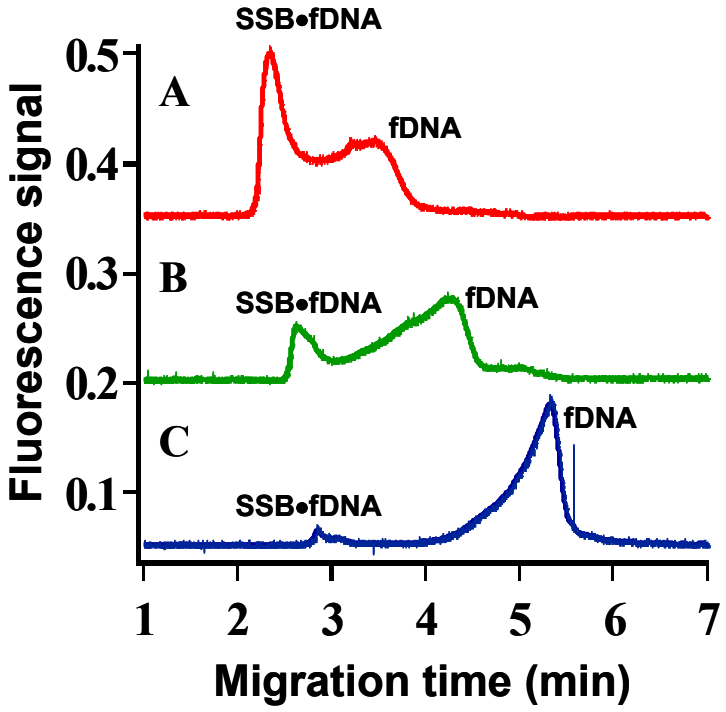

Figure 2.5. Influence of Separation Time on NECEEM Electropherograms

The separation time was changed by changing the electroosmotic velocity through using run buffers with different ionic strengths: 12.5 mM Tetraborate pH 9.4 (A), 16.7 mM Tetraborate pH 9.4 (B) and 25.0 mM Tetraborate pH 9.4 (C). Although the relative intensities of the electrophoretic features changed, the total area of the fluorescence signal remained constant with changing separation time. The total concentrations of the protein and fDNA in the equilibrium mixture were $[SSB]_0 = 0.80$ μM and $[fDNA]_0 = 0.10$ μM. The electropherograms are offset for the clarity of presentation.

2.2.4. Determination of k_{off} and k_{on}

The monomolecular rate constant of complex decay, k_{off}, can be determined from the exponential part 3 of the electropherogram by fitting the experimental data (**Figure 2.6**) with a single exponential function:

$$I_t = I_{t_0} \exp\left\{ k_{off} \frac{t_{SSB \bullet fDNA}}{t_{fDNA} - t_{SSB \bullet fDNA}} (t - t_0) \right\} \quad (2.9)$$

where I_t and I_{t_0} are the fluorescence intensities at times t and t_0, respectively, and t_{fDNA} and $t_{SSB \bullet fDNA}$ are migration times of fDNA and SSB•fDNA, respectively. The $t_{SSB \bullet DNA}/(t_{fDNA} - t_{SSB \bullet DNA})$ coefficient reflects the apparent shortening of the time window in which the complex decay is monitored: $t_{SSB \bullet fDNA}$ to t_{fDNA} instead of 0 to t_{fDNA}. The value of k_{off} for the decay of the SSB•fDNA complex was determined to be $(3.3 \pm 1.6) \times 10^{-2}$ s^{-1}. Using expression (2.2) and the values of K_d and k_{off} I calculated the bimolecular rate constant of the SSB•fDNA complex formation, $k_{on} = (11.7 \pm 5.6) \times 10^4$ $M^{-1}s^{-1}$. It is worthwhile to emphasize that the values of K_d and k_{off} can be determined from a single electropherogram.

If the monomolecular rate constant of complex decay, k_{off}, is too small or separation of the two peaks is not sufficient to resolve the exponential part, then the value of k_{off} can be determined by measuring the area of peak 2 (corresponding to the amount of the protein-DNA complex) as a function of peak 2 migration time. Migration time can be varied by changing one or more of the following 4 parameters: (i) capillary length, (ii) electric field, (iii) run buffer composition, and (iv) differential pressure applied to

capillary ends. The area will decrease with increasing time exponentially, and the value of k_{off} can be calculated from this data.

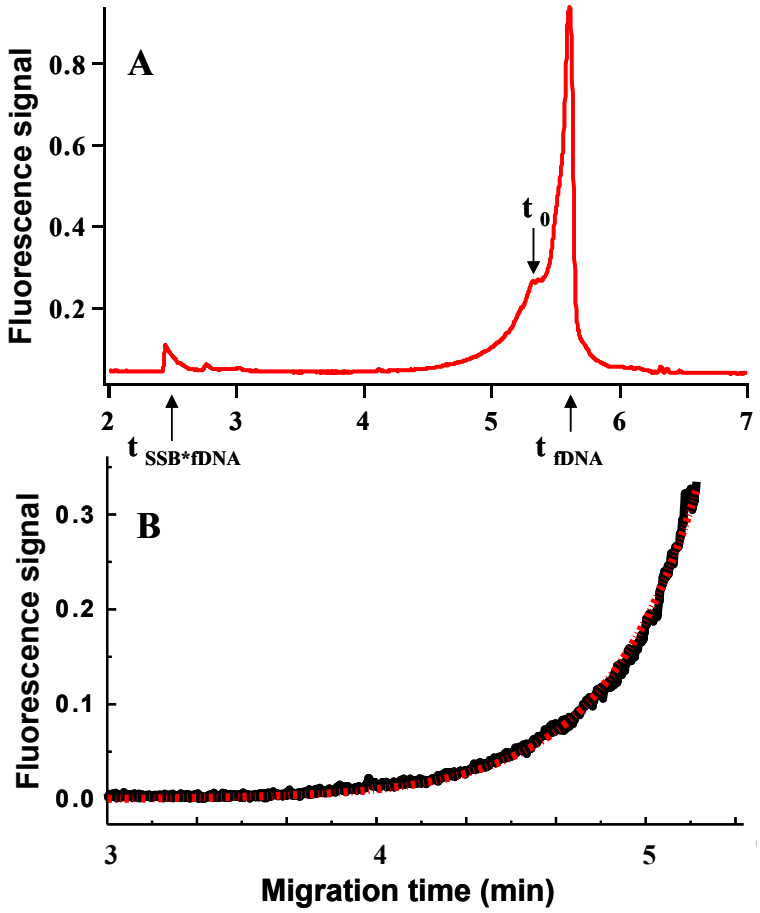

Figure 2.6. Determination of k_{off} .

The value of k_{off} can be found by fitting the exponential part of the electropherogram with a single exponential function, represented by Equation (2.9). Frame A shows the whole electropherogram and illustrates the assignment of times t_0, t_{fDNA} and $t_{SSB•fDNA}$. Frame B shows the best fit of experimental data with a single exponential function.

2.3. CONCLUSION

NECEEM takes the advantage of a rapidly decaying complex to calculate equilibrium and kinetic parameters of complex formation and decay in a single experiment. Knowledge of these constants is essential for understanding the dynamics of regulatory biological processes. Only slight modification of the NECEEM separation conditions may be needed to optimize this method for another protein-DNA complex. The parameters to be optimized are: the buffer concentration, pH, the capillary length, its type (coated or uncoated), and the strength of the electric field used for NECEEM. Another unique feature of NECEEM is its extremely high sensitivity. I was able to determine the parameters of the protein-DNA interaction with the amount of the protein as low as 10^{-18} moles. The next exciting application of NECEEM will include extremely sensitive analyses of proteins using oligonucleotide aptamers as affinity probes.

2.4. EXPERIMENTAL METHODS

2.4.1. Chemicals and Materials

E. coli single-stranded DNA binding protein (SSB), and buffer components were from Sigma-Aldrich (Oakville, ON). A fluorescently labeled 15-mer oligonucleotide, 5'-fluorescein-GCGGAGCGTGGCAGG (fDNA), was kindly donated by Dr. Yingfu Li (McMaster University, Hamilton, ON). Fused-silica capillaries were purchased from Polymicro (Phoenix, AZ). Deionazed water of Milli-Q quality was used for all solutions.

2.4.2. Capillary Electrophoresis

NECEEM separation of protein-DNA complexes was performed using a laboratory-built CE instrument with fluorescence detector described in detail elsewhere [35]. Uncoated fused silica capillaries of 40 cm × 20 μm I.D. × 150 μm O.D. were used in all experiments. Electrophoresis was run in a positive-polarity mode (positive electrode at the injection end) using a Spellman CZE 1000 power supply (Plainview, NY, USA) as a source of high voltage. A 488 nm line of an Ar-ion laser (Melles Griot, Ottawa, ON) was utilized to excite fluorescence of fDNA. Fluorescence was filtered from stray and scattered laser light with a band pass filter centered at 520 nm (Omega Optical, Brattleboro, VT). An R1477 photo multiplier tube (Hamamatsu, Middlesex, NJ) was used as a fluorescence light detector.

Fluorescence anisotropy was measured with the same CE instrument slightly modified as described elsewhere [33]. The value of anisotropy was calculated according to the following expression:

$$r = \frac{I_{\parallel} - I_{\perp}}{I_{\parallel} + 2I_{\perp}} \tag{2.10}$$

where $I_{\parallel}$ and $I_{\perp}$ are the intensities of fluorescence in the planes parallel and perpendicular to the plane of polarization of the excitation light.

Three run buffers were used for NECEEM: 25 mM, 16.7 mM and 12.5 mM tetraborate at pH 9.4. The run buffer for ACE was 25 mM tetraborate at pH 9.4 supplemented with 1 μM SSB. The samples were injected into the capillary by a pressure pulse of 1 s × 9.1 kPa; the length of the corresponding sample plug was 0.93 mm as was

calculated using the Poiseuille equation. The electrophoresis was carried out with an electric field of 600 V/cm at ambient temperature. The capillary was rinsed with the run buffer solution for 2 min prior to each run. At the end of each run, the capillary was rinsed with 100 mM NaOH for 2 min, followed by a rinse with deionized water for 2 min.

2.4.2. Equilibrium Mixtures

To prepare an equilibrium mixture of the protein, DNA and the protein-DNA complex, I mixed solutions of 16 μM SSB and 205 nM fDNA in the NECEEM run buffer at a desired volume ratio and incubated at room temperature prior to the analysis to reach the equilibrium.

Equation Chapter 3 Section 3 # CHAPTER 3

MATHEMATICAL MODEL OF NECEEM

3.1. INTRODUCTION

I have introduced a new KCE method for finding kinetic parameters of complex formation, nonequilibrium capillary electrophoresis of equilibrium mixtures (NECEEM) [36, 37]. Uniquely, NECEEM allows for the determination of both a bimolecular rate constant k_{on}, and a monomolecular rate constant, k_{off} and K_d from a single electropherogram. Conceptually, the equilibrium mixture of A and B is prepared, which contains three components, A, B, and C.

$$A + B \underset{k_{off}}{\overset{k_{on}}{\rightleftharpoons}} C \tag{3.1}$$

A plug of the equilibrium mixture is injected onto the capillary by pressure, and the run buffer that does not contain any of the three components is used for electrophoresis. As a result of the electrophoretic separation, the complex formation reaction is excluded from the dynamic equilibrium (3.1), and the complex dissociates exponentially with a monomolecular rate constant k_{off}. NECEEM electropherograms consist of peaks and exponential dissociation lines whose migration times and areas are used to calculate k_{off} and K_d. In this chapter, I want to show theoretical bases of NECEEM by developing a mathematical model of the method and applying it to fit experimental data and determine binding parameters through nonlinear regression of experimental data. The math model was developed in close collaboration with a

mathematician, Dr Victor Okhonin, from Krylov group. It provides adequate description of experimental NECEEM electropherograms and offers a simple and robust theoretical platform for understanding the influence of intermolecular complexes on CE electropherograms.

3.2. RESULTS AND DISCUSSION

3.2.1. Major Assumptions

The goal of this study was to develop a mathematical model of NECEEM that could qualitatively and quantitatively describe experimental NECEEM electropherograms. We based our consideration on a hypothesis that solving for reaction (3.1) under conditions of efficient electrophoretic separation of A, B, and C could provide a simple but satisfactory model. Technically, we aimed at obtaining analytical solutions for concentrations of A, B, and C in NECEEM as functions of time passed from the beginning of separation and position in the capillary. Such analytical solutions can be then used to model experimental data and determine binding parameters of complex formation. We obtained the analytical solutions under the following major assumptions.

We assume that electrophoretic zones of A and B are separated fast so that the forward reaction is negligible with respect to the reverse reaction (3.1) during the NECEEM separation. This assumption allows us to find solutions for concentrations of A, B, and C using the linear approximation. Due to the small diameter of the capillary in comparison to its length, a one-dimensional model can be used in which the x coordinate starts in the beginning of the injection end of the capillary and co-directs with its axis.

The following system of partial differential equations describes mass transfer of the three components with diffusion during NECEEM [38]:

$$\frac{\partial A(t,x)}{\partial t} + v_{\mathrm{A}} \frac{\partial A(t,x)}{\partial x} - \mu_{\mathrm{A}} \frac{\partial^2 A(t,x)}{\partial x^2} = \mathrm{k}_{\mathrm{off}} C(t,x) \tag{3.2}$$

$$\frac{\partial B(t,x)}{\partial t} + v_{\mathrm{B}} \frac{\partial B(t,x)}{\partial x} - \mu_{\mathrm{B}} \frac{\partial^2 B(t,x)}{\partial x^2} = \mathrm{k}_{\mathrm{off}} C(t,x) \tag{3.3}$$

$$\frac{\partial C(t,x)}{\partial t} + v_{\mathrm{C}} \frac{\partial C(t,x)}{\partial x} - \mu_{\mathrm{C}} \frac{\partial^2 C(t,x)}{\partial x^2} = -\mathrm{k}_{\mathrm{off}} C(t,x) \tag{3.4}$$

Here, A, B, and C are the concentrations of A, B and C, respectively; v_{A}, v_{B}, and v_{C} are effective velocities of A, B, and C in electrophoresis, respectively; μ_{A}, μ_{B}, and μ_{C} are diffusion coefficients of A, B, and C, respectively, and $\mathrm{k}_{\mathrm{off}}$ is the unimolecular constant of the dissociation of C. We assume that v_{A}, v_{B}, v_{C}, μ_{A}, μ_{B}, and μ_{C} do not change during electrophoresis.

The plug of the equilibrium mixture, which is injected into the capillary, has a length of l. We assume that the three components in the plug undergo little diffusion before the separation starts. Therefore, the initial distribution (at $t = 0$) of the components in the capillary is described by the following:

$$\begin{aligned} &A(x) = A_0, B(x) = B_0, C(x) = C_0; x \in \{0, l\} \\ &A(x) = 0, B(x) = 0, C(x) = 0; x \notin \{0, l\} \end{aligned} \tag{3.5}$$

where A_0, B_0, and C_0 are the equilibrium concentrations of A, B, and C, respectively, in the equilibrium mixture. The solutions of differential equations (3.2), (3.3), (3.4) can be presented as integrals using the Green's function, G(t, x, v, μ, k), (**Appendix 3.6.1**) and the initial conditions (3.5).

3.2.2. Solution for C

The solution for C is simpler than those for A and B; therefore, we find it first. The differential equation for C (see Equation (3.4)) has a zero source function. Therefore, its solution consists of a single term:

$$C(t,x) = C_0 \int_0^l dx' G(t, x-x', v_C, \mu_C, k_{off}) = C_0 \frac{\exp(-tk_{off})}{\sqrt{2\pi}} \int_{(x-tv_C)/\sqrt{2t\mu_C}}^{(l+x-tv_C)/\sqrt{2t\mu_C}} d\gamma \exp(-\gamma^2/2) \quad (3.6)$$

where x' is the integration parameter along the length of the injected plug of the equilibrium mixture and $\gamma = (x' - x + v_C t)/(4\mu_C t)^{1/2}$. The integral at the right hand side of (3.6) can be expressed *via* the tabular function *erf* resulting in the following expression for C:

$$C(t,x) = C_0 \frac{\exp(-tk_{off})}{2} (erf((l-x+tv_C)/\sqrt{4t\mu_C}) - erf((tv_C - x)/\sqrt{4t\mu_C})) \quad (3.7)$$

3.2.3. Solutions for A and B

The differential equations for A and B (see Equations (3.2) and (3.3)) are similar. Therefore, their solutions will be also similar. Therefore, we find the solution for A first and then extend it to B. Equation (3.2) has a non-zero source function; therefore its solution is a sum of two terms:

$$A(t,x) = A_{eq}(t,x) + A_{dis}(t,x) \quad (3.8)$$

$A_{eq}(t, x)$ describes the migration of the electrophoretic zone of the equilibrium fraction of A. The solution for $A_{eq}(t, x)$ is found in the way similar to that for C:

$$A_{eq}(t,x) = A_0 (erf((l-x+tv_A)/\sqrt{4t\mu_A}) - erf((tv_A - x)/\sqrt{4t\mu_A}))/2 \quad (3.9)$$

$A_{dis}(t, x)$ describes the migration of the electrophoretic zone of the A produced from the dissociation of C:

$$A_{dis}(t,x) = k_{off} \int_{-\infty}^{+\infty} dx' \int_{0}^{t} dt' G(t-t', x-x', v_A, \mu_A, 0) C(t', x') \tag{3.10}$$

where t' and x' are integration parameters for t and x, respectively.

If we substitute $C(t', x')$ in equation (3.10) with its expression through the Green's function (see equation (3.6)), we can present A_{dis} in the following form:

$$A_{dis}(t,x) = k_{off} C_0 \int_{0}^{l} dx'' \int_{-\infty}^{+\infty} dx' \int_{0}^{t} dt' G(t-t', x-x', v_A, \mu_A, 0) G(t', x'-x'', v_C, \mu_C, k_{off}) \tag{3.11}$$

where x" is the integration parameter along the length of the injected plug. Using the solution for the integral of the multiplication product of two Gauss functions (**Appendix 3.6.2**), we can integrate equation (3.10) with respect to x' and obtain:

$$A_{dis}(t,x) = k_{off} C_0 \int_{0}^{l} dx'' \int_{0}^{t} dt' \frac{\exp(-t' k_{off})}{\sqrt{4\pi(\mu_C t' + \mu_A (t-t'))}} \exp\left(-\frac{(x'' + (v_C - v_A)t' - x + v_A t)^2}{4(\mu_C t' + \mu_A (t-t'))} \right) \tag{3.12}$$

The last integral can be solved precisely only if $\mu_C = \mu_A$. Otherwise, the approximate solution of this integral can be found using the saddle-point method. For this method to be applicable, diffusion of A and C must be slow in comparison to their translational movement (it is certainly true if A and B are large molecules, such as proteins and nucleic acids): $\mu_A t + (\mu_C - \mu_A)(x - v_A t)/(v_C - v_A) << (x - v_A t)^2$. We assume that the last inequality is satisfied and that $l << x$. With these assumptions, integral (3.12) can be transformed to:

$$A_{\text{dis}}(t,x) \approx \frac{\mathrm{k}_{\text{off}} C_0 \exp((x - v_{\text{A}}t)\mathrm{k}_{\text{off}}/(v_{\text{C}} - v_{\text{A}}))}{(v_{\text{C}} - v_{\text{A}})} \varepsilon_{\text{A}} \int_0^{l/\varepsilon_{\text{A}}} d\psi \int_{(v_{\text{A}}t - x)/\varepsilon_{\text{A}}}^{(v_{\text{C}}t - x)/\varepsilon_{\text{A}}} \frac{d\varphi}{\sqrt{\pi}} \exp(-(\psi + \varphi)^2) \quad (3.13)$$

where $\varepsilon_{\text{A}} = 2\sqrt{(\mu_{\text{C}}(x - v_{\text{A}}t) - \mu_{\text{A}}(x - v_{\text{C}}t))/(v_{\text{C}} - v_{\text{A}})}$ and ψ and φ are the parameters of integration linearly dependent on *x*" and *t*', respectively.

Integral (3.13) can be solved through the *erf* functions (see **Appendix 3.6.3**):

$$A_{\text{dis}}(t,x) \approx \frac{\mathrm{k}_{\text{off}} C_0 \exp((x - v_{\text{A}}t)\mathrm{k}_{\text{off}}/(v_{\text{C}} - v_{\text{A}}))}{2(v_{\text{C}} - v_{\text{A}})} \varepsilon_{\text{A}} I(l/\varepsilon_{\text{A}}, (v_{\text{C}}t - x)/\varepsilon_{\text{A}}, (v_{\text{A}}t - x)/\varepsilon_{\text{A}}) \quad (3.14)$$

The solution for B is similar to that for A. Accordingly, equations (3.8),(3.9), and (3.14) can be modified for B:

$$B(t,x) = B_{\text{eq}}(t,x) + B_{\text{dis}}(t,x) \quad (3.15)$$

$$B_{\text{eq}}(t,x) = B_0(erf((l - x + tv_{\text{B}})/\sqrt{4t\mu_{\text{B}}}) - erf((tv_{\text{B}} - x)/\sqrt{4t\mu_{\text{B}}}))/2 \quad (3.16)$$

$$B_{\text{dis}}(t,x) \approx \frac{\mathrm{k}_{\text{off}} C_0 \exp((x - v_{\text{B}}t)\mathrm{k}_{\text{off}}/(v_{\text{C}} - v_{\text{B}}))}{2(v_{\text{C}} - v_{\text{B}})} \varepsilon_{\text{B}} I(l/\varepsilon_{\text{B}}, (v_{\text{C}}t - x)/\varepsilon_{\text{B}}, (v_{\text{B}}t - x)/\varepsilon_{\text{B}}) \quad (3.17)$$

where $\varepsilon_{\text{B}} = 2\sqrt{(\mu_{\text{C}}(x - v_{\text{B}}t) - \mu_{\text{B}}(x - v_{\text{C}}t))/(v_{\text{C}} - v_{\text{B}})}$.

The concentrations of A, B, and C for given *t* and *x* can be calculated using expressions (3.7), (3.8), (3.13), (3.14), and (3.15)-(3.17) and any spreadsheets-type software with built-in mathematical functions. In this work we used the Excel program.

3.2.4. Simulated Electropherograms

We used equations (3.7), (3.8), (3.13), (3.14), and (3.15)-(3.17), which describe $A(t, x)$, $B(t, x)$, and $C(t, x)$, to build simulated electropherograms. To be comparable with experimental electropherograms, which are typically generated with a detector placed in a

fixed position on the capillary or past the capillary, we assume that x is constant. Thus, the simulated electropherograms contain solutions for concentrations as functions of t for fixed x: $A(t)$, $B(t)$, and $C(t)$. For graphical presentation, these solutions should be multiplied by the velocities of corresponding species, v_A, v_B, and v_C, if the simulated electropherograms are to model the experimental data obtained with sheath-flow-type off-column detection. The areas under the features in velocity-corrected electropherograms correspond to the amounts of separated species.

The solution for $C(t)$ has one term (see Equation (3.7)), while the solutions for $A(t)$ and $B(t)$ consist of two terms: $A_{eq}(t)$ and $A_{dis}(t)$ (see Equations (3.8), (3.9), and (3.14)) and $B_{eq}(t)$ and $B_{dis}(t)$ (see Equations (3.15)-(3.17)), respectively. $A_{eq}(t)$, $B_{eq}(t)$, and $C(t)$ are Gaussian peaks, while $A_{dis}(t)$ and $B_{dis}(t)$ are lines corresponding to the production of A and B due to the dissociation of C (**Figure 3.1a**). We cannot distinguish $A_{eq}(t)$ from $A_{dis}(t)$ and $B_{eq}(t)$ from $B_{dis}(t)$ in experiment. Therefore, to be comparable with experimental electropherograms, simulated ones have to contain $A(t) = A_{eq}(t) + A_{dis}(t)$ and $B(t) = B_q(t) + B_{is}(t)$ instead of $A_{eq}(t)$, $A_{dis}(t)$, $B_{eq}(t)$, and $B_{dis}(t)$ (**Figure 3.1b**).

There are three qualitatively distinct types of simulated NECEEM electropherograms, depending on the value of the dissociation rate constant, k_{off}, with respect to the reciprocal migration time of C, $1/t_C$ (**Figure 3.2**). If $k_{off} << 1/t_C$, the dissociation of C is not significant and three peaks corresponding to equilibrium fractions of A, B, and C are observed in a NECEEM electropherogram (**Figure 3.2a**). This is the simplest case, in which NECEEM is reduced to the equilibrium separation of A, B,

and C. If $k_{off} \sim 1/t_C$, the dissociation of C during separation is significant, but a detectable amount of C reaches the detector.

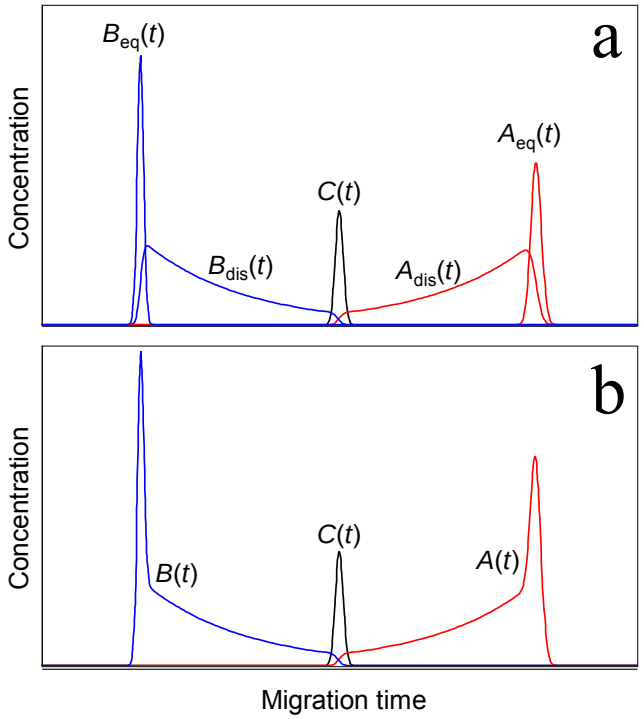

Figure 3.1. Simulated NECEEM electropherograms

Panel **a** illustrates characteristic features produced by: (i) peaks $A_{eq}(t)$ and $B_{eq}(t)$ corresponding to equilibrium fractions of A and B, (ii) exponential decay lines $A_{dis}(t)$ and $B_{dis}(t)$ corresponding to A and B, produced from the dissociation of C, and (iii) peak $C(t)$ corresponding to the fractions of intact C reaching the detection point. Panel **b** shows simulated electrophoretic features generated by experimentally distinguishable species: $A(t)$, $B(t)$, and $C(t)$.

The simulated NECEEM electropherogram still contains three peaks corresponding to equilibrium fractions of A and B and the fraction of intact C, which reached the detector (**Figure 3.2b**). In addition to the three peaks, it contains two lines, corresponding to A and B produced from the dissociation of C.

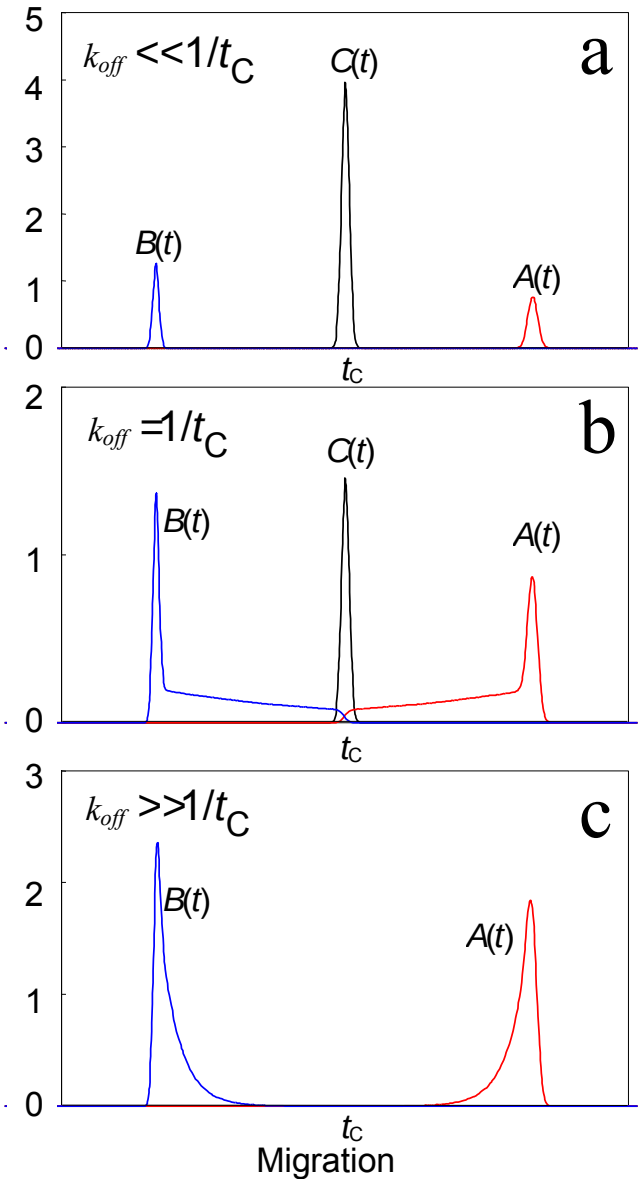

Figure 3.2. Simulated NECEEM Electropherograms for Different Rate Constants

Simulated NECEEM electropherograms obtained for different values of the rate constant, k_{off}, of the dissociation of complex C with respect to the reciprocal migration time of C ($1/t_C$): $k_{off} << 1/t_C$ (panel a), $k_{off} = 1/t_C$ (panel b), and $k_{off} >> 1/t_C$ (panel c).

Finally, if $k_{off} >> 1/t_C$, then C dissociates to undetectable levels and the electropherogram does not contain peak C (**Figure 3.2c**). The extent of the dissociation can be changed by varying t_C via, for example, changing the effective length of the capillary (the distance from the injection end to the detection point) or the velocity of C, which depends on the electric field. Despite the absence of peak C, the electropherogram depicted in **Figure 3.2c** can still be used to obtain binding parameters, k_{off} and K_d (see Chapter 4).

It is worthwhile to mention that the electropherogram shown in **Figure 3.2c** suggests that tailing and fronting, which are often observed in CE, can originate from complex formation between the analyte and components of the sample matrix. If the run buffer is different from the sample buffer, the complex will be decaying during the separation, and complex decay will lead to electropherogram features similar to those in **Figure 3.2c**.

3.2.5. Determination of K_d and k_{off}

Simulated NECEEM electropherograms can help to understand the principles of finding binding parameters from experimental NECEEM electropherograms. By definition, the value of the equilibrium dissociation constant, K_d, can be determined from equilibrium amounts, A_{eq}, B_{eq}, and C_{eq}, of the three components in the equilibrium mixture if they all are detectable:

$$K_d = \frac{A_{eq} B_{eq}}{C_{eq}} \tag{3.18}$$

Alternatively, K_d can be determined from equilibrium amounts of two components if the third one is undetectable. For example, if B cannot be detected, K_d can

be determined based on equilibrium amounts of A (A_{eq}) and C (C_{eq}) and total concentrations of A (A_{tot}) and B (B_{tot}) mixed:

$$K_d = \frac{B_{tot}(1 + A_{eq} / C_{eq}) - A_{tot}}{1 + C_{eq} / A_{eq}} \tag{3.19}$$

By definition, the unimolecular rate constant of the dissociation of C can be determined if C_{eq} and the amount of C remaining intact (C_{intact}) at time t_C are known:

$$k_{off} = \frac{\ln(C_{eq} / C_{int\,act})}{t_C} \tag{3.20}$$

To find K_d and k_{off} using formulas (3.19) and (3.20) we need to determine A_{eq}/C_{eq}, C_{eq}/C_{intact}, and t_C. These three parameters can be determined precisely from a single NECEEM electropherogram if it was of the type presented in **Figure 3.1a**. Indeed, t_C is simply the migration time of C. The areas under $A_{eq}(t)$ and $B_{eq}(t)$ correspond to A_{eq} and B_{eq}, respectively. The areas under $A_{dis}(t)$ and $B_{dis}(t)$ are equal due to the mass balance; therefore, both the area under $C(t) + A_{dis}(t)$ and the area under $C(t) + B_{dis}(t)$ are equal to C_{eq}. However, in the experiment, we cannot distinguish $A_{eq}(t)$ from $A_{dis}(t)$ and $B_{eq}(t)$ from $B_{dis}(t)$. This requires that such a distinction be made from an electropherogram comprised of $A(t) = A_{eq}(t) + A_{dis}(t)$ and $B(t) = B_{eq}(t) + B_{dis}(t)$ (**Figure 3.1b**). The overlap between $A_{eq}(t)$ and $A_{dis}(t)$ as well as $B_{eq}(t)$ and $B_{dis}(t)$ leaves some uncertainty in how to distinguish between them. This emphasizes the need for a more accurate way of finding A_{eq}/C_{eq} and C_{eq}/C_{intact} from NECEEM electropherograms, which would lead to unambiguous determination of K_d and k_{off}. One of the approaches to accurate finding of A_{eq}/C_{eq} is described in the following paragraph.

Here, we demonstrate that K_d and k_{off} can be found by non-linear regression of experimental NECEEM electropherograms using the mathematical model developed. The experimental data modeled were obtained for the interaction between a fluorescently labeled 15-mer DNA oligonucleotide (A) and single-stranded DNA binding protein (B). Due to the fluorescence label on A, both A and C were detectable while B was not. Therefore, experimental NECEEM electropherograms contained fluorescence traces of A and C only. Non-linear regression was based on minimizing the deviation between the experimental trace and a model function $A(t) + C(t)$ using the least square method. The parameters optimized in the regression analysis were: k_{off}, v_A, v_C, μ_A, μ_C, and the A_{eq}/C_{eq} ratio. Thus, k_{off} was found directly from the regression procedure, while K_d was calculated using equation (3.19) with the A_{eq}/C_{eq} value found in the regression. Due to the analytical nature of the model, satisfactory fitting of one electropherogram is rapidly calculated even with the relatively slow Excel solver. Experiments were conducted with three different sets of concentrations of A and B to generate three qualitatively different NECEEM electropherograms. The results of the regression of representative experimental data are shown in **Figure 3.3**. Binding parameters were determined by averaging those for the three sets of different experimental conditions (5 repeats for every set): $k_{off} = (4.5 \pm 1.2) \times 10^{-3} s^{-1}$ and $K_d = (1.9 \pm 0.7) \times 10^{-8}$ $M^{-1}s^{-1}$. These values are lower than those measured earlier, due to adjustments to a standard NECEEM procedure. Namely, we lowered the temperature inside the capillary and kept it constant by using a CE apparatus with liquid-cooled capillary.

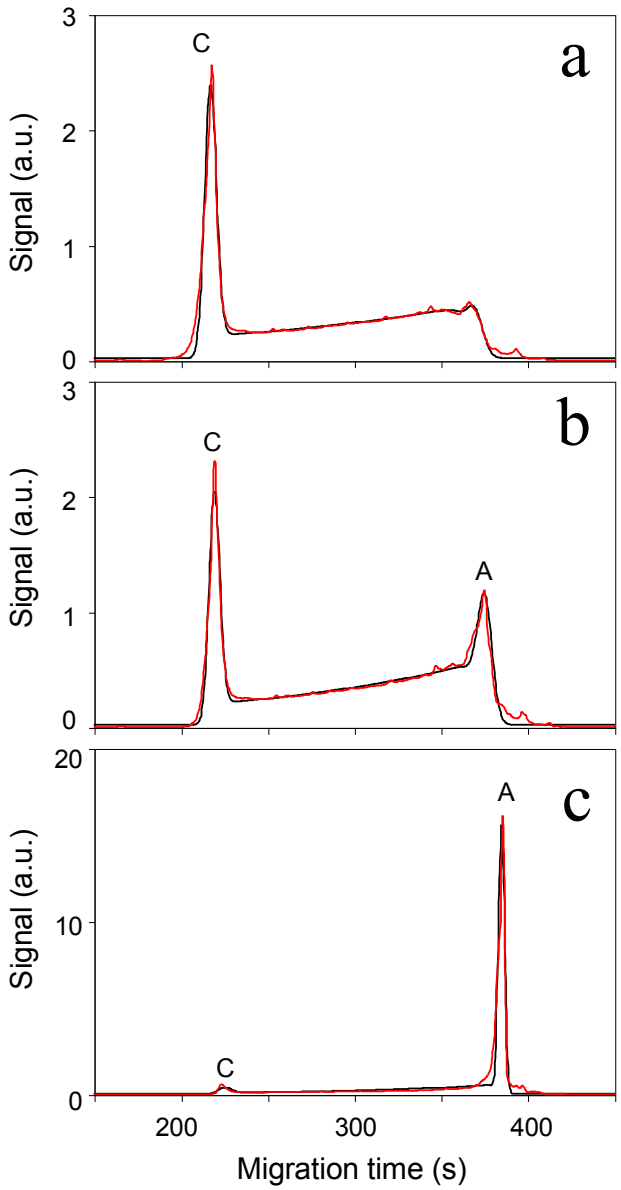

Figure 3.3. Fitting Experimental NECEEM Electropherograms with Simulated Ones

Experimental NECEEM electropherograms (red lines) were obtained for the interaction between a fluorescently labeled DNA 15-mer oligonucleotide (0.1 μM) and a single-stranded DNA-binding protein: 1 μM (panel a), 0.5 μM (panel b), and 0.25 μM (panel c). Simulated NECEEM electropherograms (black lines) were obtained by non-linear regression of the experimental data using the least square method. A denotes the DNA and C denotes the protein-DNA complex.

Also, to demonstrate more pronounced peaks of the complex we used higher concentrations of the protein, at which it is known to form mutlimers, whose affinity to DNA is greater than that of a monomer protein [39].

3.3. CONCLUSION

A mathematical model of NECEEM has been developed, which provides the analytical solution for concentrations of interacting components in the linear approximation with diffusion. The model satisfactorily explains the experimental results and the origin of features (peaks, tailing, and fronting) in electropherograms obtained from samples that include dissociating complexes. The model allows for finding binding parameters, K_d and k_{off}, from a single experimental electropherogram in a fast and accurate way, providing the bases for using KCE as a powerful analytical method in studies of non-covalent molecular complexes.

3.4. EXPERIMENTAL METHODS

3.4.1. Chemicals and Materials

Single-stranded DNA binding protein from *E. coli* and buffer components were obtained from Sigma-Aldrich (Oakville, ON). Fluorescently labeled 15-mer DNA oligonucleotides, fluorescein-5'-GCGGAGCGTGGCAGG, was kindly donated by Dr. Yingfu Li (McMaster University, Hamilton, ON). Fused-silica capillaries were purchased from Polymicro (Phoenix, AZ). All solutions were made using Milli-Q quality deionized water and filtered through a 0.22 μm filter (Millipore, Nepean, ON).

3.4.2. Capillary Electrophoresis

Capillary electrophoresis analyses were performed using a Beckman-Coulter P/ACE MDQ instrument (Missisauga, ON) with on-column fluorescence detection. A 488 nm line of an Ar-ion laser was utilized to excite fluorescence of the fluorescein label on the DNA molecule. Uncoated fused silica capillary of 50 cm × 50 μm I.D. × 375 μm O.D. (effective length of 40 cm) was used. Electrophoresis was carried out with a positive electrode at the injection end biased at +30 kV, resulting in the electric field of 600 V/cm across the 50-cm long capillary. The NECEEM run buffer was 12.5 mM sodium tetraborate at pH 9.4. The samples were injected into the capillary by a pressure pulse of 3 s × 3.5 kPa; the length and the volume of corresponding sample plug were approximately 1.7 mm and 3.3 nL as was calculated using the Poiseuille equation. The capillary was rinsed with the run buffer solution for 2 min prior to each run. At the end of each run, the capillary was rinsed with 100 mM NaOH for 2 min, followed by a rinse with deionized water for 2 min. The temperature of the capillary was maintained at 20°C by liquid-based cooling of the capillary in all NECEEM experiments.

3.4.3. Equilibrium Mixtures

NECEEM experiments were performed with three different equilibrium mixtures of the single-stranded DNA-binding protein and the fluorescently labeled 15-mer DNA oligonucleotide (5 repeats for every mixture). The protein and DNA were mixed in the NECEEM run buffer to have the final concentration of DNA equal to 100 nM and final

concentrations of the protein equal to 0.25 μM, 0.5 μM, and 1 μM. The mixtures were incubated at room temperature for 1 hour to reach the equilibrium prior to the analysis.

3.4.4. Calculations

All calculations were carried out with built-in functions in Excel software. Non-linear regression analysis of experimental NECEEM electropherograms was performed with the Excel Solver.

3.6. APPENDIXES

Appendix 3.6.1. Green's Function

Mass transfer with diffusion is described by the following generalized equation:

$$\frac{\partial G(t,x)}{\partial t} + v\frac{\partial G(t,x)}{\partial x} - \mu\frac{\partial^2 G(t,x)}{\partial x^2} = -kG$$

where v, μ, and k are numeric parameters. If the x-distribution of G at time zero is a delta function, then, by definition, the solution of the above equation is the Green's function:

$$G(t,x,v,\mu,k) = \begin{cases} (\exp(-kt - (x-vt)^2 / 4\mu t) / \sqrt{4\pi\mu t}; t > 0 \\ 0; t < 0. \end{cases}$$

Appendix 3.6.2. Integral of Multiplication Product of Two Gauss Functions

Integral of the product of two Gauss functions with infinite limits has the following solution:

$$\int_{-\infty}^{+\infty} \frac{1}{\pi\sqrt{\lambda\omega}} \exp\left(-\frac{(x-\varepsilon)^2}{\lambda}\right) \times \exp\left(-\frac{(x-\eta)^2}{\omega}\right) dx = \frac{1}{\sqrt{\pi(\lambda+\omega)}} \exp\left(-\frac{(\eta-\varepsilon)^2}{\lambda+\omega}\right)$$

Appendix 3.6.3. Double Integral of Gauss Function in Finite Limits

Double integral of Gauss function in finite limits has the following solution:

$$I(\chi,\psi,\theta) = \frac{2}{\sqrt{\pi}} \int_0^{\chi} d\gamma \int_{\theta}^{\psi} d\varphi \exp(-(\gamma+\varphi)^2) =$$
$$= (\psi+\chi) erf(\psi+\chi) - \psi erf(\psi) - (\theta+\chi) erf(\theta+\chi) + \theta erf(\theta) +$$
$$+ (\exp(-(\psi+\chi)^2) - \exp(-\psi^2) - \exp(-(\theta+\chi)^2) + \exp(-\theta^2)) / \sqrt{\pi}$$

where $erf(x) = \frac{2}{\sqrt{\pi}} \int_0^x \exp(-y^2) dy.$

Equation Chapter 4 Section 4

CHAPTER 4

AFFINITY-MEDIATED NECEEM

4.1. INTRODUCTION

I have demonstrated non-equilibrium capillary electrophoresis of equilibrium mixtures (NECEEM) as the KCE method that allows finding kinetic and equilibrium parameters of protein-DNA interactions. In this chapter I want to introduce an affinity-mediated NECEEM method.

To explain the rationale for affinity-mediated NECEEM, I have to emphasize that NECEEM requires good separation of free DNA from the protein-DNA complex. If the separation is poor, the accuracy of the method with respect to the determination of rate constants and equilibrium constants decreases. Affinity-mediated NECEEM is based on the insight that adding to the run buffer a background affinity agent which can bind free DNA but not the protein-DNA complex can improve the separation by changing the mobility of free DNA while not affecting that of the complex.

In the study showing the proof of principle, I demonstrated affinity-mediated NECEEM of protein-ssDNA pairs by using single stranded binding protein (SSB) from *E. coli* as a background affinity agent in the run buffer. To extend affinity-mediated NECEEM to studies of dsDNA-protein interactions, a suitable dsDNA-binding protein needs to be found to serve as a background affinity agent instead of SSB. Hypothetically, affinity-mediated NECEEM can be also realized with a protein-binding affinity agent,

such as an antibody, instead of a DNA-binding agent, provided that the agent binds the protein but does not bind the protein-DNA complex.

The SELEX method (systematic evolution of ligands by exponential enrichment) developed in 1990 allows the generation of single-stranded DNA or RNA molecules (known as aptamers) for target binding [40, 41]. It has been well demonstrated that aptamers can be created relatively easily for a broad range of targets with high affinity and specificity [42, 43]. The high affinity and specificity exhibited by aptamers towards small and large molecular targets is ascribed to the ability of aptamers to incorporate small molecules into their nucleic acid structures, and to integrate themselves into the structures of large molecules such as proteins [44]. Aptamers are becoming a popular molecular-recognition tool in many analytical methods and devices. For example, aptamers have been successfully used in flow cytometry [45], biosensors [46, 47], capillary electrochromatography [48, 49], and affinity chromatography [50].

Aptamers have uniform charge to mass ratios, and therefore have predictable behavior in electrophoresis. They usually undergo structural transitions when they interact with target molecules. Such structural transitions, accompanied by the change in mass upon binding to the target, leads to changes in electrophoretic properties. This suggests that electrophoresis can be used for highly efficient separation of free aptamers from the aptamer-target complexes. Aptamers can be easily (and inexpensively) labeled with a fluorescent tag, which makes it possible to use laser-induced fluorescence for their sensitive detection in capillary electrophoresis. Moreover, binding of a relatively small aptamer molecule to a large target molecule changes the fluorescence anisotropy of the

aptamer. Fluorescence anisotropy can be a valuable addition to the toolbox for fluorescence detection of aptamer-protein complexes as has been demonstrated in Chapter 2. The separation and detection advantages of aptamers make them a very attractive affinity probe in capillary electrophoresis-based quantitative assays of proteins. Kennedy and co-authors have successfully applied DNA aptamers to quantitative analysis of proteins in capillary electrophoresis [51]. Two proteins, IgE and thrombin, were analyzed using two existing aptamers [52, 53]. In these experiments, the DNA aptamers were fluorescently labeled. The aptamer alone and the aptamer/ protein mixtures were injected into a capillary. The areas of two peaks corresponding to free and protein-bound aptamer were used for the quantification of the proteins. With this approach, the detection limits of 46 pM and 40 nM were demonstrated for IgE and thrombin, respectively. The authors pointed out that even for relatively stable aptamer-protein complexes the accuracy of the method could be affected by partial decay of the complex during the separation. Unstable aptamer-protein complexes can completely decay during the separation; as a result no peak corresponding to the protein-aptamer complex can be observed. Complex decay makes it very difficult to use aptamers with high "off" rates for quantitative analyses of proteins.

Here I demonstrate that the affinity-mediated NECEEM method allows accurate quantitative analysis of proteins even with aptamers, whose complexes with proteins completely decay during the separation. Thrombin (Thr) and the GGTTGGTGTGGTTGG oligonucleotide (**Figure 4.1**) were chosen for this work as a well-studied protein-aptamer pair [53-55].

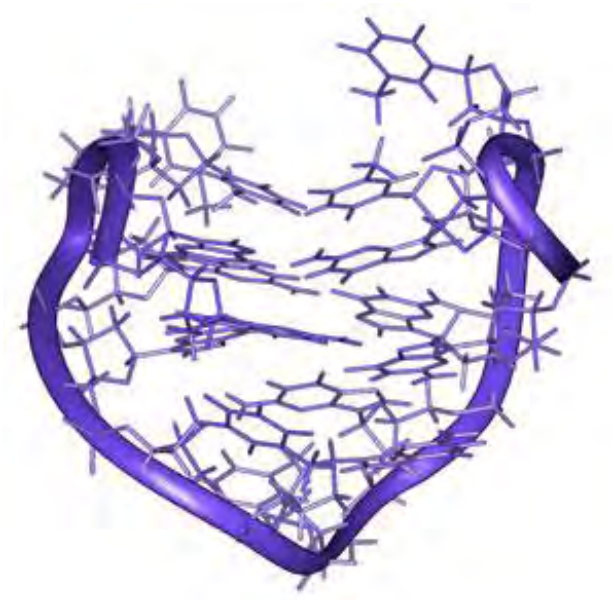

Figure 4.1. Structure of Thrombin Aptamer

The thrombin aptamer (blue) is a single-stranded DNA of 15 nucleotides that was identified by the selection of thrombin-binding molecules from a large combinatorial library of oligonucleotides. This aptamer of thrombin has a unique double G-tetrad structure capable of binding thrombin at nanomolar concentrations.

4.2. RESULTS AND DISCUSSION

4.2.1. Affinity-Mediated NECEEM

For NECEEM of a protein and its aptamers (Apt), conditions have to be found that facilitate the exclusion of the complex formation reaction by the efficient separation of free protein from free aptamer. I aimed at finding universal conditions that could be applied to a large number of protein-aptamer pairs. To achieve efficient separation of free protein and free aptamer independently on the protein physical-chemical properties I included SSB in the separation buffer. SSB binds free ssDNA non-specifically and does not bind the protein-aptamer complex since the latter does not have an exposed ssDNA

sequence. Thus, SSB present in the separation buffer is expected to bind non-specifically free aptamer and preclude the formation of the protein-aptamer complex during NECEEM. NECEEM of Thr and Apt generated electropherograms with the first peak corresponding to free Apt and an exponential curve associated with the monomolecular decay of the Apt•Thr complex (**Figure 4.2**). The second peak, which should correspond to the Apt • Thr complex, was not observed since the complex completely decayed during its migration through the capillary (see the "Determination of k_{off}" section). A small peak corresponding to the complex could be observed when the migration time was considerably reduced. The migration time could be shortened by (i) applying forward pressure [51], (ii) reducing the length of the capillary, or (iii) increasing the electroosmotic flow.

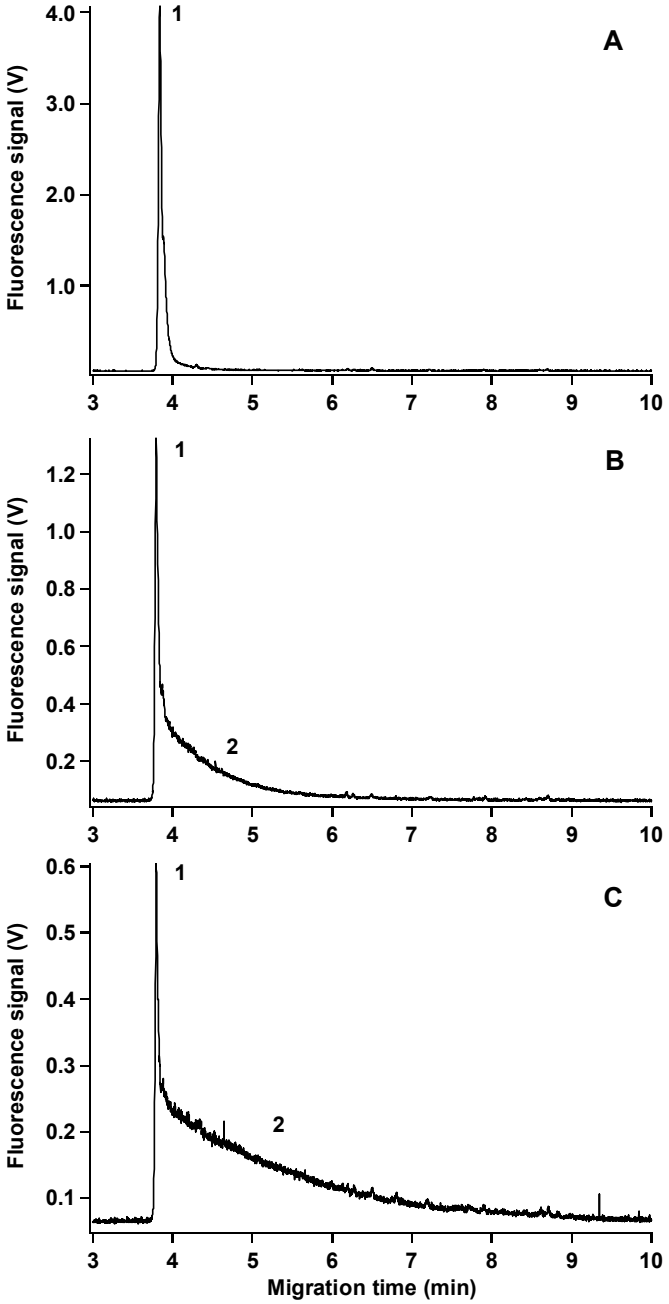

Figure 4.2. Affinity-Mediated NECEEM of Thrombin and Its Aptamer

Electropherograms generated by NECEEM of Thr and Apt (61 nM) at different concentration of Thr: 0 (A), 500 nM (B), and 2 μM (C). Peak 1 corresponds to the equilibrium fraction of free Apt. Exponential part 2 corresponds to the equilibrium fraction of the Apt•Thr complex. The conditions of separation are described in the experimental section.

4.2.2. Determination of K_d

The value of K_d is measured for the conditions of the incubation buffer. The assignment of peak 1 to the equilibrium fraction of free Apt and exponential part 2 to the equilibrium fraction of the Apt•Thr complex allows me to calculate the equilibrium dissociation constant, K_d. The equilibrium fraction of free Apt is proportional to the area of peak 1, A_1:

$$[\text{Apt}]_{eq} = cA_1 \tag{4.1}$$

where c is a constant. The equilibrium fraction of the complex is proportional to the area under exponential part 2, A_2:

$$[\text{Apt} \bullet \text{Thr}]_{eq} = cA_2 \tag{4.2}$$

In a separate experiment I proved that the quantum yields of fluorescein in Apt and Apt•Thr were identical. This justified using the same constant c in Equations (4.1) and (4.2). Using these expressions I can find the ratio, R, of the two equilibrium fractions:

$$R = \frac{[\text{Apt}]_{eq}}{[\text{Apt} \bullet \text{Thr}]_{eq}} = \frac{A_1}{A_2} \tag{4.3}$$

On the other hand the knowledge of R is sufficient for the determination of K_d:

$$K_d = \frac{[\text{Thr}]_0(1+R) - [\text{Apt}]_0}{1+1/R} \tag{4.4}$$

The areas A_1 and A_2, were calculated as illustrated in **Figure 4.3**. The control experiment without Thr (**Figure 4.2A**) showed the right border of area A_1 to distinguish two areas with 5% precision. Equations (4.3) and (4.4) were then used to calculate the

value of K_d equal to 240 ± 16 nM based on six experiments with different concentrations of Thr and Apt mixed.

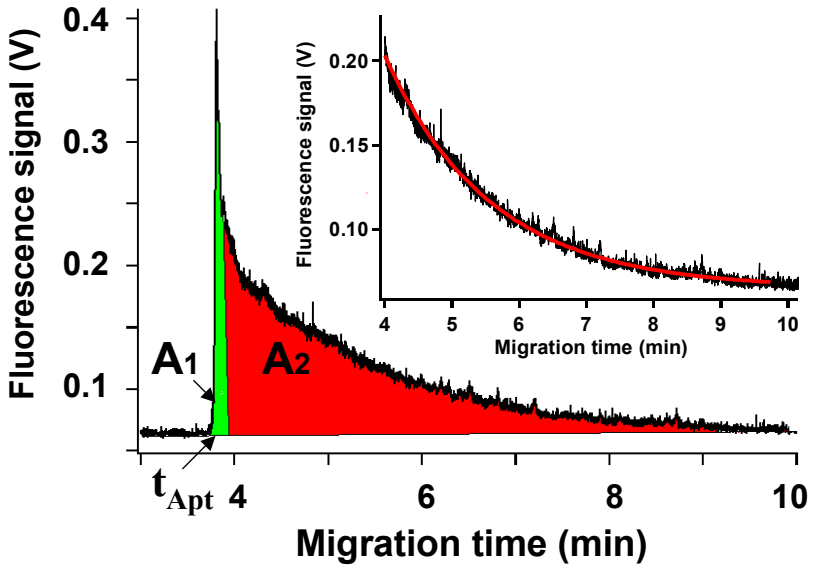

Figure 4.3. Determination of K_d and k_{off} for Thrombin and Its Aptamer

The determination of K_d and k_{off} requires a number of parameters, which can be obtained from a single NECEEM experiment. The main frame illustrates the determination of areas A_1 and A_2 as well as the migration time t_{Apt}. The inset illustrates fitting of experimental data (black line) with the single exponential function (red line).

This value is in agreement with that obtained by Bock *et al.*, 200 nM [53]. The dissociation constant obtained by Kennedy and co-authors was two times higher (450 nM) [51]. The authors suggested that this discrepancy could be due to rapid decay of an aptamer-thrombin complex during separation or perhaps due to the use of different incubation conditions. NECEEM takes into consideration the complex decay and thus eliminates the decay as a possible source of mistake in the K_d determination. Additionally, electropherograms generated by NECEEM have a memory of the dynamic

equilibrium maintained in the incubation buffer. Therefore, NECEEM can be used to measure K_d in different incubation buffers. Moreover, NECEEM allows the use of different incubation and separation buffers and thus permits their separate optimization, which is very important for method development.

4.2.3. Determination of Migration Time of Apt•Thr Complex

The knowledge of the migration time of the Apt•Thr complex was essential for the determination of the monomolecular rate constant, k_{off}, of complex decay (see the next section). The migration time of Apt•Thr was determined in ACE experiments using an approach similar to that described by Le and co-authors [32]. In ACE, Thr was a buffer component so that the Apt•Thr complex was in equilibrium with free Thr and free Apt during the course of electrophoresis. By increasing the concentration of Thr in the buffer I increased the equilibrium fraction of Thr-bound aptamer. The migration time of the peak increased with increasing [Thr] until it reached its saturation level at [Thr]>0.5 μM, indicating that most of the aptamer was in the Thr-bound state at this high concentration of Thr. This "saturated" migration time was the migration time of the Apt-Thr complex. It should be noted that the presence of Thr in the separation buffer considerably increased the electroosmotic flow (EOF). To obtain the correct information on the migration time of the Apt•Thr complex I used fluorescein, which does not bind Thr, as an internal reference to follow the change of the EOF. The migration time of the Thr-Apt complex (corrected for the EOF) was estimated to be 9.4 ± 0.2 min. No peak corresponding to the Thr-Apt complex was observed in NECEEM at 9.4 min (see **Figure**

4.2) due to complete decay of the complex during this time as will be demonstrated in the next section.

4.2.4. Determination of k_{off}

The value of k_{off} is measured in the run buffer, which may be different from the incubation buffer in which the value of K_d is measured. The monomolecular rate constant of complex decay, k_{off}, can be determined from the exponential part 2 of the electropherogram by fitting the experimental data in the time window t_{Apt} to $t_{Apt•Thr}$ (see the inset to **Figure 4.2**) with a single exponential function:

$$I_t = I_B + I_{t_{Apt}} \exp\left\{-k_{off} \frac{t_{Apt•Thr}}{t_{Apt•Thr} - t_{Apt}} (t - t_{Apt})\right\} \quad (4.5)$$

where I_t and $I_{t_{Apt}}$ are the fluorescence intensities at times t and t_{Apt}, respectively; I_B is the intensity of the fluorescence background and t_{Apt} and $t_{Apt•Thr}$ are migration times of Apt and Apt•Thr, respectively. The $t_{Apt•Thr}/(t_{Apt•Thr} - t_{Apt})$ coefficient reflects the apparent changing of the time window in which the complex decay is monitored: t_{Apt} to $t_{Thr•Apt}$ instead of 0 to $t_{Thr•Apt}$.

Using the data from **Figure 4.3** along with the value for $t_{Apt•Thr}$ found in the previous section, the value of k_{off} for the decay of the Apt•Thr complex in the separation buffer was determined to be $(8.8 \pm 1.0) \times 10^{-3}$ s^{-1}. It should be noted that this rate constant is characteristic of the separation buffer and not the incubation buffer. This high monomolecular constant results in (99.3 ± 0.3) % of the equilibrium fraction of Apt•Thr

decayed during $t_{Apt\bullet Thr}$ = 9.4 min. This is the reason why the peak corresponding to the Apt•Thr complex was not observed in NECEEM (**Figure 4.2**).

4.2.5. Determination of Unknown Protein Concentration by NECEEM

When K_d of the protein-aptamer complex was determined, the unknown concentration of the protein could be found analytically as:

$$[Thr]_0 = \frac{K_d}{R} + \frac{[Apt]_0}{1+R} \tag{4.6}$$

Knowledge of K_d is equivalent to building the calibration curve in traditional affinity approaches. As in traditional affinity analyses, the dynamic range of the method is controlled by the concentration of the affinity probe, Apt. The accuracy and precision of the method depend on the accuracy and precision in the determination of K_d, A_1 and A_2. The value of K_d is sensitive to the composition and pH of the incubation buffer in which the equilibrium mixture is prepared. Therefore, it is important that K_d be determined de novo whenever a new incubation buffer is used. In practical applications, the method development for NECEEM-based affinity analysis of a protein should include three steps: (i) the optimization of the incubation and separation buffers, (ii) the determination of K_d in the optimal incubation buffer, and (iii) the determination of $[Apt]_0$ appropriate for required dynamic ranges of protein concentrations.

The concentration and mass limits of detection for Thr quantitation in the NECEEM analyses were found to be 60 nM and 4×10^6 molecules respectively. The dynamic range of the method was two orders of magnitude of $[Thr]_0$ at the fixed concentration of Apt (61nM).

4.2.6. Using ssDNA Binding Protein for Hybridization Analysis

A large number of proteins involved in DNA replication, DNA damage control, DNA repair, and gene expression are capable of binding DNA and RNA with different affinity and sequence specificity [1-3]. This ability of DNA- and RNA-binding proteins has a yet-to-be realized potential in analytical sciences. I suggest that they can be used as highly efficient and versatile tools in analyses of DNA, RNA. Here, I utilized a single stranded DNA binding protein (SSB) to facilitate affinity analyses of DNA, RNA in gel-free electrophoresis.

This work deals with affinity assays using specific affinity probes: hybridization probes for analyses of DNA and RNA [56-58]. These types of probes are single stranded DNA (ssDNA). In such analyses in general, the probe (P) binds to a target molecule (T) and the amounts of the probe-target complex (P•T) and unbound P are determined. Distinguishing between P and P•T requires a physical-chemical property (e.g. optical spectrum, polarization, electrophoretic mobility, etc.) that differs between P and P•T. Finding such a property and optimizing its use is one of the major challenges in designing affinity analyses.

This study was inspired by the insight that any DNA-binding protein that binds differently to P and P•T can induce the required change in their physical-chemical properties. P is a ssDNA; thus, I decided to examine SSB (source *E. coli*) that binds ssDNA and ssRNA of more than 8 bases in length but does not bind double stranded DNA (dsDNA), dsRNA, or double stranded DNA-RNA hybrids [34, 59]. The affinity of ssDNA to SSB is about 10 times higher than that of ssRNA [60]. The dissociation

constant of the SSB-ssDNA complex is equal to 0.3 μM under conditions used in this work [32]. The hypothesis was that SSB could induce and control the difference in electrophoretic mobilities of P and P•T in gel-free electrophoresis (electrophoretic mobility is linearly dependent on the "charge to size" ratio of the molecule). I examined this hypothesis for two types of target molecules: DNA and RNA. CE was used to monitor apparent electrophoretic mobilities of P and P•T. SSB was added to the CE run buffer to maintain equilibrium interaction of SSB with P and P•T. The use of mediators capable of shifting analyte mobility in CE is well documented [61-63]. This work demonstrates for the first time that a mediator, such as a DNA-binding protein, can facilitate highly efficient separation of P and P•T in affinity analyses of T.

All hybridization experiments employed the same probe (P), a fluorescently labeled 15-base-long ssDNA. Two types of ssDNA and ssRNA targets were studied: (i) complementary targets (T) which had the same length as P, and (ii) elongated targets (T') which were longer than P and included the sequence complementary to P at their 5' end (see the experimental section for sequences of P, T, and T'). P and the hybridization complexes, P•T and P•T', are schematically depicted in **Figure 4.4A**. Every nucleotide base in DNA or RNA bears a single negative charge. Therefore, the "charge to size" ratio of both DNA and RNA is highly negative and does not depend on their lengths or hybridization. As a result, single stranded P, double stranded P•T, and P•T', which has a single-stranded overhang, have similar highly negative electrophoretic mobilities in gel-free electrophoresis. An SSB molecule is comprised of 178 amino acids and bears only

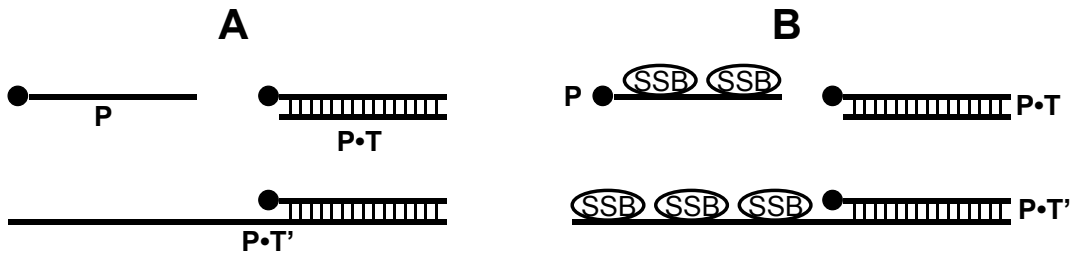

Figure 4.4. Structure of Hybridization Probe and Complex with Target

Panel A schematically depicts the hybridization probe (P), the complex of the probe with the complementary target (P•T), and the complex of the probe with the elongated target (P•T'). Panel B schematically illustrates binding of SSB to the single-stranded P and single-stranded overhang of P•T' and the lack of such binding to double-stranded P•T.

a small negative charge of –4 to –8 for pH ranging from 9.0 to 10.0. Thus, the electrophoretic mobility of SSB is much less negative than those of P, P•T, and P•T'. SSB binds to single stranded P and the single-stranded overhang of P•T' but does not bind to double stranded P•T (**Figure 4.4B**). Upon binding to P and P•T', SSB should make their electrophoretic mobility less negative while the mobility of P•T should not be affected as it does not bind SSB. P•T' contains a double-stranded region that cannot bind SSB. Therefore, P•T' binds fewer SSB molecules per base of DNA or RNA than P. As a result P•T' should have a more negative electrophoretic mobility than P. Moreover, due to lower affinity of SSB to RNA with respect to that of the affinity of SSB to DNA, P•T' with an RNA target will bind fewer SSB molecules than P•T' with a DNA target. Thus, P•T' with RNA as a target should have more negative electrophoretic mobility than P•T' with DNA as a target. The following experiments completely confirmed all these predictions.

First, I examined how SSB influences electrophoretic mobilities of P and P•T. One hundred picoliters of the mixture of P (40 nM) and P•T (60 nM) was injected into the capillary and subjected to electrophoresis in a gel-free run buffer supplemented with different concentrations of SSB. In the absence of SSB in the run buffer, P could not be separated from P•T confirming that P and P•T had similar mobilities in the gel-free electrophoresis (**Figure 4.5, lower trace**). As expected, the presence of SSB in the run buffer induced the mobility shift of P. When the concentration of SSB increased, the electrophoretic mobility of P increased while that of P•T remained the same (**Figure 4.5, middle and top traces**). The optimum difference in electrophoretic mobilities of P and P•T was achieved when the concentration of SSB was in the range of the dissociation constant of the complex between P and SSB, $K_d \approx 0.3$ μM [60]. The results were identical for RNA and DNA as a target. Thus, I demonstrated that SSB induces and effectively controls the difference in electrophoretic mobilities of P and P•T for DNA and RNA targets.

Second, I examined whether SSB can facilitate the separation of P•T' from P and P•T. One hundred picoliters of the mixture of P (40 nM) and P•T (40 nM) and P•T' (10 nM) was injected into the capillary and subjected to electrophoresis in a gel-free run buffer supplemented with 200 nM SSB. P, P•T and P•T' were baseline separated for both DNA and RNA as a target (**Figure 4.6**). As I predicted P•T' had more negative electrophoretic mobility with RNA as a target (**Figure 4.6, insert**) than with DNA as a target (**Figure 4.6, main frame**). Thus, it was demonstrated that SSB induces and

effectively controls the difference in electrophoretic mobilities of P, P•T, and P•T' for DNA and RNA targets.

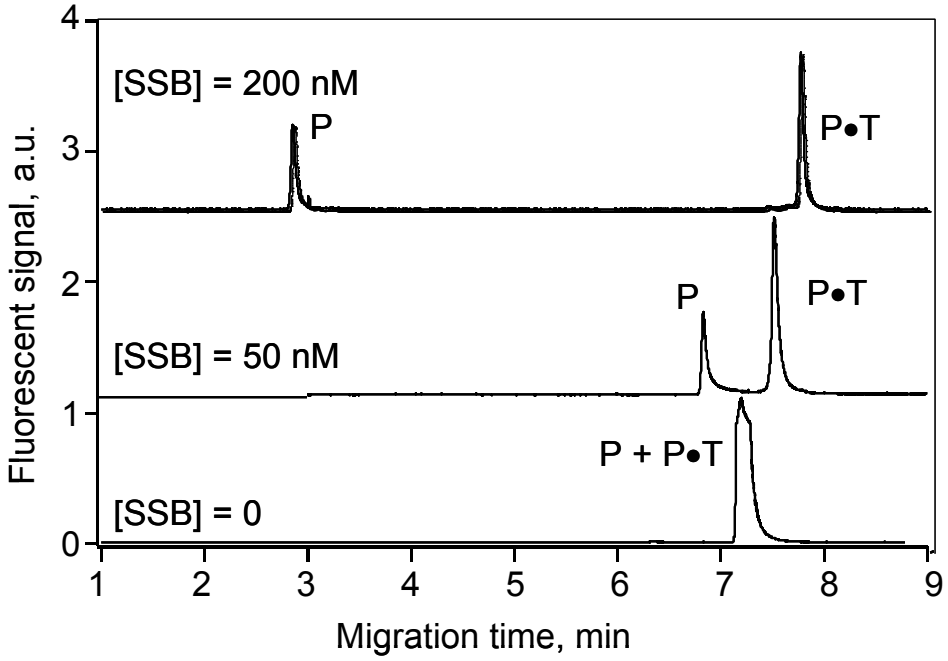

Figure 4.5. SSB-Mediated DNA Hybridization Analysis in Gel-Free CE

P is a fluorescently labeled ssDNA probe. P•T is dsDNA hybrid of P with a complementary target DNA. The amounts of P and P•T were 4×10^{-18} mol and 6×10^{-18} mol, respectively. The run buffer was 25 mM tetraborate at pH 9.4 supplemented with different concentrations of SSB (shown in the graph).

SSB provides a unique means of gel-free CE analysis of short and long DNA and RNA targets. Advanced CE instrumentation used in this work allows the quantitation of as few as 100 molecules [64], which is comparable with the sensitivity of quantitative PCR [65]. In addition, the accuracy of CE greatly exceeds that of PCR. Thus, SSB-mediated CE analyses will facilitate highly sensitive and accurate quantitation of genomic DNA and messenger RNA without time-consuming and error-prone PCR and

RT-PCR. SSB is a representative of a very large family of DNA- and RNA-binding proteins. Among them, there are proteins that bind DNA and RNA sequence non-specifically. Such proteins will facilitate universal hybridization analyses similar to those demonstrated here with SSB. Moreover, sequence-specific DNA- and RNA-binding proteins can be used to add sequence selectivity to the analyses when required. The diversity of properties of DNA- and RNA-binding proteins will allow researchers to design a comprehensive tool set for quantitative analyses of DNA and RNA.

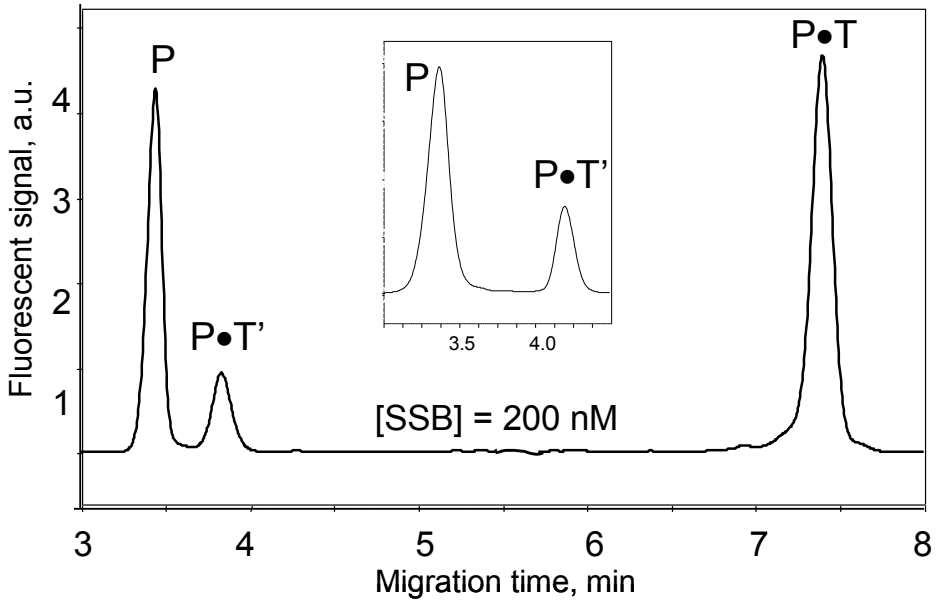

Figure 4.6. SSB-Mediated Hybridization Analysis.

SSB-mediated hybridization analysis of two target oligonucleotides: T and T'. P and T are similar to those in **Figure 4.4**. T' is an elongated target with 22 additional bases at one end of the target. The amounts of P, P•T, and P•T' were 4×10^{-18} mol, 4×10^{-18} mol and 1×10^{-18} mol, respectively. The run buffer was 25 mM tetraborate with 200 nM SSB at pH 9.4. The main frame and the insert show the results for DNA and RNA targets, respectively.

4.3. CONCLUSION

Affinity-mediated NECEEM method will be applicable to a wide variety of protein-aptamer pairs that cannot be analyzed otherwise due to the instability of the protein-aptamer complexes. The use of SSB protein as a separation buffer component, first, will enhance the removal of free aptamer from the electrophoretic zone of free protein and thus will minimize the optimization efforts for the separation buffer, second, will be utilized to design highly efficient electrophoretic affinity analyses of DNA, RNA. Such analyses will allow for the accurate quantitation of genomic DNA on ultra-small samples without error-prone PCR amplification. They will also facilitate extremely sensitive monitoring of gene expression at both mRNA and protein levels. SSB is a representative of a very large family of DNA- and RNA-binding proteins. I foresee that many proteins of this family will find their applications in analytical sciences.

4.4. EXPERIMENTAL METHODS

4.4.1. Chemicals and Materials

Single-stranded DNA binding protein from *E. coli* (SSB), human thrombin (Thr) and buffer components were from Sigma-Aldrich (Oakville, ON). Fused-silica capillaries were purchased from Polymicro (Phoenix, AZ). All solutions were made using the Milli-Q quality deionized water and filtered through a 0.22 μm filter (Millipore, Nepean, ON).

Normal and modified DNA, RNA oligonucleotides were all prepared by automated DNA/RNA synthesis using standard cyanoethylphosphoramidite chemistry (Central Facility, McMaster University). The fluorescein in 5'-Fluorescein-

GCGGAGCGTGGCAGG was introduced during DNA synthesis using 5'-fluorescein phosphoramidite (Glen Research, Sterling, Virginia) and purified by reverse phase HPLC. HPLC separation was performed on a Beckman-Coulter HPLC System Gold with a 168 Diode Array detector. The HPLC column used was an Agilent Zorbax ODS C18 Column, with dimensions of 4.5 mm × 250 mm and a 5μm particle diameter. A two-buffer system was used for purification of all DNA species with buffer A being 0.1 M triethylammonium acetate (TEAA, pH 6.5) and buffer B being 100% acetonitrile. The best separation results were achieved by a non-linear elution gradient (10% B for 10 min, 10%B to 40%B over 65 min) at a flow rate of 1 mL/min. The main peak was found to have very strong absorption at both 260 nm and 491 nm due to DNA and fluorescein, respectively.

4.4.2. Capillary Electrophoresis

NECEEM separation of protein-DNA complexes was performed using a laboratory-built CE instrument with a fluorescence detector described in detail elsewhere [35]. Uncoated fused silica capillaries of 33 cm × 20 μm I.D. × 150 μm O.D. were used in all experiments; the distance from the capillary inlet to the detector was 33 cm. The electrophoresis was run in a positive-polarity mode (anode at the injection end) using a Spellman CZE 1000 power supply (Plainview, NY, USA) as a source of high voltage. A 488 nm line of an Ar-ion laser (Melles Griot, Ottawa, ON) was utilized to excite fluorescence of the fluorescent tag. Fluorescence was filtered from stray and scattered laser light with a band pass filter centered at 520 nm (Omega Optical,

Brattleboro, VT). An R1477 photo multiplier tube (Hamamatsu, Middlesex, NJ) was used as a fluorescence light detector.

The separation buffer for NECEEM was 25 mM sodium tetraborate at pH 9.4 supplemented with 50 nM or 200 nM SSB. The separation buffers for affinity capillary electrophoresis (ACE) were 25 mM Tetraborate at pH 9.4 supplemented with Thr in the range of 0 – 1 μM. The samples were injected onto the capillary by a pressure pulse of 1 s × 9.1 kPa; the length and the volume of the corresponding sample plug were 0.36 mm and 110 pL respectively. The electrophoresis was carried out with an electric field of 400 V/cm at ambient temperature. The capillary was rinsed with the separation buffer solution for 2 min before each run. At the end of each run, the capillary was rinsed with 100 mM NaOH for 2 min, followed by a rinse with deionized water for 2 min.

4.4.3. Aptamer and Probe Design

Figure 4.7 illustrates the approach used for fluorescent tagging of the aptamer. The GGTTGGTGTGGTTGG aptamer (bold) was not directly labeled with fluorescein; instead it had an additional 16-mer oligonucleotide sequence element (italic) that was bound to the complementary 15-mer sequence labeled with fluorescein (fDNA). This arrangement allows the use of the same fDNA for labeling of different aptamers in future experiments provided that all the aptamers to be used have the same fDNA-binding sequence. It should be noted that this structure is not equivalent to an aptamer with an additional 16-mer sequence directly labeled with fluorescein at the 3' end. In my structure the additional 16-mer was bound to the complementary 15-mer and formed a double-

stranded DNA sequence that could not interact with SSB, which was a component of the separation buffer. For simplicity, the whole complex depicted in **Figure 4.7** is called the aptamer (Apt).

A fluorescein-labeled 15-mer oligonucleotide, 5'-GCGGAGCGTGGCAGG (fDNA), was utilized as a hybridization probe for analyses of DNA and RNA targets. Two types of DNA and RNA targets were examined. The first type of targets included 15-mer DNA and RNA oligonucleotides with sequences complementary to that of the hybridization probe. The second type of targets included 37-mer DNA and RNA oligonucleotides, which included the 15-mer sequence complementary to the hybridization probe at their 5' end. The remaining 22-mer region had the following sequence: 5'-TCACTGTGGTTGGTGTGGTTGG for DNA and 5'-UCACUGUGGUUGGUGUGGUUGG for RNA.

3'-**GGTTGGTGTGGTTGG**T*CGCCTCGCACCGTCC-5′* (modified aptamer)
Fluorescein-5'-*GCGGAGCGTGGCAGG-3′* (fDNA)

Figure 4.7. Structure of Extended Aptamer with Probe

The structure of the aptamer for human thrombin (bold) with an additional 16-nucleotide sequence and a fluorescein labeled probe (fDNA) that is complementary to the additional 16-mer sequence. Complementary strands are given in italic.

4.4.4. Equilibrium Mixtures

The hybridization probe was annealed with its targets in a thermocycler at 95 °C for 2 min in the incubation buffer (see below). After annealing the complexes were

cooled down to room temperature. To prepare the equilibrium mixtures of Thr, Apt and the Apt•Thr complex, the stock solutions of Thr (8 μM) and Apt (122 nM) in the incubation buffer were diluted with the same buffer and mixed to obtain desired concentration of Thr and Apt. The mixtures were then allowed to equilibrate at room temperature. The incubation buffer was 20 mM Tris-HCl at pH 8.3 supplemented with 5 mM KCl and 1 mM $MgCl_2$.

CHAPTER 5

TEMPERATURE-CONTROLLED NECEEM

5.1. INTRODUCTION

Two kinetic capillary electrophoresis methods have been introduced for quantitative studies of protein-DNA interactions: nonequilibrium capillary electrophoresis of equilibrium mixtures (NECEEM) [36, 37, 66], and affinity-mediated NECEEM [67-69]. In NECEEM, the protein and DNA are mixed and allowed to reach the dynamic equilibrium:

$$\text{Protein} + \text{DNA} \underset{k_{off}}{\overset{k_{on}}{\rightleftharpoons}} \text{Protein•DNA}$$

The equilibrium mixture contains three components: free protein, free DNA, and a protein-DNA complex. A short plug of the equilibrium mixture is injected into the capillary and the three components are separated under non-equilibrium conditions, in a run buffer that does not contain the protein or DNA. The equilibrium fractions of free protein and free DNA migrate as unchanging electrophoretic zones, while the complex does not. As the result of electrophoretic separation of the three components, the complex is no longer at equilibrium with free protein and free DNA. When out of equilibrium, the complex dissociates and its concentration decreases exponentially. The protein and the ligand dissociated from the complex broad zones with exponential concentration profiles. As a general concept NECEEM can be used in a variety of applications. The proven applications of NECEEM include: (i) determination of the rate constant, k_{off}, of complex

dissociation and the equilibrium constant, K_b, of complex formation [36, 37, 66, 70, 71], (ii) quantitative analyses of proteins using aptamers as affinity probes [68]. NECEEM requires that the complex be well separated from at least one of free components, free protein or free DNA. Finding optimal buffer conditions for acceptable separation quality may be difficult for some protein-DNA pairs. Affinity-mediated NECEEM was suggested as a generic way of achieving good separation of the protein-DNA complex from free DNA [67]. In affinity-mediated NECEEM, the run buffer is supplemented with a background affinity agent, which can bind free DNA but cannot bind the protein-DNA complex. Binding to the background affinity agent changes the mobility of free DNA, which, in turn, mediates NECEEM. Sequence-non-specific DNA-binding proteins were suggested as suitable background affinity agents for changing the mobility of free DNA [67]. I believe that affinity-mediated NECEEM can be also realized with a protein-binding affinity agent, such as an antibody, provided that it binds the free protein but does not bind the protein-DNA complex.

In this chapter, I introduce temperature-controlled NECEEM, and demonstrate its application to study the thermochemistry of protein-DNA interactions. Knowing how temperature influences kinetic and equilibrium binding parameters of non-covalent protein-DNA interactions is important for understanding fundamental biological processes, such as gene expression and DNA replication [72-76]. It is also essential for developing analytical applications of DNA aptamers and DNA-binding proteins in affinity and hybridization analyses and in optimizing the polymerase chain reaction (PCR) [67, 77-79]. Conventional methods for thermochemical studies of protein-DNA

interactions have limitations. Differential scanning calorimetry (DSC) and isothermal titration calorimetry (ITC) are not applicable to finding kinetic parameters [80-82]. Surface plasmon resonance (SPR) can serve to determine equilibrium and kinetic parameters but it is a heterogeneous method, which requires the immobilization of either DNA or protein on the surface of a sensor [83, 84]. Being a homogeneous kinetic method, temperature-controlled NECEEM uniquely allows finding temperature dependencies of equilibrium and kinetic parameters of complex formations without the immobilization of reagents on the surface. Moreover, it requires much lower quantities of the protein than DSC, ITC, and SPR.

5.2. RESULTS AND DISCUSSION

5.2.1. Temperature-Controlled NECEEM

Initially, I explain how temperature should be controlled in NECEEM for measuring temperature dependencies of protein-DNA binding parameters. The nature of the NECEEM method leads to K_b being measured under the conditions of the equilibrium mixture and k_{off} being measured under the conditions of the separation media. Thus, to determine $K_b(T)$, the temperature of the equilibrium mixture should be controlled, while to determine $k_{off}(T)$, the temperature of the separation media should be controlled. If the conditions (the buffer and the temperature) of the equilibrium mixture and separation media are identical, $k_{on}(T)$ can be calculated as $K_b(T) \times k_{off}(T)$. Therefore, it is beneficial to have the two temperatures identical.

To realize the described concept of temperature-controlled NECEEM in this work, I used a CE instrument with separate temperature controls of the sample vial (which contains the equilibrium mixture) and the separation capillary (which contains the separation media); the two temperatures were set to be identical so that the k_{on} value could be calculated. Moreover, the incubation buffer for the equilibrium mixture and the electrophoresis run buffer were also identical: 25 mM sodium tetraborate at pH 9.3. DNA was labeled with fluorescein to facilitate fluorescence detection of free DNA and protein-DNA complexes. NECEEM was driven by an electric field at which thermo-stabilization was efficient. The values of K_b and k_{off} were determined from NECEEM electropherograms as depicted in **Figure 5.1** [36, 37, 66, 68].

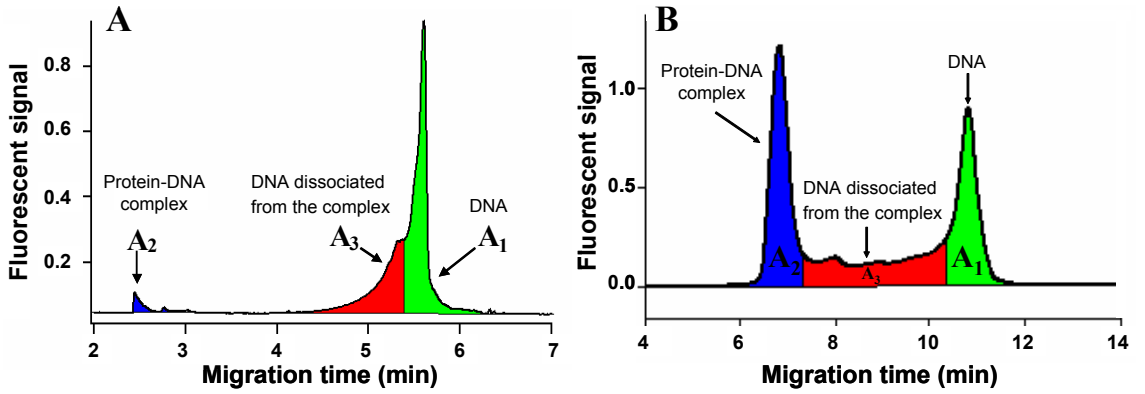

Figure 5.1. NECEEM for Two Protein-DNA Systems

NECEEM electropherograms allow to measure equilibrium and kinetic binding parameters in single run for two protein-DNA complexes: (A) *E. coli* ssDNA-binding protein (250 nM) with a 20-base long ssDNA (200 nM), and (B) *Taq* DNA polymerase (70 nM) with its DNA aptamer (75 nM). The incubation buffer and the running buffer were 25 mM tetraborate at pH 9.3.

5.2.2. *Taq* DNA Polymerase/Aptamer System

I first applied temperature-controlled NECEEM to study the *Taq* DNA polymerase/aptamer system. This model was chosen for the proof-of-principle work because some aspects of its temperature-dependent behavior are known [78, 79]. The aptamer for *Taq* DNA polymerase was selected for a specific temperature behavior to promote hot-start PCR. Accordingly, the aptamer inhibits the *Taq* DNA polymerase activity at low temperatures but its inhibition efficiency decreases rapidly at temperatures exceeding 35 °C [79]. Temperature dependencies of K_b, k_{off}, and k_{on} for this protein-DNA pair are shown in the left three panels of **Figure 5.2.** The $K_b(T)$ data indicate that the equilibrium stability of the complex does not change significantly between 15 and 36 °C but decreases rapidly with temperatures exceeding the threshold level of 36 °C. This sharp suppression of complex stability at $T > 36°C$ is in perfect agreement with the data on temperature-dependent inhibition of Taq DNA polymerase [78]. The phase-transition-like behavior of $K_b(T)$ suggests temperature-dependent conformational changes in the structure of either the protein or the aptamer or both of them. Taq DNA polymerase is extremely temperature-stable, while the aptamer's hairpin structure is, in contrast, known to be temperature-sensitive [79]. Hence, the abrupt temperature-dependent transition in the stability of the protein-aptamer complex is most likely due to conformational changes in the aptamer secondary structure. Temperature dependencies of k_{on} and k_{off} provide an insight into how the conformational changes affect two opposite processes: binding and dissociation. The rapid increase of k_{off} and abrupt decrease of k_{on} at $T > 36$ °C indicate

that both complex dissociation and association are affected by conformational changes occurring at high temperatures. The magnitude of change in k_{on} is, however, greater than that in k_{off} implying that the conformational transition affects binding to a greater extent than dissociation.

5.2.3. SSB/ssDNA System

After the method was evaluated with the *Taq* DNA polymerase/aptamer system, I applied it to study the interaction between SSB and ssDNA, for which temperature data for binding parameters was not available. Temperature dependencies of K_b, k_{off}, and k_{on} for this system are shown in the right three panels of **Figure 5.2**. The $K_b(T)$ data indicate that the equilibrium stability decreases rapidly with temperature in the range of 10-25 °C, but increases gradually with temperature rising from 25 to 50 °C. The phase-transition point in $K_b(T)$ suggests that this system also experiences temperature-dependent conformational changes in the structure of either the protein or DNA or both of them. ssDNA used in this work (see the Experimental section for the chapter) does not form stable hybrids to a considerable extent, thus excluding DNA from a list of potential culprits. As for the protein, it is known to be thermostable and to form homodimers and homotetramers in a temperature-dependent fashion [39, 85]. Therefore, I associate the observed phase-transition-like behavior in $K_b(T)$ for the SSB/ssDNA system with temperature-dependent multimerization of the protein. Similar to the Taq DNA polymerase/aptamer system, temperature dependencies of k_{on} and k_{off} for the SSB/ssDNA system can be used to understand how conformational changes affect binding and

dissociation of the complex. The value of k_{off} grows with T exponentially within the whole studied range of temperatures, indicating that the conformational changes do not affect complex dissociation. The value of k_{on} behaves differently: it does not change in the range of 10-25 °C, but grows for temperatures exceeding the threshold of 25 °C. From this analysis I can conclude that the temperature-dependent conformational changes in SSB mainly influence the ability of the protein to form a complex with ssDNA rather than the ability of the complex to dissociate.

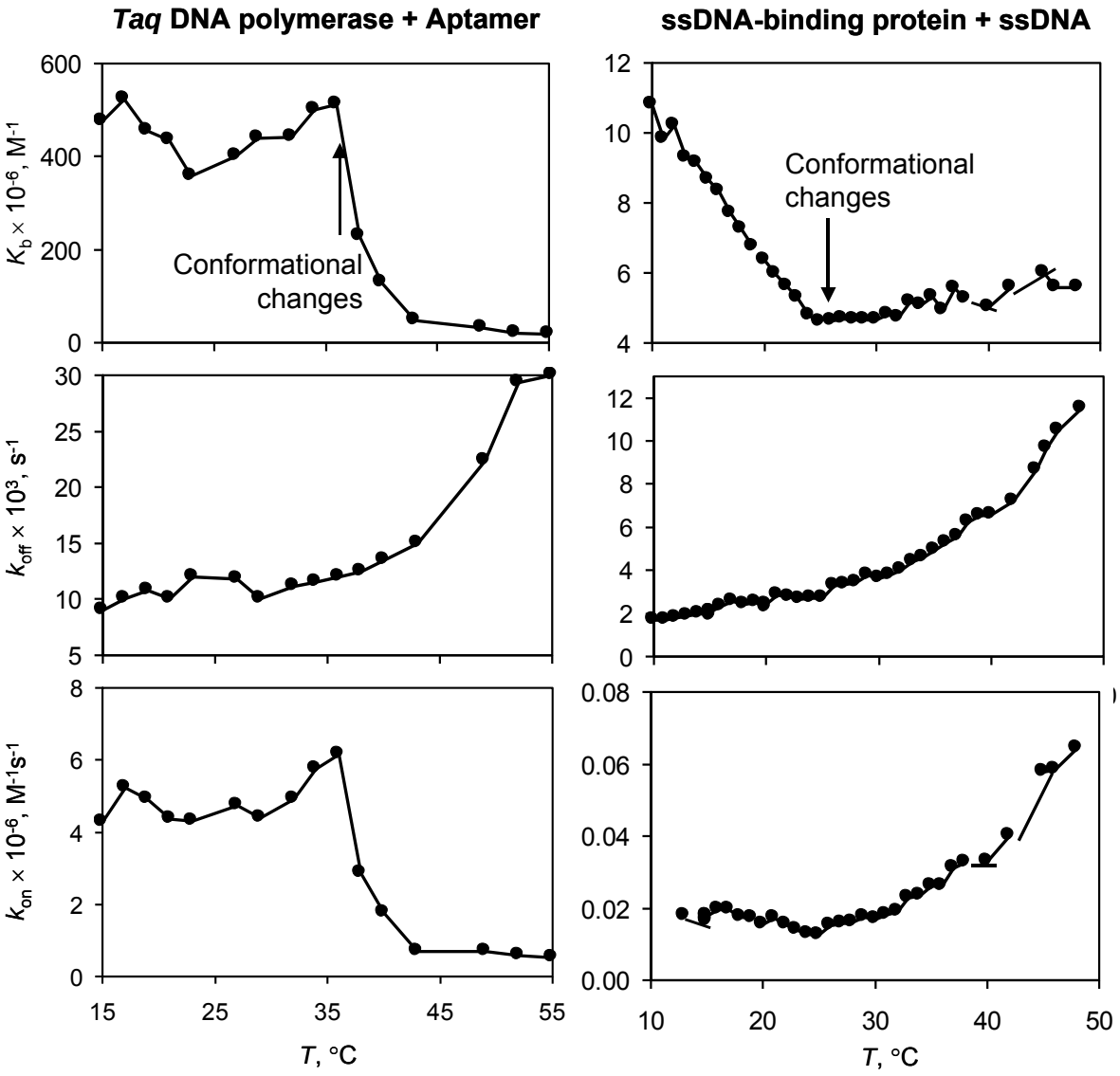

Figure 5.2. Temperature Dependences for Equilibrium and Kinetic Binding parameters

NECEEM-measured temperature dependencies of equilibrium and kinetic binding parameters for two protein-DNA complexes: (i) *Taq* DNA polymerase (70 nM) with its DNA aptamer (75 nM) and (ii) *E. coli* ssDNA-binding protein (250 nM) with a 20-base long ssDNA (200 nM). Every point represents the mean of data obtained in 3 experiments.

5.2.4. Determination of Thermodynamic Parameters

I used Van't Hoff plots of the temperature data for K_b to find ΔH and ΔS for complex formation (**Figure 5.3**). Experimental errors for values of ΔH and ΔS presented in the graphs were in the range of 10-20%. Temperature regions corresponding to different conformations had significantly different ΔH and ΔS. For the Taq DNA polymerase/aptamer system, the process is entropy-driven at low temperatures and enthalpy-driven at high temperatures. For the SSB/ssDNA system, the driving forces are opposite.

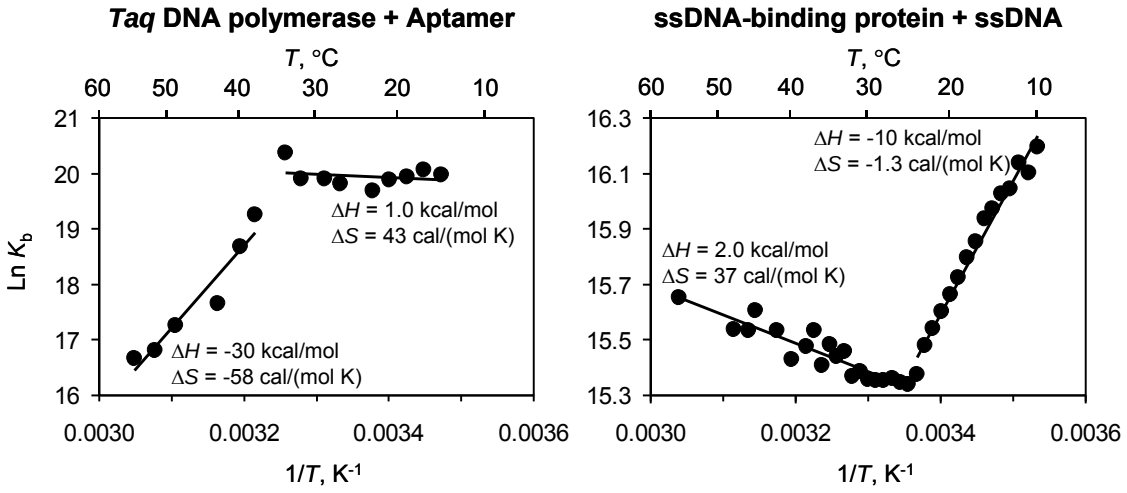

Figure 5.3. Van't Hoff plots.

Van't Hoff plots used for the determination of ΔH and ΔS for complex formation in two protein-DNA pairs: (i) *Taq* DNA polymerase with its DNA aptamer and (ii) *E. coli* ssDNA-binding protein with a 20-base long ssDNA.

5.2.5. Using NECEEM for Determination of Temperature in CE

Here I want to introduce a bonus application of temperature-controlled NECEEM as a nonspectroscopic approach to determining temperature in CE. It is based on measuring a temperature-dependent rate constant of complex dissociation by means of the kinetic CE method. In this work, I used the dissociation of a protein-DNA complex to demonstrate that the new method allows for temperature determination in CE with a precision of 2 °C. I applied the new method to study heat dissipation efficiency in CE instruments with active and passive cooling of the capillary. The result indicates that even CE instruments with active heat dissipation from the capillary have to be tested for the quality of heat dissipation for every set of experimental conditions before being used in temperature-sensitive analyses. The results also suggest that, in general, CE instruments with passive heat exchange should not be used for temperature-sensitive analyses. With a number of advantages over conventional spectroscopic approaches, NECEEM-based temperature determination will find practical applications in CE method development for temperature-sensitive analyses, such as hybridization and affinity assays.

CE is rapidly becoming an indispensable tool in studies of biomolecular interactions, such as protein-protein, protein-DNA, protein-small molecule, and DNA-small molecule. These affinity interactions are highly sensitive to temperature; therefore, they may be affected by Joule heat generated during CE. The reliable use of CE in such studies requires a means of accurately measuring the temperature inside the capillaries or channels during the course of electrophoresis. The use of temperature-sensing devices for

measuring the temperature inside capillaries and channels during electrophoresis is technologically challenging. It is much more practical to use liquid probes, which can be sampled in CE without influencing the parameters of CE and the temperature of the separation media. Until now, all approaches for temperature sensing in CE relied on molecular probes with temperature-dependent spectral/optical properties. Temperature in capillaries and channels was measured with a number of spectroscopic techniques including NMR spectroscopy of water [86], backscattering of light [87], Raman spectroscopy of hydrogen bonds [88], light absorption by thermochromic liquid crystals and nanocrystals [89, 90], and fluorescence spectroscopy of molecular fluorophores [91, 92]. The applicability of spectroscopic probes is obviously limited to specific spectroscopic detection schemes.

In this work, I exploited the dissociation kinetics of a noncovalent complex between a SSB and fluorescently labeled 15-mer single stranded DNA (fluorescein-5'-GCGGAGCGTGGCAGG- 3'):

$$\text{SSB•fDNA} \xrightarrow{k_{off}} \text{SSB} + \text{fDNA}$$

The rate constant, k_{off}, of complex dissociation depends on temperature, *T*, according to the Arrhenius equation:

$$k_{off} = Ae^{-E_a/RT}$$

where A is a preexponential factor, E_a is the activation energy of the reaction, and R is the gas constant.

First, I used NECEEM and a reference CE instrument (P/ACE MDQ) with controlled temperature of the capillary to study the dependence of complex dissociation

kinetics on temperature. The instrument was equipped with a laser-induced fluorescence detector to monitor the fluorescently labeled DNA and its complex with SSB; free SSB was not detectable. The equilibrium mixture of SSB and fDNA was injected into the thermostabilized capillary by pressure, and its components were separated under nonequilibrium conditions. NECEEM electropherograms changed drastically with the temperature of the capillary (**Figure 5.4**). These changes reflected temperature dependencies of the electroosmotic flow (shortening of the migration time with increasing T) and the dissociation rate constant, k_{off} (decreasing peak area of the complex). The rate constants at different temperatures were calculated using a standard NECEEM approach described in the chapter 2. The dependence of k_{off} on T was exponential, confirming the conformational integrity of the protein and a satisfactory quality of temperature stabilization in the reference CE instrument within the studied range of temperatures (**Figure 5.5**). This dependence can be used as a calibration curve for measuring an unknown temperature during CE with any CE instrument under any conditions with the only requirement being that the electrophoresis run buffer be the same. It should be noted that "the same buffer" requirement is not unique for NECEEM-based temperature determinations spectroscopic probes are also sensitive to buffer conditions so spectroscopic methods require calibration in the same buffer and with the same CE instrument. The calibration curve for the NECEEM-based method can be built with another CE instrument (e.g., the one with active cooling) or even with a non-CE method, such as surface plasmon resonance (SPR). The precision of the NECEEM-based method ranges from 1 to 3 °C, depending on the temperature region.

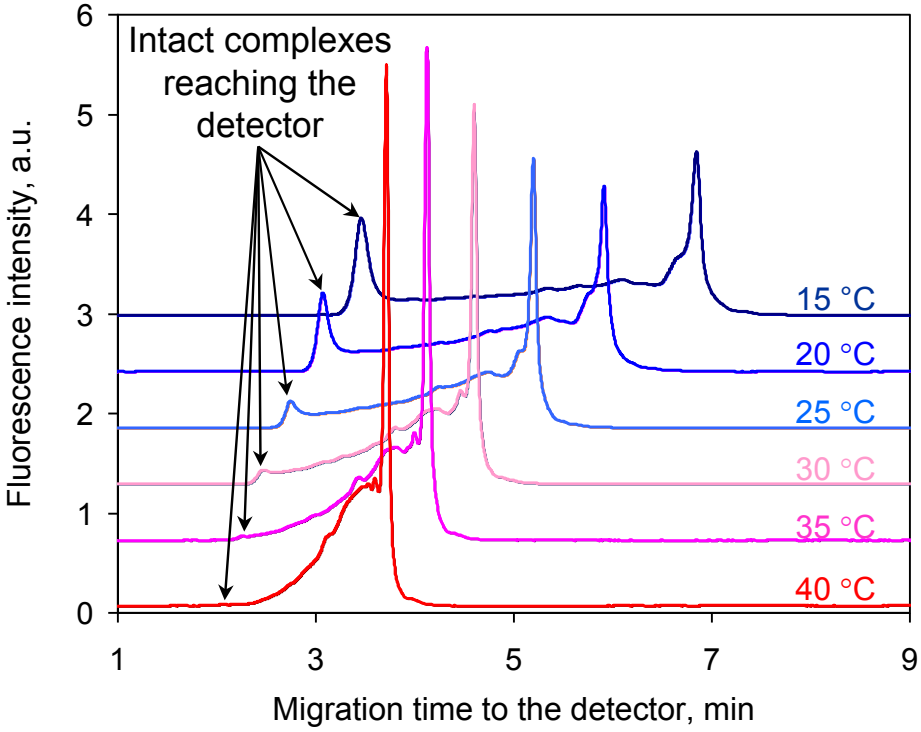

Figure 5.4. Dependence of Dissociation Kinetics of Protein-DNA Complex on Temperature of Capillary

The equilibrium mixture of SSB (250 nM) and fluorescently labeled DNA (100 nM) was prepared in 25 mM sodium tetraborate buffer at pH 9.4. NECEEM was carried out in the same electrophoresis run buffer by a 400 V/cm electric field. The arrows indicate peaks of the intact complex reaching the detector.

Second, I used the new temperature determination method to study the quality of Joule heat dissipation in the reference CE instrument under different electric fields used to drive electrophoresis. The temperature of the capillary in the reference instrument was controlled by placing the capillary in a liquid heat exchanger. Joule heat is inevitably generated during electrophoresis, and if it does not dissipate efficiently, the temperature in the capillary will be greater than the temperature of the heat exchanger. Increasing heat

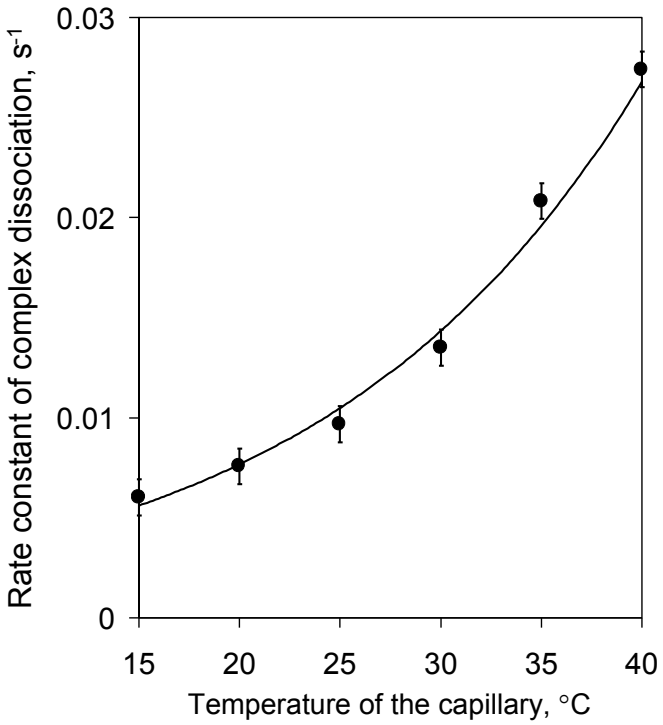

Figure 5.5. Temperature Dependence of Dissociation Rate Constant

Dependence of the rate constant of protein-DNA complex dissociation measured with NECEEM on the temperature of the capillary. The experimental conditions were similar to those in **Fig. 5.4.**

generation, e.g., by increasing the electric field, when its dissipation is inefficient would lead to a further increase of temperature inside the capillary despite the constant temperature of the heat exchanger. To examine whether heat dissipation was efficient in the reference instrument, I measured the temperature in the capillary as a function of an electric field under constant temperature of the heat exchanger. The temperature did not change with the electric field rising from 50 to 600 V/cm but increased dramatically when the electric field grew over 600 V/cm, suggesting that heat dissipation became inefficient when the electric field exceeded 600 V/cm (**Figure 5.6**). This result indicates

that even CE instruments with temperature control of the capillary have to be tested for the quality of heat dissipation for every set of experimental conditions before being used in temperature-sensitive analyses.

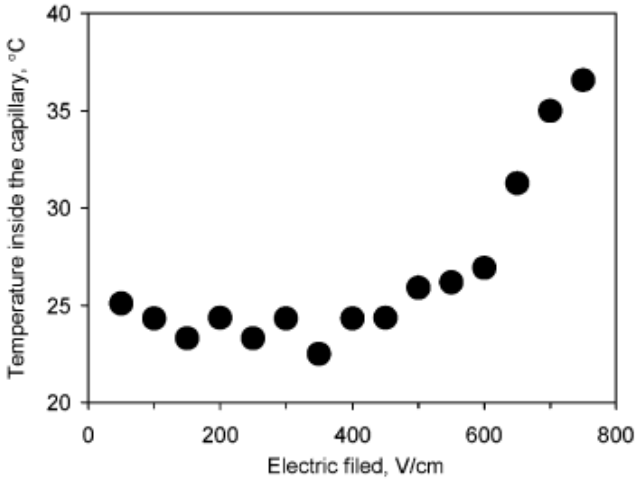

Figure 5.6. Temperature Dependence of Electric Field in CE.

Measurements were performed at the constant temperature, 25 °C, of the heat exchanger used to thermostabilize the capillary. The experimental conditions other than the electric field were similar to those in **Figure 5.4**.

Third, I applied the NECEEM-based temperature determination method to study heat dissipation efficiency in a CE instrument with passive cooling of the capillary through heat exchange with ambient air. The conditions of NECEEM were identical to those used in **Figure 5.4** except for a capillary, which had thinner walls (65 instead of 165 μm) to promote more efficient heat dissipation. I found that even with thinner walls the temperature in the capillary during CE was 35 ± 2 °C when the ambient air temperature was 20 °C. This result suggests that, in general, CE instruments with passive heat exchange should not be used for temperature-sensitive analyses.

Finally, I outline the major characteristics of the NECEEM-based method for temperature determination in CE. The rate constant of complex dissociation measured by NECEEM depends only on the temperature and the buffer composition. It does not depend on other CE conditions such as capillary dimensions, capillary coating, or electric filed. Thus, the calibration curve, k_{off} versus T, measured with any reference instrument under any separation conditions (e.g., the one presented in **Figure 5.5**) can be used to determine the temperature for any other CE instrument, provided the complex-forming system and the electrophoresis run buffer are the same. Moreover, the calibration curve built with a non- CE method, such as SPR, can equally be used. This makes NECEEM-based temperature measurements simple and reliable. All spectroscopic methods, in contrast, require that a calibration curve be built with a CE instrument in which the temperature is to be determined. This is often difficult, especially for CE on a chip. Another advantage of the NECEEM-based temperature determination is that, in contrast to spectroscopic methods, it can be performed with nonspectroscopic detection (e.g., electrochemical detection). In addition, NECEEM provides much more reliable temperature information than spectroscopic methods, when used in CE with single-point detection (the majority of CE instruments employ this type of detection). NECEEM integrates temperature along the capillary length, while spectroscopic methods measure temperature in the detection point only. The temperature in the detection point may be considerably different from that in the rest of the capillary due to heating by interrogating light or difficulties with cooling in this point. As a result, spectroscopic methods may lead to significant systematic errors, while NECEEM should provide much more accurate

temperature data. I would like to emphasize that a "kinetic probe" (e.g., DNA-SSB mixture) can be loaded into a capillary along with a sample for in situ temperature determination. To realize this mode, the sample must not interact with the components of the "kinetic probe" and a means should be provided for separate detection of the sample and the "kinetic probe" (e.g., by using different fluorescent dyes to label the sample and the detectable component of the "kinetic probe").

5.3. CONCLUSION

To conclude, I present here the first application of temperature-controlled NECEEM, a novel method for thermochemical studies of non-covalent protein-DNA interactions. Temperature-controlled NECEEM is a homogeneous kinetic method that allows finding temperature dependencies of equilibrium and kinetic parameters of protein-DNA complex formation without immobilizing DNA or the protein on the surface of a solid substrate. Moreover, the new method can be potentially applicable to other types of macromolecular interaction, such as protein-protein, protein-small molecule, and DNA-small molecule. The NECEEM-based method represents the first nonspectroscopic technique for measuring temperature in CE. With a number of advantages over conventional spectroscopic approaches, it will find practical applications in CE method development for temperature-sensitive analyses, such as hybridization and affinity assays.

5.4. EXPERIMENTAL METHODS

5.4.1. Chemicals and Materials

Single-stranded DNA binding protein (SSB) from *Escherichia coli* and buffer components were obtained from Sigma-Aldrich (Oakville, ON). An extended 62-mer DNA aptamer for Taq DNA polymerase and a fluorescently-labeled 20-mer ssDNA, 5'-FAM-AACGAGAAGCGCGATCACAT-3', were custom-synthesized by IDT (Coralville, IA, USA). The extension in the aptamer sequence was made to fluorescently label the aptamer by making its hybrid with a fluorescently labeled 15-mer DNA oligonucleotide, 5'-FAM-GCGGAGCGTGGCAGG, which was kindly donated by Dr. Yingfu Li (McMaster University, Hamilton, ON). Fluorescein was attached to oligonucleotides by using 6-carbon spacer arm to eliminate some problems with the protein binding. The structure of the aptamer is shown in **Figure 5.7**. Fused-silica capillaries were purchased from Polymicro (Phoenix, AZ). All solutions were made using Milli-Q quality deionized water and filtered through a 0.22-μm filter (Millipore, ON).

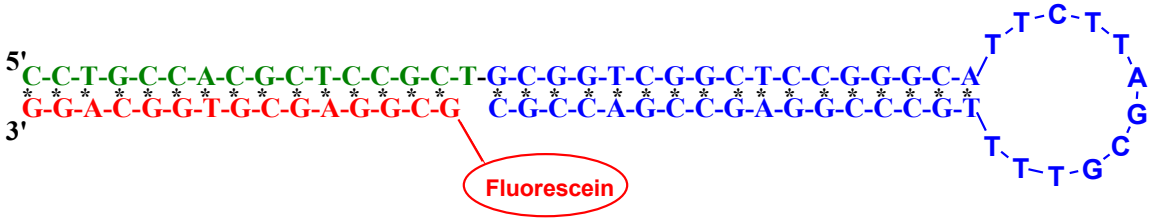

Figure 5.7. DNA Aptamer for Taq Polymerase

The aptamer is shown in blue, the extension in green and the fluorescently-labeled hybridization probe in red.

5.4.2. NECEEM

Temperature-controlled NECEEM was performed with two CE instruments were used in this work: a commercial P/ACE MDQ machine (Beckman-Coulter) with thermo-stabilization of the capillary (the outer walls of the capillary were washed with a liquid heat exchanger maintained at a fixed temperature) and a custom-made CE machine without thermo-stabilization of the capillary (the capillary was exposed to the ambient air) [32]. Both machines employed laser-induced fluorescence detection with a 488 nm line of an argon-ion laser for fluorescence excitation. Uncoated fused silica capillaries were used with the following dimensions: 40 cm × 20 μm I.D. × 350 μm O.D. in the commercial instrument and 40 cm × 20 μm I.D. × 150 μm O.D. in the custom-made instrument. Electrophoresis was run with a positive electrode at the injection end biased at +16 kV if not indicated otherwise. The run buffer for all CE experiments was 25.0 mM sodium tetraborate at pH 9.4. The samples were injected into the capillary by a pressure pulse of 1 s × 9.1 kPa; the length of corresponding sample plug was 0.93 mm as was calculated using the Poiseulle equation. The capillary was rinsed with the run buffer solution for 2 minutes prior to each run. At the end of each run, the capillary was rinsed with 100 mM NaOH for 2 minutes, followed by a rinse with deionized water for 2 minutes. Temperature-controlled NECEEM experiments were performed in three repeats for every temperature point.

5.4.3. Equilibrium Mixtures

Equilibrium mixtures were prepared by mixing the protein and DNA in the incubation buffer and preincubated at a room temperature for 1 h prior analysis. The incubation buffer was 25 mM tetraborate at pH 9.4. For the *Taq* DNA polymerase-aptamer mixture the concentrations of the protein and the aptamer were 70 and 75 nM, respectively. For the SSB-ssDNA mixture the concentrations of the protein and DNA were 250 and 200 nM, respectively.

NECEEM experiments for temperature determination were performed with three different equilibrium mixtures of the single-stranded DNA-binding protein and the fluorescently labeled 15-mer DNA oligonucleotide (five repeats for every mixture). The protein and DNA were mixed in the NECEEM run buffer to have the final concentration of DNA equal to 100 nM and final concentrations of the protein equal to 0.25, 0.5, and 1 μM. The mixtures were incubated at room temperature for 1 h to reach the equilibrium prior to the analysis.

The rate constant of complex dissociation was calculated from a single NECEEM electropherogram by two methods: by fitting the dissociation curve with a single-exponential function and through peak areas as described in Chapter 2 and 3.

Equation Chapter 6 Section 6# CHAPTER 6

SweepCE

6.1. INTRODUCTION

Non-covalent protein-DNA complexes play an important role in gene expression, DNA replication, DNA integrity control, and DNA damage repair [1-3]. In order to understand the dynamics of these biological processes it is essential to know the kinetic parameters of the formation and dissociation of relevant complexes (C) between the protein (P) and DNA (D):

$$P + D \underset{k_{off}}{\overset{k_{on}}{\rightleftharpoons}} C$$

The knowledge of these parameters is also required for the development and optimization of analytical and molecular biology methods based on protein-DNA interactions. The monomolecular rate constant of complex dissociation, k_{off}, can be determined by either surface plasmon resonance (SPR) [4, 5], or by non-equilibrium capillary electrophoresis of equilibrium mixtures (NECEEM) [36, 37, 66]. As for the bimolecular rate constant of complex formation, k_{on}, until now, the only technique available for its direct measurements was stopped flow spectroscopy [93-95]. Stopped-flow spectroscopy relies on the change of spectral properties of either protein or DNA during complex formation. Such changes are often insignificant, which limits the applicability of stopped-flow methods to studies of protein-DNA interactions. Here I introduce sweeping capillary electrophoresis (SweepCE), a new KCE method

for directly measuring k_{on}, and demonstrate its use for studying protein-DNA interactions. In contrast to stopped-flow spectroscopy, SweepCE does not rely on spectral changes of the protein or DNA upon complex formation. It requires only that electrophoretic mobilities of the protein and DNA be different, which is always achievable. Moreover, SweepCE is complementary to NECEEM; the two methods constitute a powerful kinetic capillary electrophoresis platform for comprehensive studies of protein-DNA interactions.

6.2. RESULTS AND DISCUSSION

6.2.1. SweepCE

The concept of SweepCE is based on the sweeping of slowly migrating DNA by a fast migrating protein during electrophoresis. The capillary is pre-filled with a solution of DNA and electrophoresis is then carried out from a solution of the protein in a continuous mode. Because the electrophoretic mobility of the protein is greater than that of DNA, the protein continuously mixes with DNA and forms the protein-DNA complex. The complex migrates with a velocity higher than that of DNA and causes sweeping of DNA. The value of k_{on} for complex formation can be determined from the time-profile of DNA concentration using a simple mathematical model of the sweeping process. Mathematical analysis is an essential part of SweepCE.

At the beginning, I demonstrated the phenomenon of DNA sweeping by a DNA-binding protein in capillary electrophoresis (CE). The capillary (bare silica) was pre - filled with 10 nM fluorescently labeled DNA (5'-fluorescein-

GCGGAGCGTGGCAGG) in 25 mM sodium tetraborate buffer at pH 9.0. The injection end of the capillary was then immersed into a solution of 100 nM SSB

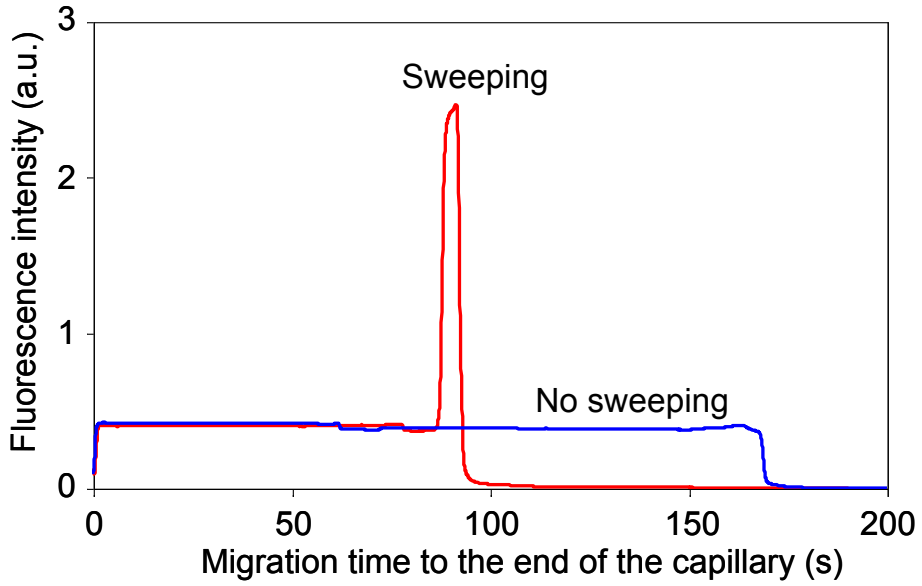

Figure 6.1. Sweeping of DNA by DNA-Binding Protein in CE.

The capillary (bare silica) was pre-filled with 10 nM fluorescently labeled DNA in 25 mM sodium tetraborate buffer at pH 9.0. The injection end of the capillary was then immersed into a solution of 100 nM SSB protein in the same buffer and a positive voltage was applied to the protein solution. The "no-sweeping" control experiment was performed in the absence of SSB.

protein in the same buffer and a positive voltage of 20 kV was applied to the protein solution. SSB is a single-stranded DNA- binding protein [34, 59], which migrates faster than DNA and binds ssDNA sequence-non-specifically [67]. Fluorescence detection was used in these experiments so that only DNA and its complex with the protein were detectable. In the absence of the protein, DNA gradually eluted from the outlet end of the capillary while the capillary was gradually filled with a bare run buffer from its inlet end. This DNA replacement process generated an

electropherogram with a characteristic plateau, which ended at 170 s, when the tail of DNA exited the capillary (**Figure 6.1, blue line**). In the presence of the protein, the tail of DNA was swept by the faster moving protein, which resulted in a "sweeping region" with an increased overall concentration of DNA (**Figure 6.1, red line**). It is the shape of the "sweeping region" that can be used for the determination of the bimolecular rate constant, k_{on}, of protein-DNA interaction.

6.2.2. Mathematical Model of SweepCE

In collaboration with a mathematician, Dr. Victor Okhonin, from Krylov lab, we developed a mathematical model of the sweeping process that facilitates finding k_{on} from the shape of the "sweeping region". Sweeping of DNA by the protein is governed by the rate of complex formation between them and by the velocities of the protein, DNA, and the complex in electrophoresis: v_P, v_D, v_C, respectively. The overall mass transfer process is described by the following system of non-linear partial differential equations:

$$\begin{aligned}
&\frac{\partial P(t,x)}{\partial t} + v_P \frac{\partial P(t,x)}{\partial x} = -k_{on} D(t,x) P(t,x) \\
&\frac{\partial D(t,x)}{\partial t} + v_D \frac{\partial D(t,x)}{\partial x} = -k_{on} D(t,x) P(t,x) \\
&\frac{\partial C(t,x)}{\partial t} + v_C \frac{\partial C(t,x)}{\partial x} = k_{on} D(t,x) P(t,x)
\end{aligned} \tag{6.1}$$

Here P, D, and C are the concentrations the protein, DNA and complex, respectively; t is time passed from the beginning of separation and x is the distance from the inlet of the capillary to the point of observation. Complex dissociation can

be neglected if $t << 1/k_{off}$, where t is the time of analysis and k_{off} is the monomolecular rate constant of dissociation. Diffusion can be neglected if $t << \delta x^2/\mu$, where μ is a typical coefficient of diffusion and δx is a characteristic width of electrophoretic peaks. We assume that both of these conditions are satisfied, allowing us to use equations (6.1). Typically, systems of non-linear partial differential equations do not have general analytical solutions. There are only very few physical processes for which such solution can be found, typically by using the inverse scattering problem technique. In our case, the exact general solution can be found using a simpler approach. The general solution for the first two equations in (6.1) has the following form:

$$\begin{aligned} D(t,x) &= \frac{\partial \lambda(t,x)}{\partial t} + v_P \frac{\partial \lambda(t,x)}{\partial x} \\ P(t,x) &= \frac{\partial \lambda(t,x)}{\partial t} + v_D \frac{\partial \lambda(t,x)}{\partial x} \end{aligned} \tag{6.2}$$

where

$$\lambda(t,x) = \frac{1}{k_{on}} \ln(A(x - v_P t) + B(x - v_D t)) \tag{6.3}$$

Direct substitution of $P(t,x)$ and $D(t,x)$ from (6.2) to (6.1) proves this statement. Concrete forms of functions $A(\xi)$ and $B(\xi)$ can be determined from initial conditions. If we assume that at time $t = 0$ concentrations of the protein and DNA are $\tilde{P}(x)$ and $\tilde{D}(x)$, respectively, then for $A(\xi)$ and $B(\xi)$ we can write the following differential equations:

$$\frac{dA(\xi)}{d\xi} = -\mathrm{k}_{\mathrm{on}}\tilde{P}(\xi)(A(\xi)+B(\xi))/(v_P - v_D)$$
$$\frac{dB(\xi)}{d\xi} = \mathrm{k}_{\mathrm{on}}\tilde{D}(\xi)(A(\xi)+B(\xi))/(v_P - v_D) \tag{6.4}$$

From system (6.3) we can obtain a single linear equation for $A(\xi)$ + $B(\xi)$; functions $A(\xi)$ and $B(\xi)$ can be then found by solving this equation. For the illustration of this general approach we consider a practically interesting case when the velocity of the protein is higher than that DNA, $v_{\mathrm{P}} > v_{\mathrm{D}}$. At time $t = 0$, the concentrations of DNA ($\tilde{D}(x)$) is equal to 0 for $x < 0$ and equal to D_0 for $x \geq 0$; the concentration of the protein ($\tilde{P}(x)$), in contrast, is equal to 0 for $x \geq 0$ and equal to the constant value of P_0 for $x \leq 0$. In this case, solutions for $A(\xi)$ and $B(\xi)$ are:

$$A(\xi) = (A_0 + B_0)\left\{\exp\left(\frac{-\mathrm{k}_{\mathrm{on}}P_0\xi}{v_P - v_D}\right) - 1\right\}\theta(-\xi) + A_0$$
$$B(\xi) = (A_0 + B_0)\left\{\exp\left(\frac{\mathrm{k}_{\mathrm{on}}D_0\xi}{v_P - v_D}\right) - 1\right\}\theta(\xi) + B_0 \tag{6.5}$$

where

$$\theta(\xi) = \begin{cases} 0, \xi < 0 \\ 1, \xi \geq 0 \end{cases}$$

For λ in expression (6.3) we will have:

$$\lambda(t,x) = \frac{1}{\mathrm{k}_{\mathrm{on}}}\ln\left(A(x - v_P t) + B(x - v_D t)\right) =$$
$$= \frac{1}{\mathrm{k}_{\mathrm{on}}}\ln\left[\begin{array}{l}\left\{\exp\left(-\mathrm{k}_{\mathrm{on}}P_0\frac{(x - v_P t)}{v_P - v_D}\right) - 1\right\}\theta\left(-(x - v_P t)\right) + \\ + \left\{\exp\left(\mathrm{k}_{\mathrm{on}}D_0\frac{(x - v_D t)}{v_P - v_D}\right) - 1\right\}\theta((x - v_D t)) + 1\end{array}\right] + \frac{1}{\mathrm{k}_{\mathrm{on}}}\ln(A_0 + B_0) \tag{6.6}$$

And, finally, the concentration of the protein, DNA, and the complex are equal to:

$$P(t,x) = P_0 \frac{\exp\left(\mathrm{k_{on}} P_0 \dfrac{x - v_\mathrm{P} t}{v_\mathrm{P} - v_\mathrm{D}}\right)\theta(-x + v_\mathrm{P} t)}{\left[\begin{array}{l}\left\{\exp\left(-\mathrm{k_{on}} P_0 \dfrac{x - v_\mathrm{P} t}{v_\mathrm{P} - v_\mathrm{D}}\right) - 1\right\}\theta(-x + v_\mathrm{P} t) + \\ + \left\{\exp\left(\mathrm{k_{on}} D_0 \dfrac{x - v_\mathrm{D} t}{v_\mathrm{P} - v_\mathrm{D}}\right) - 1\right\}\theta(x - v_\mathrm{D} t) + 1\end{array}\right]}$$

$$D(t,x) = D_0 \frac{\exp\left(\mathrm{k_{on}} D_0 \dfrac{x - v_\mathrm{D} t}{v_\mathrm{P} - v_\mathrm{D}}\right)\theta(x - v_\mathrm{D} t)}{\left[\begin{array}{l}\left\{\exp\left(-\mathrm{k_{on}} P_0 \dfrac{x - v_\mathrm{P} t}{v_\mathrm{P} - v_\mathrm{D}}\right) - 1\right\}\theta(-x + v_\mathrm{P} t) + \\ + \left\{\exp\left(\mathrm{k_{on}} D_0 \dfrac{x - v_\mathrm{D} t}{v_\mathrm{P} - v_\mathrm{D}}\right) - 1\right\}\theta(x - v_\mathrm{D} t) + 1\end{array}\right]}$$

$$C(t,x) = \mathrm{k_{on}} \int_0^t D(t - \tau, x - \tau v_\mathrm{C}) P(t - \tau, x - \tau v_\mathrm{C}) d\tau$$

Here, P_0 and D_0 are the concentrations of the protein and DNA, respectively, before the start of the sweeping process; θ is the parameter which equals 0 if $x < 0$ and equals 1 if $x \geq 0$. The three expressions can be used to build simulated electropherograms. All parameters in the three expressions, except for $\mathrm{k_{on}}$, are either defined (θ) or controlled (P_0, D_0) or can be found in independent CE experiments (v_P, v_D, and v_C). Therefore, fitting experimental electropherograms with the simulated ones requires the optimization of a single parameter, $\mathrm{k_{on}}$, only. Standard procedures

for non-linear regression of experimental data can be used for fast and accurate determination of k_{on}.

6.2.2. Determination of k_{on}

I examined the proposed SweepCE approach of finding k_{on} for the interaction of SSB and the fluorescently labeled 15-mer DNA nucleotide described above. Due to the fluorescence label, both DNA and the protein-DNA complexes were detectable. SweepCE electropherograms for three different concentrations of DNA are presented in **Figure 6.2 (blue lines).** The fluorescent signal corresponds to a sum concentration of DNA and the protein-DNA complex. To fit such a signal with my model, the fitting function should be $D(t) + C(t)$. The detector was placed in a single point at the end of the capillary; therefore, x was not a variable but a fixed parameter. I measured v_P, v_D, and v_C in separate capillary electrophoresis experiments and used this values along with specified P_0 and D_0 in the non-linear regression analysis to find k_{on}. Simulated SweepCE electropherograms, which provide the best fitting of experimental data are shown in **Figure 6.2 by red lines**. The k_{on} value obtained from SweepCE analyses was $(3.4 \pm 0.6) \times 10^6\ M^{-1}s^{-1}$. This value is in satisfactory agreement with that indirectly determined as $k_{on} = k_{off}/K_d = 1 \times 10^6\ M^{-1}s^{-1}$ using $k_{off} = 0.01\ s^{-1}$ and $K_d = 10$ nM obtained by NECEEM under identical to SweepCE experimental conditions. Fitting the experimental data with k_{on}, which deviated from the correct one, can be found in **Figure 6.3**.

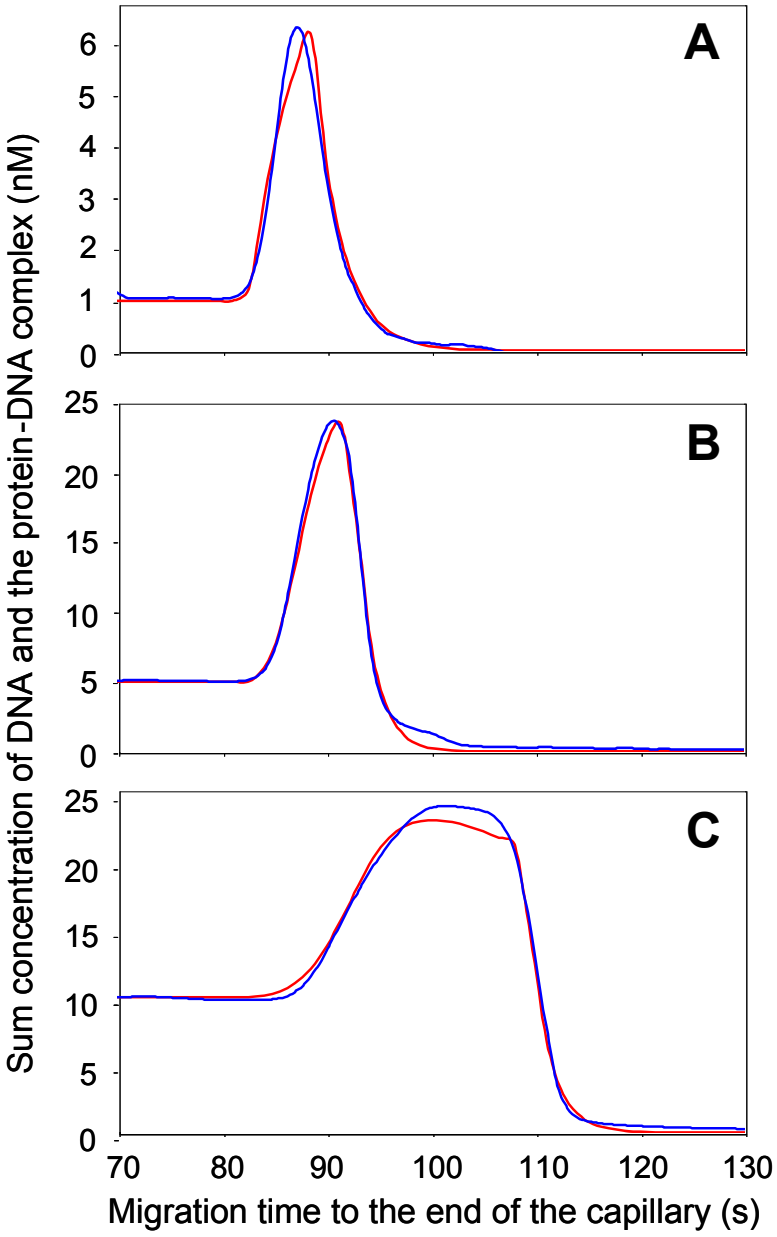

Figure 6.2. Fitting Experimental SweepCE Electropherograms with Simulated SweepCE Electropherograms

Experimental SweepCE electropherograms (blue lines) were obtained for the interaction between single-stranded DNA binding protein (60 nM) and a 15-mer fluorescently labeled DNA: 1 nM (panel A), 5 nM (panel B), and 10 nM (panel C). Simulated SweepCE electropherograms (red lines) were obtained by nonlinear regression of the experimental data using the least-squares method.

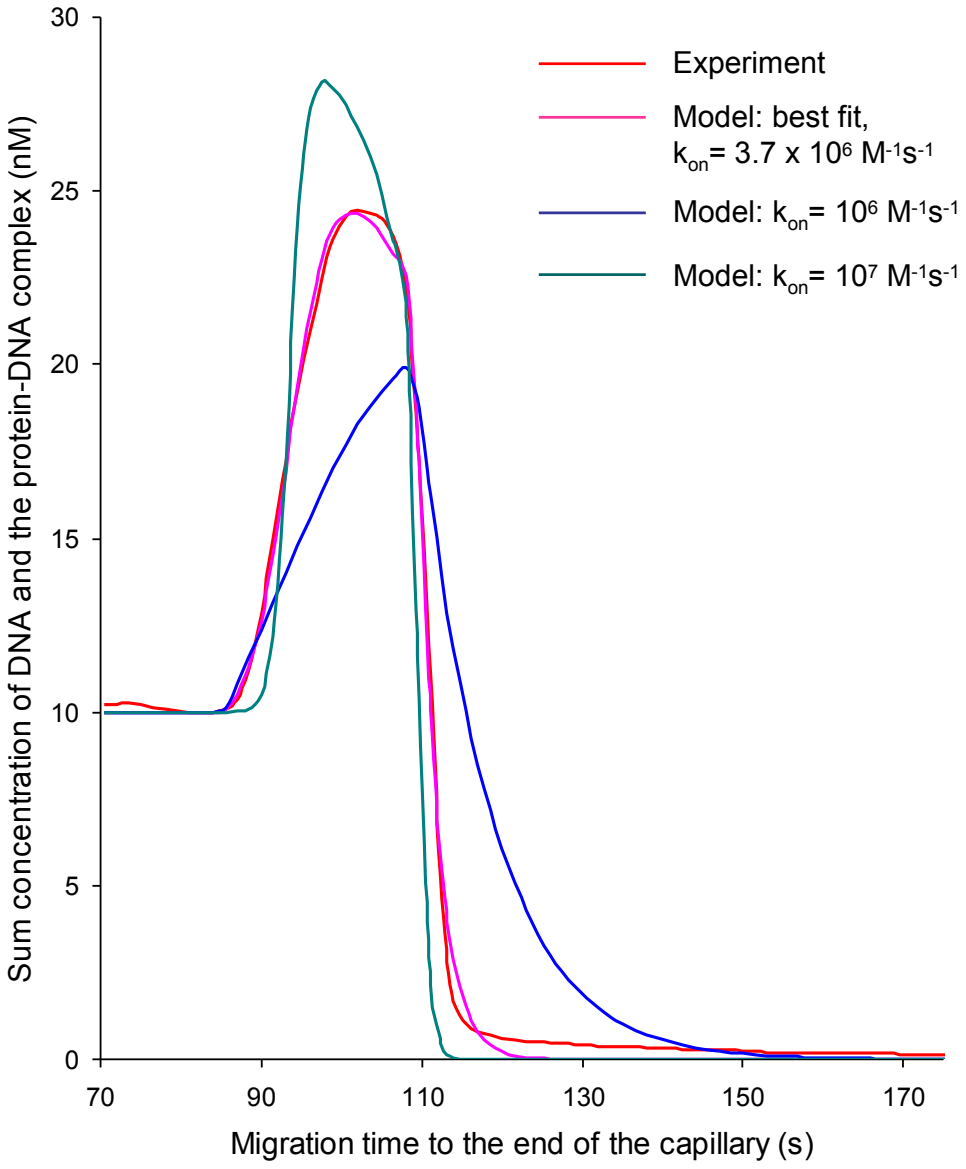

Figure 6.3. Fitting Experimental Data with k_{on} Value Different from Correct One

The incorrect fitting is to illustrate the sensitivity of SweepCE electropherograms to k_{on}. Experimental data are identical to those presented in **Figure 6.2.** The correct value of k_{on} is 3.4×10^6 $M^{-1}s^{-1}$. The incorrect values of k_{on} used here were 10^6 $M^{-1}s^{-1}$ and 10^7 $M^{-1}s^{-1}$.

6.3. CONCLUSION

Finally, I want to outline major characteristics of SweepCE. The simple mathematical model of SweepCE works if complex dissociation during the time of SweepCE separation is negligible. With the shortest separation times in CE being on the order of a few seconds, the simple model can be used for finding k_{on} of complexes, whose k_{off} values are as high as 0.1 s^{-1}. For greater k_{off}, the system of partial differential equations should include the rate of complex dissociation and should be solved numerically. The numerical solution is more complex technically, but can reveal both k_{on} and k_{off}. In SweepCE, very low concentrations of reacting components can be used, allowing for reliable measurements of k_{on} values as high as diffusion controlled ones ($\sim 10^9$ $M^{-1}s^{-1}$). Mixing of the reacting components in SweepCE proceeds in a continuous mode, thus excluding "dead" time, inevitable for stopped-flow methods.

To conclude, SweepCE represents the first non-stopped flow technique for directly measuring the bimolecular rate constant of complex formation. Along with NECEEM, which measures K_d and k_{off}, SweepCE establishes a powerful KCE method for comprehensive studies of protein-ligand interactions, which uses a universal instrumental platform.

6.4. EXPERIMENTAL METHODS

6.4.1. Chemicals and Materials

Single-stranded DNA binding protein from *Escherichia coli* and buffer components were obtained from Sigma-Aldrich (Oakville, ON). Fluorescently labeled 15-mer DNA oligonucleotides, fluorescein-5'-GCGGAGCGTGGCAGG, was kindly donated by Dr. Yingfu Li (McMaster University, Hamilton, ON). Fused-silica capillaries were purchased from Polymicro (Phoenix, AZ). All solutions were made using Milli-Q quality deionized water and filtered through a 0.22-μm filter (Millipore, Nepean, ON).

6.4.2. SweepCE

All CE procedures were performed using the following instrumentation and common settings and operations. CE was carried out with a P/ACE MDQ apparatus (Beckman Coulter, Mississauga, ON) equipped with absorption and fluorescence detectors; a 488-nm line of an Ar-ion laser was utilized to excite fluorescence. An 50-cm long (40 cm to a detection window) uncoated fused silica capillary with an inner diameter of 75 μm and outer diameter of 360 μm was used. The capillary was pre-filled with 1-10 nM fluorescently labeled DNA (5'-fluorescein-GCGGAGCGTGGCAGG) in the electrophoresis run buffer - 25 mM sodium tetraborate at pH 9.0. The injection end of the capillary was then immersed into a solution of 50-100 nM SSB protein in the same buffer and a positive voltage of 20 kV

was applied to the protein solution. The temperature of the separation capillary was maintained at 20 ± 0.2 °C. The capillary was rinsed with the run buffer solution for 2 min prior to each run. At the end of each run, the capillary was rinsed with 100 mM HCl for 2 min, 100 mM NaOH for 2 min, followed by a rinse with deionised water for 2 min.

CHAPTER 7

NECEEM – COMREHENSIVE KCE METHOD FOR SELECTION OF APTAMERS

7.1. INTRODUCTION

Aptamers are DNA (or RNA) oligonucleotides capable of binding different classes of targets with high affinity and selectivity. Due to their unique properties, aptamers promise to revolutionize many areas of natural and life sciences ranging from affinity separation to diagnostics and treatment of diseases.

A general approach to aptamer selection from libraries of random DNA sequences (applicable to RNA libraries as well) was introduced by Gold's and Szostak's groups in 1990 [40, 41]. It is termed selection of ligands by exponential enrichment (SELEX) and involves multiple rounds of the following procedure. The library is allowed to react with the target so that DNA forms dynamic complexes with the target. At equilibrium, DNA molecules with high affinity are predominantly bound to the target while those with low affinity are predominantly unbound. DNA-target complexes are partitioned from free DNA and the target-bound DNA is PCR-amplified to obtain a new affinity-enriched library. The enriched library is used for the next round of selection. The procedure is repeated for several rounds until the enriched library reaches a certain level of bulk affinity, after which, individual DNA molecules from the enriched library are selected by bacterial cloning, PCR-amplified, sequenced, and chemically synthesized.

Major requirements for methods of aptamer selection include: (i) high and well controlled efficiency of partitioning of DNA-target complexes from free DNA, (ii) the ability to accurately determine binding parameters (K_d, k_{on} and k_{off}) of the aptamer-target interaction, and (iii) the ability to select aptamers with pre-defined ranges of the binding parameters. None of the conventional methods of partitioning [96-101] satisfies the three requirements. I have introduced a new kinetic capillary electrophoresis method, termed non-equilibrium capillary electrophoresis of equilibrium mixtures (NECEEM) [36, 66]. In this chapter I want to demonstrate that NECEEM provides a unique way of highly efficient selection of aptamers, which can satisfy the three requirements. First, I describe the theoretical foundation of NECEEM-based selection of aptamers including selection of aptamers with pre-defined ranges of binding parameters. Then, I present results of theoretical and experimental studies of the efficiency of NECEEM-based partitioning of aptamers from non-aptamers. Finally, I illustrate the application of the new method to selection of aptamers for protein farnesyltransferase (PFTase), the enzyme involved in posttranslational modification of Ras proteins, which are important signal transducers. My results suggest that the efficiency of NECEEM-based partitioning exceeds that of the conventional methods by as much as 2 orders of magnitude. Due to the high efficiency, NECEEM-based SELEX requires fewer rounds of selection than SELEX based on conventional methods of partitioning. Uniquely, a single round of NECEEM-based partitioning and PCR amplification was sufficient for obtaining a pool of aptamers for PFTase with K_d in the range of 1 nM. To the best of my knowledge, it is the first report of selecting an aptamer with nanomolar affinity in a single

step. Interestingly, the aptamers exhibited no significant inhibitory effect on PFTase activity, thus suggesting that they may be used for monitoring PFTase *in vivo* without affecting its function.

7.2. RESULTS AND DISCUSSION

7.2.1. Concept of NECEEM-Based Selection

The concept of NECEEM-based selection of aptamers is illustrated in **Figure 7.1**. In the first step, the DNA library is mixed with the target (T) and incubated to form the equilibrium mixture (EM). DNA molecules with high affinity are predominantly bound to the target while those with low affinity are predominantly unbound. Thus, EM consists of free DNA, DNA-target complexes (DNA•T) and free T (**Figure 7.1a**). In the second step, a plug of EM is introduced into the capillary and high voltage is applied to separate the equilibrium fraction of DNA•T from the equilibrium fraction of DNA by gel-free capillary electrophoresis (CE) under non-equilibrium conditions (**Figure 7.1b**). Non-equilibrium conditions imply that the separation buffer does not contain the components of the library or the target. The unique feature of NECEEM is that all free DNA molecules have similar electrophoretic mobilities, independent of their sequences [102, 103]. Therefore, they migrate as a single electrophoretic zone. In my particular example, I assume that the conditions of NECEEM are chosen so that the mobility of T is higher than that of DNA. The mobility of DNA•T will typically be intermediate to those of DNA and T. In the electric field, the zones of DNA, DNA•T, and T are separated. The equilibrium between DNA and DNA•T is no longer maintained and DNA•T starts

dissociating, which results in smears of DNA and T. The order in which the components reach the end of the capillary is the following: 1) the equilibrium part of free T, 2) free T formed by dissociation of DNA•T during NECEEM, 3) the remains of intact DNA•T, 4) free DNA formed from the dissociation of DNA•T during NECEEM, and 5) the equilibrium part of free DNA. In the final step, a fraction is collected from the output of the capillary in a time window, which depends on specific goals (**Figure 7.1c**). Positive selection is defined as the collection of the equilibrium part of the target-bound DNA. Negative selection is defined as collection of the equilibrium part of free DNA. Positive and negative selection can be combined to realize specific selection modes. Positive selection from the equilibrium mixture that contains T can be used to select aptamers to T. Negative selection from the equilibrium mixture that does not contain T but contains the incubation buffer can be used to exclude from the library aptamers for buffer components. Negative selection from the equilibrium mixture that does not contain target 1 but contains target 2 can be used to exclude from the library aptamers for target 2. The last approach can be used for the elimination of aptamers with cross-reactivity for targets 1 and target 2. It can also be used for parallel selection of aptamers to multiple targets.

Being a homogeneous method with comprehensive kinetic features, NECEEM provides a means for selection of DNA aptamers with pre-defined ranges of binding parameters (K_d, k_{off}, and k_{on}) of complex formation:

$$DNA + T \underset{k_{off}}{\overset{k_{on}}{\rightleftharpoons}} DNA\bullet T$$

where k_{on} and k_{off} are the rate constant of complex formation and dissociation, respectively. The two rate constants define the equilibrium dissociation constant, $K_d = k_{off}/k_{on}$. In the equilibrium mixture of the DNA library and the target, DNA molecules with K_d less than the concentration of the equilibrium part of free target, [T], are predominantly bound to the target, while those with $K_d > [T]$ are predominantly unbound. Therefore, positive selection (see **Figure 7.1c**) leads to DNA molecules with $K_d < [T]$, while negative selection leads to DNA molecules with $K_d > [T]$. Alternating positive selection using higher concentration of free target, $[T]_1$, with negative selection using lower concentration of free target, $[T]_2$, can facilitate selection of aptamers with a limited range of affinity: $[T]_2 < K_d < [T]_1$. The unique feature of NECEEM is that it allows direct measurement of the concentration of free target if it exceeds the limit of detection [66]. If this concentration is lower than the limit of detection, it can be estimated under certain conditions using approaches described in detail elsewhere [104]. Another unique feature of NECEEM is that the time window used for positive selection accurately defines the range of k_{off} values of selected DNA. Selection within the $t_1 - t_2$ time window (**Figure 7.1c**) leads to DNA molecules with the following k_{off} range:

$$k_{off} = \frac{t_{DNA} - t_{DNA\bullet T}}{t_{DNA\bullet T}(t_1 - t_2)} \ln\left(\frac{t_{DNA} - t_2}{t_{DNA} - t_1}\right)$$

where $t_{DNA\bullet T}$ and t_{DNA} are migration times in NECEEM of the DNA-target complex and free DNA, respectively.

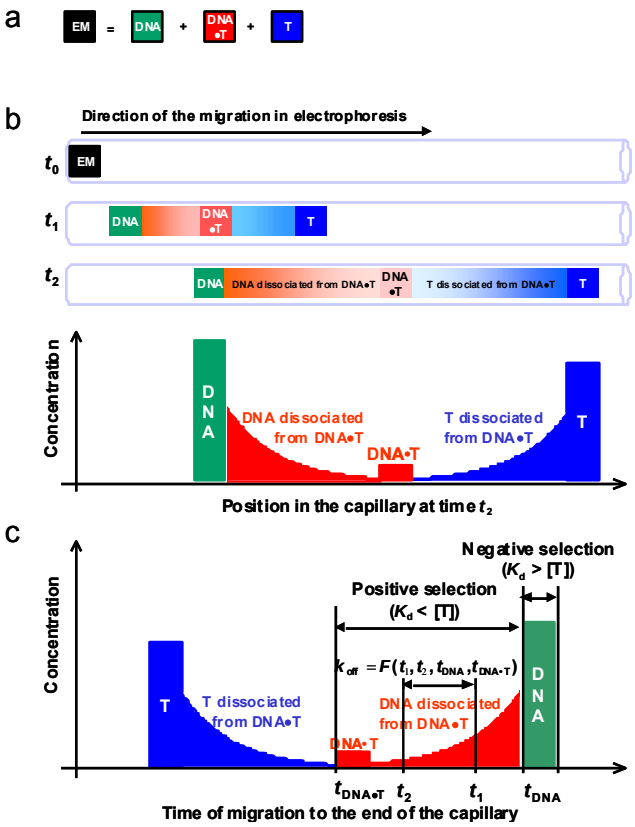

Figure 7.1. Schematic Representation of NECEEM-Based Selection of DNA Aptamers

(a) Step 1: Preparation of the equilibrium mixture (EM) of the DNA library and the target (T). The equilibrium mixture contains free DNA, DNA-target complex (DNA•T) and free T. **(b)** Step 2: NECEEM-based separation of the equilibrium fraction of target-bound DNA (red) from the equilibrium mixture of free DNA (green). The top of the panel shows spatial distribution of the separated components in the capillary at different times ($t_0 = 0$, $t_2 > t_1 > t_0$) from the beginning of separation. The graph at the bottom of panel **b** shows concentrations of the separated components as functions of the position in the capillary at time t_2. **(c)** Step 3: Aptamer collection at the exit of the capillary in different time windows. Positive selection corresponds to collecting the equilibrium fraction of target-bound DNA (red), which preferably contains DNA with high affinity to the target ($K_d < [T]$). Negative selection corresponds to collecting the equilibrium fraction of free DNA (green), which preferably contains DNA with low affinity to the target ($K_d > [T]$). The parameters of the time window for positive selection define k_{off} values of the DNA-target complexes for selected DNA. The denotations used are: $t_{DNA•T}$ and t_{DNA} are migration times in NECEEM of DNA•T and free DNA, respectively, $F(t_1, t_2, t_{DNA}, t_{DNA•T}) \rightarrow (t_{DNA} - t_{DNA•T})/(t_{DNA•T} \times (t_1 - t_2)) \times \ln((t_{DNA} - t_2)/(t_{DNA} - t_1))$ with the increasing number of rounds of SELEX.

When aptamers are selected with limited ranges of K_d and k_{off}, the range of k_{on} is also defined due to the relation between the three constants: $k_{on} = k_{off}/K_d$.

Another way for selecting aptamers with a certain range of k_{on} is to control the incubation time of the equilibrium mixture so that only DNA molecules with high k_{on} reach equilibrium, while those with low k_{on} do not. Alternating positive selection using a longer incubation time, τ_1, with negative selection using a shorter incubation time, τ_2, can facilitate selection of aptamers with the following range of k_{on}: $1/[T]\tau_1 < k_{on} < 1/[T]\tau_2$.

7.2.2. Efficiency of NECEEM-Based Selection

If aptamers are not obtained after 15-20 rounds of selection, further selection is typically considered impractical. The number of rounds required for selecting aptamers depends critically on the efficiency of partitioning of target-bound DNA from free DNA [98, 104-106]. In this section I demonstrate that NECEEM-based partitioning of DNA aptamers provides the efficiency, which exceeds those of the best conventional methods by as much as 100 times.

A general partitioning procedure is shown in **Figure 7.2a**. Amounts of DNA•T and DNA at the output of partitioning ($DNA•T_{out}$ and DNA_{out}) depend on the amounts of DNA•T and DNA at the input of partitioning ($DNA•T_{in}$ and DNA_{in}) and efficiencies of collection for DNA•T and DNA ($k_{DNA•T}$ and k_{DNA}). The efficiency of partitioning is defined as $k_{DNA•T}/k_{DNA}$: in ideal partitioning, $k_{DNA•T} = 1$ and $k_{DNA} = 0$, so that the efficiency of partitioning is equal to ∞. In conventional methods, the efficiency of partitioning is limited by non-specific adsorption of DNA to the surface of the

chromatographic support or filter. The values of $k_{DNA} < 10^{-3}$ are hardly achievable; therefore, the upper limit for the efficiencies of partitioning by conventional methods is 10^3. Typical values of $k_{DNA•T}/k_{DNA}$ lie in the range of 10-100 [96, 98-101, 106-108].

The efficiency of NECEEM-based partitioning depends on how well DNA•T and DNA can be separated in gel-free CE. **Figure 7.1c** schematically illustrates ideal NECEEM-based partitioning with $k_{DNA•T} = 1$, $k_{DNA} = 0$, and $k_{DNA•T}/k_{DNA} = \infty$ (positive selection in the wide window). In practice, peak broadening due to interaction with capillary walls, diffusion, etc. leads to the overlap between the peaks and makes the efficiency of NECEEM-based partitioning finite. The efficiency depends not only on the resolution of DNA•T and DNA but also on the width and position of the aptamer-collection window. **Figure 7.2b** shows simulated NECEEM-based partitioning of DNA•T from DNA in the presence of peak broadening; the parameters used in simulation are typical for NECEEM of protein-DNA systems [66]. For conservative estimates, I assume in this simulation that DNA•T is relatively unstable ($k_{off} = 10^{-2}$ s^{-1}) so that most of it dissociates during separation. The efficiency of partitioning increases rapidly with shifting the right boundary of the aptamer collection window to the left. This is achieved due to the significant decrease of k_{DNA} when $k_{DNA•T}$ remains almost unchanged. Thus, the position and width of the aptamer collection window can be used to control the efficiency of partitioning.

I experimentally determined k_{DNA} for different aptamer-collection windows in NECEEM using only a DNA library and no target. A plug of the DNA library (total of 9×10^{11} molecules) was injected into the capillary and high voltage was applied under

the conditions (run buffer, geometry of the capillary, and the electric field), which would be later used for NECEEM-based selection of aptamers. Consecutive 1-minute fractions were collected and the number of DNA molecules in each was determined using quantitative PCR. When the right-hand side boundary of the aptamer collection window was at 19 min or shorter, a value of k_{DNA} of 10^{-5} or less was achieved, which corresponded to the efficiency of partitioning, $k_{DNA\bullet T}/k_{DNA}$, of approximately 10^5 (assuming that $k_{DNA\bullet T} \approx 1$). This efficiency exceeds those of the best conventional methods by as much as 2 orders of magnitude. I expected that the adsorption of DNA to the capillary walls, followed by its slow desorption, would lead to tailing of the library peak along with an increased k_{DNA} value for the aptamer collection window at the right-hand side of the peak. In contrast to my expectations, the library peak had no tailing and efficiencies of partitioning for aptamer collection at the right of the DNA library peak should be in the same range of values, ~10^5. The negligible DNA adsorption to capillary walls can be explained by very intensive electrostatic repulsion of negatively-charged DNA molecules from negatively-charged capillary walls [109]. These results suggest that aptamers can be collected with approximately equal efficiency at both sides of the DNA library peak. It makes the method more versatile by allowing aptamer selection for proteins with a very large range of electrophoretic mobilities.

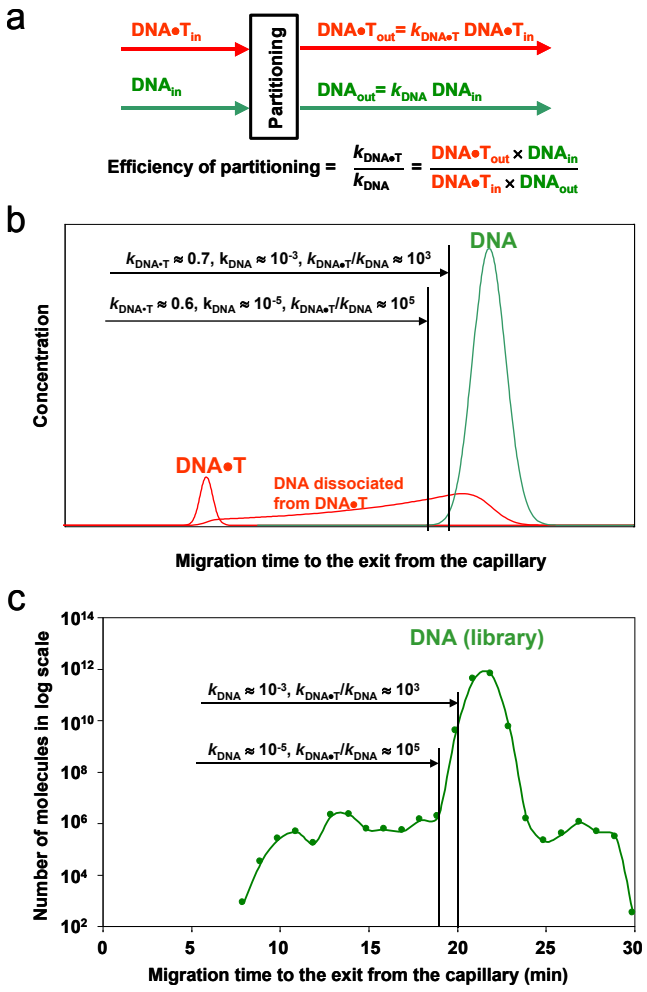

Figure 7.2. Efficiency of NECEEM-Based Partitioning

Efficiency of NECEEM-based partitioning of target-bound DNA (DNA•T) and free DNA. (a) Schematic representation of partitioning. $DNA\bullet T_{in}$ and DNA_{in} are amounts of DNA•T and DNA, respectively, at the input of partitioning. $DNA\bullet T_{out}$ and DNA_{out} are amounts of DNA•T and DNA, respectively, at the output of partitioning. $k_{DNA\bullet T} = DNA\bullet T_{out}/DNA\bullet T_{in}$ and $k_{DNA} = DNA_{out}/DNA_{in}$ are efficiencies of collection of DNA•T and DNA, respectively, at the output of partitioning. The efficiency of partitioning is defined as $k_{DNA\bullet T}/k_{DNA}$. (b) Efficiencies of simulated NECEEM-based partitioning for different aptamer collection windows. (c) Experimentally determined k_{DNA} and estimated $k_{DNA\bullet T}/k_{DNA}$ (based on assumption that $k_{DNA\bullet T} \approx 1$) for different aptamer collection windows. The sample of the DNA library was subjected to electrophoresis and fractions were collected in time windows shown in the graph. The amounts of DNA in the fractions were determined by quantitative PCR. The value of k_{DNA} for two windows was calculated as the ratio between the amount of DNA in the corresponding fraction and total amount of DNA sampled (9×10^{11} copies). The limit of detection of quantitative PCR was 1000 copies of the template per sample.

7.2.3. One-Step Selection of Aptamers for PFTase

Using NECEEM I selected aptamers with nanomolar affinity to PFTase in a single round of partitioning and PCR amplification. To decide on the suitable aptamer collection window, I first determined migration times of the DNA library and the protein from the inlet to the outlet of the capillary under conditions (run buffer, geometry of the capillary, and the electric field) similar to those which would be used for aptamer selection. In gel-free CE, migration times of molecules depend linearly on their "size to charge" ratios [102, 103]. Every nucleotide base in DNA has approximately the same size and bears a single negative charge. Since all DNA molecules in the library have the same number of nucleotide bases, their "size to charge" ratios are similar and, thus, migration times are also similar.

This explains why the DNA library migrated as a single zone and elutes from the capillary as a single peak (**Figure 7.3a**). Heterogeneous hybridization of DNA molecules in the library (including self-hybridization) introduces a certain degree of heterogeneity in the sizes of the DNA molecules, which leads to the width of the library peak being ~10 times greater that that of an individual DNA molecule from the library (not shown). In contrast to DNA, proteins are expected to have different "size to charge" ratios and, thus, different migration times due to the heterogeneity of "size to charge" ratios of amino acids. Accordingly, a sample of PFTase contained at least 4 components with different migration times, which were detectable with light absorbance at 280 nm (**Figure 7.3b**). The large widths of peaks with migration times of 11-12 min and 15-16 min suggest that

each of the two peaks may contain more than 1 species with slightly different migration times. Although exact identities of the multiple species in the PFTase sample are not known, my data (see below) indicate that all of them contain a recognition site for the aptamer, which allows me to suggest that they likely correspond to the monomer and different multimers of the protein [110]. A monomer of PFTase consists of two subunits and contains, in total, 814 amino acids and bears a negative charge of –60 (at pH 9.0 of the CE run buffer). PFTase monomer and multimers are expected to have different migration times because the hydrodynamic size of the molecule is not an additive function, while the charge is. The size to charge ratios of the PFTase monomer and multimers are greater than that of DNA, which bears a total charge of –122; therefore, all PFTase species migrated faster than the DNA library (compare **Figure 7.3a** and **Figure 7.3b**).

I, then, exploited the ability of NECEEM to measure binding parameters in order to determine the bulk affinity of the library to the protein. The equilibrium mixture containing a fluorescently labeled library and 70 nM PFTase was subjected to electrophoresis in the run buffer that did not contain the library and protein. In addition to the peak of free DNA, a set of low-intensity peaks, corresponding to PFTase-DNA complexes was observed in the range of migration times of 15-20 min (**Figure 7.3c**). Five peaks of complexes had detectable levels of intensity; 2 of the 5 peaks (with migration times around 18 min) were not baseline-resolved. These data suggest that the PFTase sample contained at least 5 targets, which bound DNA and whose complexes with DNA had different migration times. Using the NECEEM-based procedure described in earlier

chapters [36], the effective equilibrium dissociation constant of the interaction between the library and PFTase was determined from the analysis of the areas of peaks of PFTase-DNA complexes and free DNA: K_d = 1.5 μM. The 5 detectable peaks of the complexes had migration times intermediate to those of PFTase and DNA, which is expected for protein-DNA complexes [37, 66]. The data on the migration times of the library, PFTase, and PFTase-DNA complexes in bulk analyses were used to decide on the aptamer collection window. To ensure that no aptamers are missed the aptamer collection window was chosen to span from the first PFTase component to the close proximity of the library (**Figure 7.3d**). Using the data of **Figure 7.2c**, the efficiency of NECEEM-based partitioning with this aptamer collection window was estimated to be approximately 10^5.

The next step was NECEEM-based partitioning of PFTase-DNA complexes from free DNA. I targeted selection of aptamers with nanomolar affinity; therefore, the equilibrium mixture used for partitioning contained only 0.2 nM PFTase. As I expected, no peaks of PFTase-DNA complexes were detectable with UV absorbance detection (**Figure 7.3d**) or even with fluorescence detection, which indicates that their amount was below the limit of detection of the instrument (10^5 molecules for fluorescence detection).

Undetectable PFTase-DNA complexes were collected blindly within the aptamer collection window and then the DNA was amplified using PCR with a fluorescently labeled forward primer, and a biotin-labeled reverse primer. DNA strands were separated using streptavidin immobilized on the surface of super paramagnetic iron oxide beads and the fluorescently labeled strands were collected to establish the affinity-enriched DNA library. When sampled for CE without the protein, this enriched DNA library generated a

relatively narrow peak (with migration time of 22 min) suggesting that its level of heterogeneity was lower than that of the initial library (compare **Figure 7.3e** and **Figure 7.3a**). I then prepared the equilibrium mixture of the enriched DNA library with 50 nM PFTase and subjected it to NECEEM. A set of peaks corresponding to PFTase-DNA complexes was observed in a time window of 15-20 min and only a small peak of free DNA was observed with a migration time of 22 min. The bulk affinity of K_d = 5 nM for the interaction of the enriched library and PFTase was found from the data of **Figure 7.3f**. Thus, one round of NECEEM-based partitioning led to 300-fold increase in the bulk affinity of the DNA library, which was possible due to the very high efficiency of NECEEM-based partitioning.

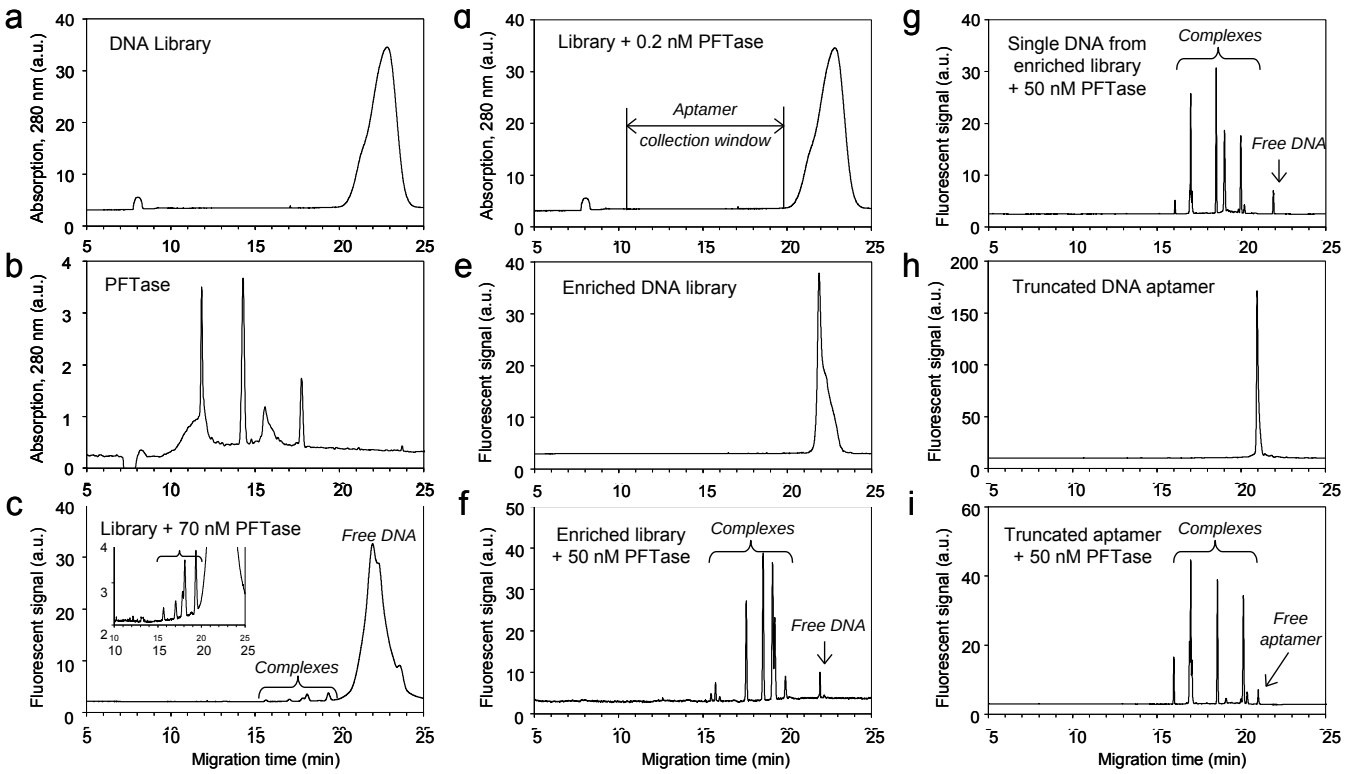

Figure 7.3. One-Step Selection of Aptamers for Protein Farnesyltransferase (PFTase)

(a) Electrophoretic migration of the DNA library (10 μM). **(b)** Electrophoretic migration of PFTase (1 μM). **(c)** NECEEM-based determination of bulk affinity of the DNA library to PFTase. The equilibrium mixture contained 5 nM fluorescently labeled DNA library and 70 nM PFTase. The inset shows the peaks of the complexes with a larger scale of the fluorescent signal. **(d)** NECEEM-based partitioning of aptamers for PFTase. The equilibrium mixture contained 10 μM library and 0.2 nM PFTase. The aptamer collection window was chosen to facilitate the efficiency of partitioning $k_{DNA \bullet T}/k_{DNA} \approx 10^5$ (see **Figure 7.2c**). **(e)** Electrophoretic migration of the PCR-amplified enriched DNA library obtained in NECEEM-based partitioning. **(f)** NECEEM-based determination of affinity of the enriched DNA library to PFTase. The equilibrium mixture contained approximately 10 nM of fluorescently labeled enriched DNA library and 50 nM PFTase. (**g**) NECEEM-based determination of affinity of a singe DNA molecule cloned from the enriched DNA library to PFTase. The equilibrium mixture contained approximately 10 nM of fluorescently labeled DNA and 50 nM PFTase. (**h**) Electrophoretic migration of a truncated aptamer, which was synthesized without constant regions. (**i**) NECEEM-based determination of affinity of the truncated aptamer to PFTase by NECEEM. The equilibrium mixture contained approximately 10 nM of the aptamer and 50 nM PFTase.

Subsequently, I cloned individual DNA molecules from the enriched library in *E. coli* and PCR-amplified them with a fluorescent primer. Individual DNA molecules revealed NECEEM electropherograms (**Figure 7.3g**) qualitatively similar to those of the enriched library (**Figure 7.3f**). Individual molecules had affinity to PFTase ranging between 0.5 and 10 nM. Sequences of the individual DNA molecules were determined and aptamers with truncated constant regions were synthesized and fluorescently labeled (**Table 7.1**). Individual truncated aptamers generated a narrow peak when sampled for CE (**Figure 7.3h**), which is expected for a highly homogeneous DNA sample. The NECEEM electropherogram of the individual aptamers with PFTase had a small peak of the free aptamer and several high peaks of PFTase-aptamer complexes. The general pattern and the migration times of the PFTase-aptamer complexes (**Figure 7.3i**) were slightly different from the PFTase-DNA complexes of the enriched library (**Figure 7.3e**) and the cloned aptamer (**Figure 7.3f**). This is most likely due to the truncated aptamer's being considerably shorter than the DNA in the library (36 bases versus 77 bases). Every aptamer was able to bind all PFTase species, indicating that all of them contained a recognition site for the aptamer. This allows me to suggest that the multiple PFTase components correspond, most likely, to a monomer and different multimers of the protein. The best of the eight examined aptamers had a K_d value of 0.5 nM (**Table 7.1**). The secondary structures of the eight aptamers have melting temperatures in a range of 32-42 °C. The affinity of the best aptamer was confirmed with filter-binding assay. To examine the selectivity of aptamers, I studied their binding to other proteins (albumin, Ras, MutS, tau, GFP, and myoglobin); no cross-reactivity was observed. After obtaining

an aptamer in a single round of selection I performed a *de novo* three-round NECEEM-SELEX (**Figure 7.4**). NECEEM-based binding assay revealed the general pattern similar to that in **Figure 7.3f** and the affinities of the selected aptamers were similar to those obtained in a single round. Thus, the minimum number of rounds of SELEX required for the selection of the best aptamer (for the given target-library system) was one.

Table 7.1. Sequences and Affinities of Truncated Aptamers

Sequence	K_d, nM
AACAATCTATCCGATAATATCTGTATTCTTCTTTGG	2
TGAGTTCATGAACCTTCGATCTTGTGATTGTTGAAC	5
CATCACCTCAAGTTCTTAGAGACCAATGTCCAGCTT	10
TGGTACACCTTCGGTTTGACGATGTATTAACGACAT	1
CGTCTCTATTGCTTTCTACATGGCGATTATAACAAT	8
AAGAGGCCAGTAGTAAAGTTTAAGTGGACAATGCAC	0.5
AGACATGCCTTAGTCAACTTGCCTCTACCTTCAAGC	5
TAAAGTTCATAACCTTTCACAAGATTTCAAACGCTA	10

Using the NECEEM-based procedure described earlier in chapter 2 and 3 [66], I measured the aggregate rate constant of complex dissociation, $k_{off} = 10^{-4}$ s^{-1} for all PFTase-aptamer complexes. The rate constant is so small that the dissociation of the complex during the duration of NECEEM is negligible. The corresponding bimolecular rate constant of complex formation was calculated as $k_{on} = k_{off}/K_d = 10^5$ $M^{-1}s^{-1}$.

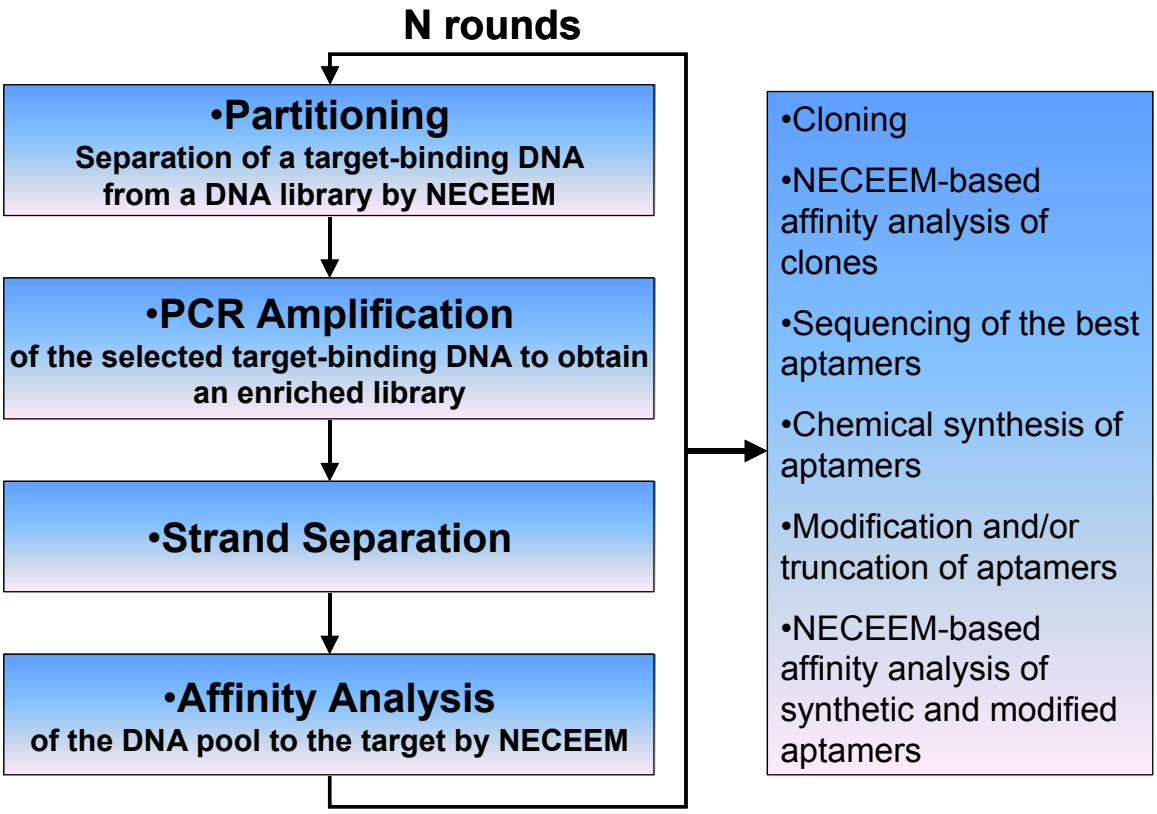

Figure 7.4. Scheme of NECEEM-SELEX of DNA Aptamers

This scheme depicts a simplified flowchart of *in vitro* selection of DNA aptamers. A random DNA pool containing ~10^{11} – 10^{15} unique individual sequences is incubated with a target. The next steps are NECEEM-based determination of bulk affinity of a DNA library to the target, and NECEEM-based partitioning of a DNA-target complex from free DNA. The collected DNA is amplified using PCR with a fluorescently labeled forward primer, and a biotin-labeled reverse primer. DNA strands are separated using streptavidin beads and the fluorescently labeled strand is collected to establish the affinity-enriched DNA library. This lower diversity pool is then incubated with a new aliquot of the target to examine its binding affinity to the target using NECEEM. If the affinity is not high enough, the new selection round starts again. After reaching the desirable affinity the enriched library is bacterially cloned. Clones are screened, and the best aptamers are sequenced. Some of them could be truncated or modified to improve binding or other specific properties.

7.2.4. Influence of Aptamer on PFTase Activity

Finally, I studied the influence of the aptamer on PFTase activity. PFTase activity was examined using a fluorescently-labeled pentapeptide substrate, 2',7'-difluorofluorescein-5-Gly-Cys-Val-Ilu-Ala (dff-GCVIA), which mimics Ras proteins with respect to farnesylation (**Figure 7.5**) [111-113]. The reaction also involves the second substrate, farnesyl pyrophosphate (FPP), as a source of the farnesyl group. I found that the two substrates added to PFTase separately or together did not noticeably affect binding of the aptamer to the enzyme. I also found that the enzymatic activity of aptamer-bound PFTase was undistinguishable from that of the unbound enzyme. These data indicate that the aptamer binding site of the protein is different from its active site, suggesting that the aptamer can be used to detect the enzyme *in situ* in its active state.

7.3. CONCLUSION

In two decades after its introduction, CE has established a solid reputation as a powerful analytical method, which combines highly efficient separation and highly sensitive quantitative detection with natural suitability for automation and parallelism. Due to these advantages, CE has become an instrumental platform for a number of important applications including industrial genome sequencing. However, there are only very few works on CE-based selection of binding ligands from complex mixtures [114, 115]. My work for the thesis was inspired by the insight that it is the development of kinetic methods in CE, which will eventually make it a practical tool in high-throughput screening of combinatorial libraries. In this chapter, I demonstrate that NECEEM can

serve as a "Swiss army knife" in the development and utilization of oligonucleotide aptamers. Using a single instrumental and conceptual platforms, NECEEM facilitates: (i) the highly efficient selection of aptamers, (ii) the accurate determination of their binding parameters, and (iii) the use of aptamers for quantitation of targets. Not only is the efficiency of NECEEM-based partitioning exceptionally high but also it can be easily controlled by adjusting the aptamer collection window. Uniquely, NECEEM can facilitate selection of aptamers with pre-defined binding parameters. The designing of advanced aptamer-based diagnostics and therapeutics requires aptamers with pre-defined kinetic and/or thermodynamic parameters of aptamer-target interaction. I forecast that being a comprehensive kinetic method, NECEEM will be an essential tool in studying fundamental issues of aptamer selection, such as the distribution of ligands in DNA libraries with respect to their binding parameters to the target. Due to its outstanding separation capabilities NECEEM can be used for parallel selection of aptamers for targets in a complex mixture. It is very intriguing to wonder to what extent NECEEM will be applicable to screening combinatorial libraries of a non-nucleotide nature. To conclude, I believe that further development of kinetic methods in CE will provide a variety of methodological schemes for high-throughput screening of combinatorial libraries using a universal instrumental platform.

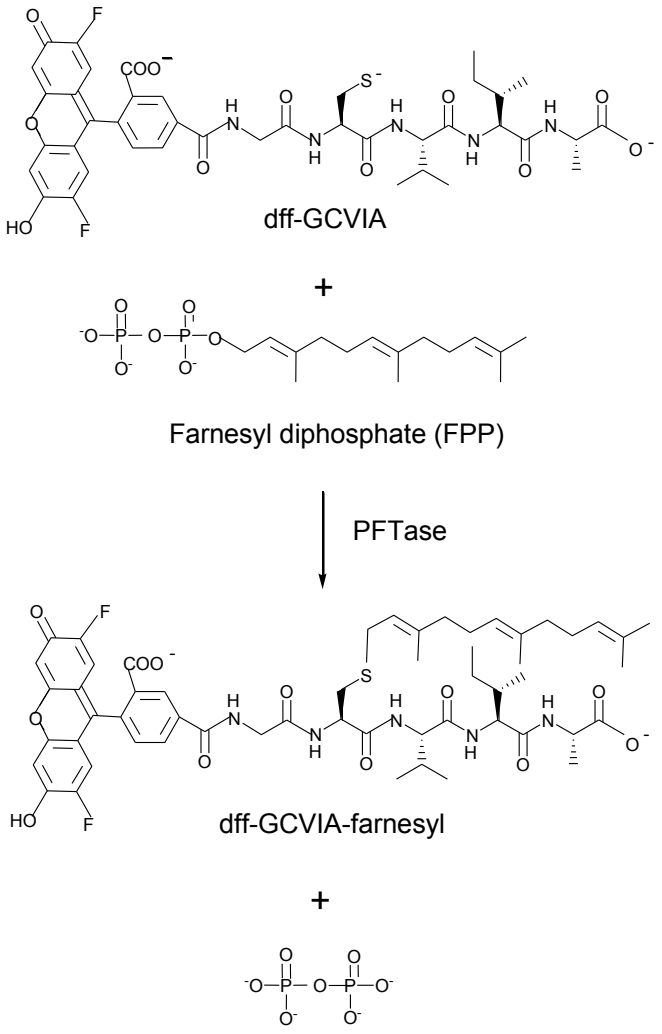

Figure 7.5. PFTase-Catalyzed Farnesylation of Cysteine Residue in dff-GCVIA Peptide

7.4. EXPERIMENTAL METHODS

7.4.1. Chemicals and Materials

Non-labeled primers, a biotin-labeled primer, a fluorescein-labeled primer, and a synthetic random DNA library were obtained from IDT (Coralville, IA, USA). Yeast *Saccharomyces cerevisiae* protein farnesyltransferase (PFTase), recombinant *Taq* DNA polymerase, farnesyl diphosphate and all other chemicals were from Sigma-Aldrich (Oakville, ON, Canada) unless otherwise stated. A non-labeled pentapeptide, Gly-Cys-Val-Ilu-Ala, was synthesized by Dalton Chemicals (Toronto, ON). A fluorescently-labeled pentapeptide, 2',7'-difluorofluorescein-5-Gly-Cys-Val-Ilu-Ala (dff-GCVIA), was kindly donated by Dr. D.C. Poulter (University of Utah). A fused-silica capillary was purchased from Polymicro (Phoenix, AZ, USA). All solutions were made using Milli-Q-quality deionized water filtered through a 0.22 μm filter (Millipore, Nepean, ON).

7.4.2. DNA Library and Primers

The agarose gel-purified library contained a central randomized sequence of 36 nucleotides flanked by 19- and 22-nt primer hybridization sites (5' CTTCTGCCCGCCTCCTTCC-N36-GGAGACGAGATAGGCGGACACT 3').

A reverse phase HPLC purified 6-carboxyfluorescein-labeled 5'-primer (5' FAM CTTCTGCCCGCCTCCTTCC 3') and a biotinylated 5'-primer (5' Biotin AGTGTCCGCCTATCTCGTCTCC 3') were used in PCR reactions for the

synthesis of double-labeled double-stranded DNA molecules. The library (5 nanomoles) was dissolved in 50 μL of water to get 100 μM stock solution and stored at –20 °C.

7.4.3. Capillary Electrophoresis

All CE procedures were performed using the following instrumentation and common settings and operations unless otherwise stated. CE was carried out with a P/ACE MDQ apparatus (Beckman Coulter, Mississauga, ON) equipped with absorption and fluorescence detectors; a 488-nm line of an Ar-ion laser was utilized to excite fluorescence. An 80-cm long (70 cm to a detection window) uncoated fused silica capillary with an inner diameter of 75 μm and outer diameter of 360 μm was used. Both, the inlet and the outlet reservoirs contained the electrophoresis run buffer – 25 mM sodium tetraborate at pH 9.3. The samples were injected into the capillary, pre-filled with the run buffer, by a pressure pulse of 8 s × 2 psi (13.4 kPa). The length and the volume of the corresponding sample plug were 25 mm and 110 nL, respectively. Electrophoresis was carried out for a total of 30 min by an electric filed of 375 V/cm with a positive electrode at the injection end of the capillary; the direction of the electroosmotic flow was from the inlet to the outlet reservoir. The temperature of the separation capillary was maintained at 20 ± 0.2 °C. When needed, fractions were collected in an automated mode by replacing the regular outlet reservoir with a fraction-collection vial containing 5 μL of water. The capillary was rinsed with the run buffer solution for 2 min prior to each run. At the end of each run, the capillary was rinsed with 100 mM HCl for 2 min, 100 mM NaOH for 2 min, followed by a rinse with deionised water for 2 min.

7.4.4. Selection of Aptamers

The equilibrium mixture for NECEEM-based selection of aptamers was prepared in the selection buffer – 25 mM Tris-HCl and 2.5 mM $MgCl_2$ at pH 8.3 – using the following two-step procedure. First, 5 μL of the 20 μM DNA library solution in the selection buffer was denatured by heating at 95 °C for 10 min with subsequent cooling down to 20 °C at a rate of 7.5 deg/min. Second, 5 μL of the 0.4 nM PFTase solution in the selection buffer was mixed with the DNA library sample and incubated at 20 °C for 30 min. The resulting equilibrium mixture contained 10 μM DNA library and 0.2 nM PFTase. A 25 mm long (110 nL) plug of the equilibrium mixture was injected into the capillary pre-filled with the run buffer; the plug contained approximately 10^{12} molecules of DNA and 10^7 molecules of PFTase. The injected equilibrium mixture was subjected to NECEEM at an electric filed of 375 V/cm and with the temperature of the capillary biased at 20 ± 0.2 °C. Eleven minutes and twenty two seconds (different from 10 min due to the 10-cm distance from the detection point on the capillary to its outlet) after the beginning of NECEEM, the regular outlet reservoir was replaced with a fraction-collection vial containing 5 μL of water. For the following 9 min, electrophoresis was carried out into this vial and a fraction of DNA ligands of approximately 3.7 μL was collected. The regular outlet vial was placed instead of the fraction collection vial and electrophoresis was run additional 11 minutes to record the complete electropherogram.

DNA in the collected fraction was PCR-amplified in a thermocycler (MasterCycler 5332, Eppendorf, Germany). In addition to the collected DNA ligands, the

PCR mixtures contained 50 mM KCl, 10 mM Tris-HCl (pH 8.6), 2.5 mM $MgCl_2$, all four dNTPs at 200 μM each, primers (1 μM each), and 0.05 units/μL *Taq* DNA polymerase. The total volume of the PCR reaction mixture was 50 μL. Twenty-eight thermal cycles were conducted with every cycle consisting of: melting at 94 °C for 30 sec, annealing at 56 °C for 15 sec, and extension at 72 °C for 15 sec. The 6-carboxyfluorescein-labeled ssDNA was separated from the complementary biotinylated ssDNA strand on streptavidin-coated super paramagnetic iron oxide particles (product number S2415, Sigma-Aldrich, Oakville, ON, Canada) according to the supplier's instructions.

DNA ligands obtained from the first and third rounds of selection were PCR-amplified using unlabeled primers and cloned into Nova Blue Singles Competent cells (*E. coli*) using the pT7 Blue-3 Perfectly Blunt Cloning Kit (Novagen, Madison, WI). Colonies grown on agar plates were picked randomly for sequencing of DNA. A plasmid from each colony was prepared using a GenElute Plasmid Miniprep Kit and sequenced at the Core Molecular Biology Facility at York University.

NECEEM-selected DNA ligands were full-length sequences containing the "random" region and two constant regions that facilitated PCR amplification. Constant regions are typically not involved in aptamer interaction with the target and thus can be removed from the final aptamer product without affecting its binding capacity. Therefore, final aptamers (truncated aptamers) were synthesized (IDT, Coralville, IA, USA) without the constant regions and contained 36 DNA bases and a 6-carboxyfluorescein fluorescent label at the 5'-end of the aptamer.

7.4.5. Finding Binding Parameters

All PFTase-DNA equilibrium mixtures for NECEEM-based measurements of binding parameters were prepared in the selection buffer – 25 mM Tris-HCl and 2.5 mM $MgCl_2$ at pH 8.3 – using the following two-step procedure. First, 5 μL of the solution of fluorescently labeled DNA in the selection buffer was denatured by heating at 95 °C for 10 min with subsequent cooling down to 20 °C at a rate of 7.5 deg/min. Second, 5 μL of the PFTase solution in the selection buffer was mixed with the DNA sample and incubated at 20 °C for 30 min. A plug of the equilibrium mixture was injected into the capillary and subjected to NECEEM in the run buffer at 375 V/cm. Laser-induced fluorescence detection was used to record NECEEM electropherograms. The equilibrium dissociation constant, K_d, of protein-DNA complexes was found from a single NECEEM electropherogram using the areas of peaks of free DNA, A_{DNA}, and the target-bound DNA, $A_{DNA \cdot T}$:

$$K_d = \frac{[T]_0 \ (1 + R) - [DNA]_0}{1 + 1/R}$$

$$\text{where } R = \frac{[DNA]_{eq}}{[DNA \cdot T]_{eq}} = \frac{A_{DNA}}{A_{DNA \cdot T}}$$

Here, $[T]_0$ and $[DNA]_0$ are total concentrations of the protein target and DNA, respectively, $[DNA]_{eq}$ and $[DNA \cdot T]_{eq}$ are the concentrations of free DNA and the DNA-target complex in the equilibrium mixture. The aggregate value of the unimolecular rate constant, k_{off}, of PFTase-aptamer complex dissociation was estimated by analyzing the areas corresponding to the intact complexes, $A_{DNA \cdot T}$, and dissociated complexes, A_{diss}:

$$k_{off} = (\ln \frac{A_{DNA \cdot T} + A_{diss}}{A_{DNA \cdot T}})/t_{complex}$$

where $t_{complex}$ was an average value of the migration times of all detectable protein-DNA complexes, 18.6 min. To obtain correct values of A_{DNA} and A_{diss}, the apparent areas of the corresponding peaks in NECEEM electropherograms were divided by the migration time of free DNA. To obtain correct value of $A_{DNA \cdot T}$, the apparent area of the corresponding peak in NECEEM electropherograms was divided by the migration time of this peak.

7.4.6. Finding Dissociation Constants of Aptamers with Ultra-Filtration and Fluorescence Detection

The NECEEM K_ds were verified by an independent measurement using ultra-filtration and fluorescence detection. Samples containing 10 nM of the aptamers were incubated with different amounts of PFTase using the same buffer as was used in the NECEEM selections. The samples were then placed in Amicon Ultra-4 centrifugal filter devices (Millipore Corporation, Bedford, MA) and spun at 7500 g for 10 min. The filtrate containing the free aptamer was collected. The amount of free aptamer was quantitated using fluorescence detection with excitation at 488 nm and emission at 520 nm. The equilibrium dissociation constant, K_d, of protein-DNA complexes was found from ultra-filtration using the fluorescent signal from the free aptamer, I_{DNA}, and the target-bound DNA, $I_{DNA \cdot T}$:

$$K_d = \frac{[T]_0(1 + R) - [DNA]_0}{1 + 1/R} \text{ where } R = \frac{[DNA]_{eq}}{[DNA \cdot T]_{eq}} = \frac{I_{DNA}}{I_{DNA \cdot T}}$$

7.4.7. Background of NECEEM-Based Partitioning

Ten μL of 10 μM ssDNA library in the selection buffer was denatured by heating at 95 °C for 10 min, and slowly cooled down to 20 °C at a rate of 7.5 deg/min. A 150 nL plug of the library containing a total of 9×10^{11} molecules was injected into the capillary pre-filled with the run buffer and subjected to electrophoresis at the electric filed of 375 V/cm with a capillary biased at 20 ± 0.2 °C. Thirty 400 nL fractions were collected during 1 min each starting from the very beginning of separation into individual vials containing 5 μL of water. Fractions 26 to 30 were diluted 10^4 times to avoid overloading PCR. The collected fractions were amplified by real-time PCR with a 7300 RT-PCR system (Applied Biosystems, Foster City, CA) using a SYBR Green PCR Master Mix from Applied Biosystems with unlabeled primers (100 nM each). Thermal cycle parameters were: 94 °C for 15 sec, 56 °C for 34 sec, and 72 °C for 15 sec. The instrument's software was used to determine the initial number of DNA molecules in each fraction. DNA standards, used to build a calibration curve, contained DNA library in amounts varying from 0 to 10^{10} molecules.

7.4.8. Measuring PFTase Activity in Presence of Aptamer

Reaction mixtures for measuring PFTase activity contained: 0.3–30 μM dff-GCVIA, 15 μM farnesyl diphosphate (FPP), 0-600 nM truncated aptamer, and 30 nM PFTase in a total of 150 μL of the assay buffer (50 mM Tris-HCl at pH 7.0 supplemented with 10 mM $MgCl_2$, 10 μM $ZnCl_2$, and 5 mM dithiothreitol). The enzymatic reaction was: (i) initiated by the addition of PFTase, (ii) incubated at 37.0 °C for a period ranging

from 5 min to 48 h, (iii) quenched with 10 μL of 1.2 M HCl (final pH 1), and (iv) placed on ice. The amount of the reaction product (farnesylated 2',7'-difluorofluorescein-5-Gly-Cys-Val-Ilu-Ala) was measured using CE with the laser induced fluorescent detection (CE-LIF) (**Figure 7.6**). Four different running buffers were utilized in CE: (i) 2.5 mM Tetraborate at pH 9.1, (ii) 25 mM tetraborate/25 mM SDS at pH 9.3, (iii) 50 mM Tetraborate/20 mM β-cyclodextrine at pH 9.5, and (iv) 50 mM TES/50mM SDS at pH 7.3. The samples were injected electrokineticly at 50 V/cm $\times$ 2 s. The electrophoresis was carried out at 400 V/cm at 20°C [111-113].

7.4.9. Influence of Substrates on Aptamer Binding

To assess the influence of the substrates (Gly-Cys-Val-Ilu-Ala and farnesyl diphosphate) on PFTase-binding ability of the aptamer, PFTase (20-100 nM) was pre-incubated with the truncated aptamer (20-200 nM) in the assay buffer at 30 °C for 30 min, and then, either Gly-Cys-Val-Ilu-Ala (20-1000 nM) or farnesyl diphosphate (0.1-15 μM) or both of them were added to the equilibrium mixture. The equilibrium mixture was subject of NECCEM as describe above. The equilibrium dissociation constants, K_d, of protein-aptamer complexes were compared for experiments with and without the substrates.

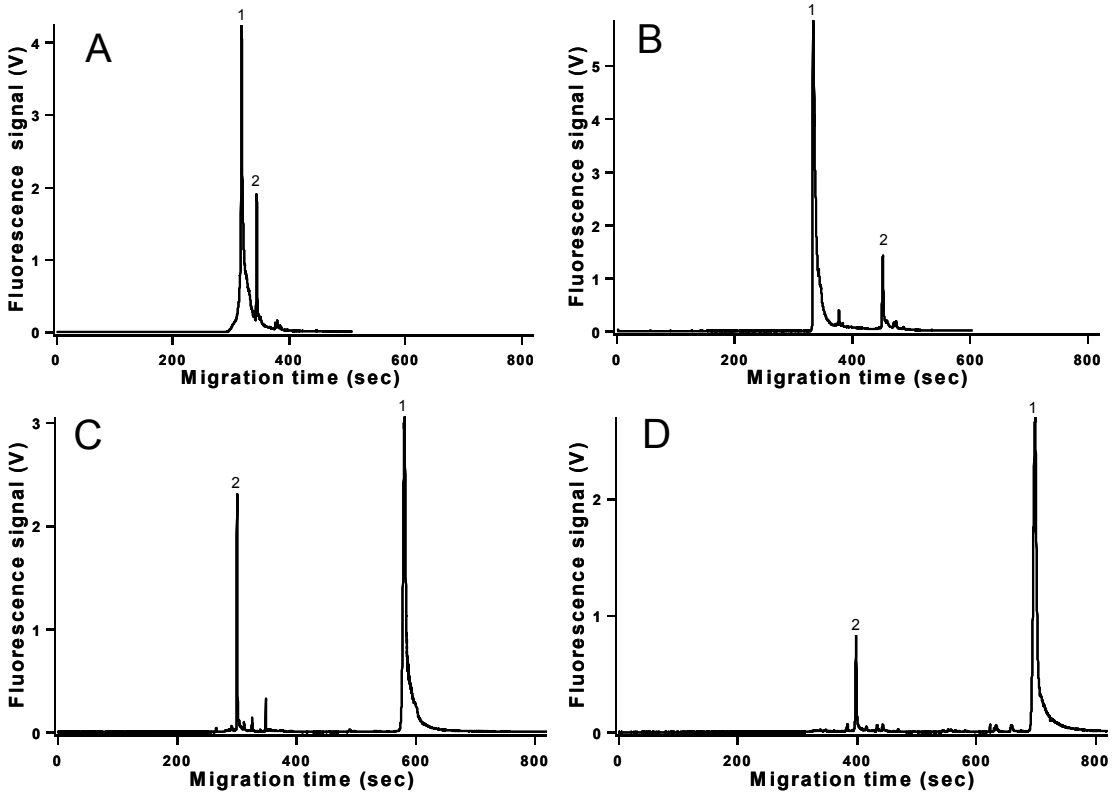

Figure 7.6. CE-LIF Separation of Product from Substrate in Farnesylation Reaction

Peak 1 is the product of the enzymatic reaction; peak 2 is the initial substrate. Running buffers: (A) 25 mM tetraborate, pH 9.1; (B) 50 mM tetraborate, 20 mM β-cyclodextrine, pH 9.5; (C) 50 mM TES, 50 mM SDS, pH 7.3; (D) 25 mM tetraborate, 25 mM SDS, pH 9.3.

CONCLUDING REMARKS

This work has a goal to establish a new paradigm: separation methods can be used as comprehensive kinetic tools. The majority of previous attempts to utilize chromatography and electrophoresis for studying biomolecular interactions were limited to assuming equilibrium between interacting molecules. Not only does such an assumption limit applications to measuring equilibrium constants, but also this assumption is conceptually mistaken since separation disturbs equilibrium. I state that kinetics must be appreciated when separation methods are used for studies of non-covalent interactions. This appreciation can dramatically enrich analytical capabilities of the methods.

To prove the benefits of the appreciation of kinetics, I introduce the concept of Kinetic Capillary Electrophoresis. Capillary electrophoresis was chosen as a methodological platform as it allows separation in solution (without a solid-phase), thus, making kinetic analysis simple and accurate. KCE is defined as CE separation of molecules, which interact during electrophoresis; KCE is not a method but a general concept. To define practical KCE methods, we need to define initial and boundary conditions for interactions.

One of the advantages of KCE methods is that mathematical modeling is not necessary for some of them. For example, k_{off} and K_d can be calculated from a single NECEEM electropherogram using trivial formulas, which involve only areas and migration times of peaks. Another example of such an “easy-math” application of KCE

methods is selection of aptamers with pre-defined binding parameters. These applications of KCE methods are accessible to researchers with no training in mathematical modeling. Although expanding the scope of "easy-math" practical applications of KCE methods is important (and is one of our primary goals), the role of mathematical modeling in KCE is difficult to overestimate. Deriving "easy" formulas is very challenging and can be impossible for many KCE methods. Having a numerical modeling approach allowed us to build a multi-method KCE toolbox for kinetic studies. Different KCE methods have different accuracies for different kinetic parameters. When used together as an integrated tool, KCE methods provide a powerful way of testing hypotheses and accurately calculating binding parameters.

To conclude, I foresee that KCE methods will find multiple applications in fundamental studies of biomolecular interactions, designing clinical diagnostics, and the development of affinity probes and drug candidates. New applications will emerge with further development of KCE.

REFERENCES

1. Ren, B., et al., *Genome-wide location and function of DNA binding proteins.* Science, 2000. **290**(5500): p. 2306-2309.

2. Leng, F. and R. McMacken, *Potent stimulation of transcription-coupled DNA supercoiling by sequence-specific DNA-binding proteins.* Proc. Natl. Acad. Sci. USA, 2002. **99**(14): p. 9139-9144.

3. Oh, D.-B., Y.G. Kim, and A. Rich, *Z-DNA-binding proteins can act as potent effectors of gene expression in vivo.* Proc. Natl. Acad. Sci. USA, 2002. **99**(26): p. 16666-16671.

4. Imanishi, M. and Y. Sugiura, *Artificial DNA-bending six-zinc finger peptides with different charged linkers: distinct kinetic properties of DNA bindings.* Biochemistry, 2002. **41**: p. 1328-1334.

5. Cheskis, B. and L.P. Freedman, *Modulation of nuclear receptor interactions by ligands: kinetic analysis using surface plasmon resonance.* Biochemistry, 1996. **35**(10): p. 3309-3318.

6. Wilson, W.D., *Tech.Sight. Analyzing biomolecular interactions.* Science, 2002. **295**(5562): p. 2103-5.

7. Carpenter, J.L., et al., *A study of the binding of vancomycin to dipeptides using capillary electrophoresis.* J. Chem. Soc., Chem. Comm., 1992. **11**: p. 804-6.

8. Heegaard, N.H.H. and F.A. Robey, *Use of capillary zone electrophoresis to evaluate the binding of anionic carbohydrates to synthetic peptides derived from human serum amyloid P component.* Anal. Chem., 1992. **64**(21): p. 2479-82.

9. Heegaard, N.H.H. and R. Kennedy, *Identification, quantitation, and characterization of biomolecules by capillary electrophoretic analysis of binding interactions.* Electrophoresis, 1999. **20**(15-16): p. 3122-3133.

10. Heegaard, N.H.H., *A heparin-binding peptide from human serum amyloid P component characterized by affinity capillary electrophoresis.* Electrophoresis, 1998. **19**(3): p. 442-7.

11. Avila, L.Z., et al., *Use of affinity capillary electrophoresis to determine kinetic and equilibrium constants for binding of arylsulfonamides to bovine carbonic anhydrase.* J. Med. Chem., 1993. **36**: p. 126-133.

12. Sowell, J., R. Parihar, and G. Patonay, *Capillary electrophoresis-based immunoassay for insulin antibodies with near-infrared laser induced fluorescence detection.* J. Chromatogr. B, 2001. **752**(1): p. 1-8.

13. Ohara, T., A. Shibukawa, and T. Nakagawa, *Capillary electrophoresis/frontal analysis for microanalysis of enantioselective protein binding of a basic drug.* Anal. Chem., 1995. **67**(19): p. 3520-5.

14. Busch, M.H.A., et al., *Comparison of five methods for the study of drug-protein binding in affinity capillary electrophoresis.* J. Chromatogr. A, 1997. **777**(2): p. 311-328.

15. Busch, M.H.A., J.C. Kraak, and H. Poppe, *Principles and limitations of methods available for the determination of binding constants with affinity capillary electrophoresis.* J. Chromatogr. A, 1997. **777**(2): p. 329-353.

16. Rundlett, K.L. and D.W. Armstrong, *Methods for the estimation of binding constants by capillary electrophoresis.* Electrophoresis, 1997. **18**(12-13): p. 2194-2202.

17. Rundlett, K.L. and D.W. Armstrong, *Methods for the determination of binding constants by capillary electrophoresis.* Electrophoresis, 2001. **22**(7): p. 1419-1427.

18. Guijt-Van Duijn, R.M., et al., *Recent advances in affinity capillary electrophoresis.* Electrophoresis, 2000. **21**(18): p. 3905-3918.

19. Tanaka, Y. and S. Terabe, *Estimation of binding constants by capillary electrophoresis.* J. Chromatogr. B, 2002. **768**(1): p. 81-92.

20. Oravcova, J., B. Boehs, and W. Lindner, *Drug-protein binding studies. New trends in analytical and experimental methodology.* J. Chromatogr. B, 1996. **677**(1): p. 1-28.

21. Rundlett, K.L. and D.W. Armstrong, *Examination of the origin, variation, and proper use of expressions for the estimation of association constants by capillary electrophoresis.* J. Chromatogr. A, 1996. **721**(1): p. 173-86.

22. Kraak, J.C., S. Busch, and H. Poppe, *Study of protein-drug binding using capillary zone electrophoresis.* J. Chromatogr. A, 1992. **608**(1-2): p. 257-64.

23. Busch, M.H.A., et al., *Critical evaluation of the applicability of capillary zone electrophoresis for the study of hapten-antibody complex formation.* J. Chromatogr. A, 1996. **744**(1+2): p. 195-203.

24. Haginaka, J., *Enantiomer separation of drugs by capillary electrophoresis using proteins as chiral selectors.* J. Chromatogr. A, 2000. **875**(1+2): p. 235-254.

25. Meisel, H. and C. Olieman, *Estimation of calcium-binding constants of casein phosphopeptides by capillary zone electrophoresis.* Anal. Chim. Acta, 1998. **372**(1-2): p. 291-297.

26. Laniel, M.-A., A. Beliveau, and S.L. Guerin, *Electrophoretic mobility shift assays for the analysis of DNA-protein interactions.* Meth. Mol. Biol., 2001. **148**: p. 13-30.

27. Bogdarina, I., D.G. Fox, and G.G. Kneale, *Equilibrium and kinetic binding analysis of the N-terminal domain of the Pf1 gene 5 protein and its interaction with single-stranded DNA.* J. Mol. Biol., 1998. **275**(3): p. 443-453.

28. LeCaptain, D.J. and A. Van Orden, *Two-beam fluorescence cross-correlation spectroscopy in an electrophoretic mobility shift assay.* Anal. Chem., 2002. **74**(5): p. 1171-1176.

29. Xian, J., *Capillary DNA-protein mobility shift assay.* Meth. Mol. Biol., 2001. **163**: p. 355-367.

30. Stebbins, M.A., et al., *Design and optimization of a capillary electrophoretic mobility shift assay involving trp repressor-DNA complexes.* J. Chromatogr. B, 1996. **683**(1): p. 77-84.

31. Foulds, G.J. and F.A. Etzkorn, *A capillary electrophoresis mobility shift assay for protein-DNA binding affinities free in solution.* Nucleic Acids Res., 1998. **26**(18): p. 4304-4305.

32. Wan, Q.-H. and X.C. Le, *Studies of protein-DNA interactions by capillary electrophoresis/laser-induced fluorescence polarization.* Anal. Chem., 2000. **72**: p. 5583-5589.

33. Le, X.C., Q.-H. Wan, and M.T. Lam, *Fluorescence polarization detection for affinity capillary electrophoresis.* Electrophoresis, 2002. **23**(6): p. 903-908.

34. Molineux, I.J., A. Pauli, and M.L. Gefter, *Physical studies of the interaction between the Escherichia coli DNA binding protein and nucleic acids.* Nucleic Acids Res., 1975. **2**(10): p. 1821-1873.

35. Wu, S. and N.J. Dovichi, *High-sensitivity fluorescence detector for fluorescein isothiocyanate derivatives of amino acids separated by capillary zone electrophoresis.* J. Chromatogr., 1989. **480**: p. 141-155.

36. Berezovski, M. and S.N. Krylov, *Nonequilibrium Capillary Electrophoresis of Equilibrium Mixtures - A Single Experiment Reveals Equilibrium and Kinetic Parameters of Protein-DNA Interactions.* J. Am. Chem. Soc., 2002. **124**(46): p. 13764-13765.

37. Krylov, S.N. and M. Berezovski, *Non-equilibrium capillary electrophoresis of equilibrium mixtures – appreciation of kinetics in capillary electrophoresis.* Analyst, 2003. **128**: p. 571-575.

38. Tang, G.Y., et al., *Modeling of Electroosmotic Flow and Capillary Electrophoresis with the Joule Heating Effect: The Nernst-Planck Equation versus the Boltzmann Distribution.* Langmuir, 2003. **19**(26): p. 10975-10984.

39. Bujalowski, W. and T.M. Lohman, *Monomers of the Escherichia coli SSB-1 mutant protein bind single-stranded DNA.* J. Mol. Biol., 1991. **217**(1): p. 63-74.

40. Tuerk, C. and L. Gold, *Systematic evolution of ligands by exponential enrichment: RNA ligands to bacteriophage T4 DNA polymerase.* Science, 1990. **249**(4968): p. 505-510.

41. Ellington, A. and J. Szostak, *In vitro selection of RNA molecules that bind specific ligands.* Nature, 1990. **346**(6287): p. 818-822.

42. Famulok, M., G. Mayer, and M. Blind, *Intramers as promising new tools in functional proteomics.* Chemistry & Biology, 2001. **8**(10): p. 931-939.

43. Jayasena, S.D., *Aptamers: an emerging class of molecules that rival antibodies in diagnostics.* Clin.Chem., 1999. **45**(9): p. 1628-1650.

44. Hermann, T. and D. Patel, *Adaptive recognition by nucleic acid aptamers.* Science, 2000. **287**(5454): p. 820-825.

45. Davis, K.A., et al., *Use of a high affinity DNA ligand in flow cytometry.* Nucleic Acids Res., 1996. **24**(4): p. 702-706.

46. Kleinjung, F., et al., *Binders in Biosensors: High-Affinity RNA for Small Analytes.* Anal. Chem., 1998. **70**(2): p. 328-331.

47. Potyrailo, R.A., et al., *Adapting Selected Nucleic Acid Ligands (Aptamers) to Biosensors.* Anal. Chem., 1998. **70**(16): p. 3419-3425.

48. Kotia, R.B., L. Li, and L.B. McGown, *Separation of Nontarget Compounds by DNA Aptamers.* Anal. Chem., 2000. **72**(4): p. 827-831.

49. Rehder, M.A. and L.B. McGown, *Open-tubular capillary electrochromatography of bovine b-lactoglobulin variants A and B using an aptamer stationary phase.* Electrophoresis, 2001. **22**(17): p. 3759-3764.

50. Deng, Q., et al., *Retention and separation of adenosine and analogues by affinity chromatography with an aptamer stationary phase.* Anal. Chem., 2001. **73**(22): p. 5415-5421.

51. German, I., D.D. Buchanan, and R.T. Kennedy, *Aptamers as Ligands in Affinity Probe Capillary Electrophoresis.* Anal. Chem., 1998. **70**(21): p. 4540-4545.

52. Weigand, T.W., et al., *High-affinity oligonucleotide ligands to human IgE inhibit binding to Fc epsilon receptor I.* J. Immunol., 1996. **157**(1): p. 221-230.

53. Bock, L.C., et al., *Selection of single-stranded DNA molecules that bind and inhibit human thrombin.* Nature, 1992. **355**(6360): p. 564-566.

54. Schultze, P., R.F. Macaya, and J. Feigon, *Three-dimensional solution structure of the thrombin-binding DNA aptamer d(GGTTGGTGTGGTTGG).* J. Mol. Biol., 1994. **235**(5): p. 1532-1547.

55. Wang, K.Y., et al., *A DNA aptamer which binds to and inhibits thrombin exhibits a new structural motif for DNA.* Biochemistry, 1993. **32**(8): p. 1899-1904.

56. Pease, A.C., et al., *Light-generated oligonucleotide arrays for rapid DNA sequence analysis.* Proc. Natl. Acad. Sci. USA, 1994. **91**(11): p. 5022-5026.

57. Mullaart, E., et al., *Parallel genome analysis by two-dimensional DNA typing.* Nature, 1993. **365**(6445): p. 469-471.

58. Higuchi, R., et al., *DNA typing from single hairs.* Nature, 1988. **332**(6164): p. 543-546.

59. Krauss, G., et al., *Escherichia coli single-strand deoxyribonucleic acid binding protein: stability, specificity, and kinetics of complexes with oligonucleotides and deoxyribonucleic acid.* Biochemistry, 1981. **20**(18): p. 5346-5352.

60. Overman, L.B., W. Bujalowski, and T.M. Lohman, *Equilibrium binding of Escherichia coli single-strand binding protein to single-stranded nucleic acids in the (SSB)65 binding mode. Cation and anion effects and polynucleotide specificity.* Biochemistry, 1988. **27**(1): p. 456-471.

61. Shimura, K. and B.L. Karger, *Affinity probe capillary electrophoresis: analysis of recombinant human growth hormone with a fluorescent labeled antibody fragment.* Anal. Chem., 1994. **66**(1): p. 9-15.

62. Chu, Y.-H., et al., *Affinity Capillary Electrophoresis.* Acc. Chem. Res., 1995. **28**(11): p. 461-468.

63. Gomez, F.A., et al., *Determination of Binding Constants of Ligands to Proteins by Affinity Capillary Electrophoresis: Compensation for Electroosmotic Flow.* Anal. Chem., 1994. **66**(11): p. 1785-1791.

64. Zhao, J.Y., et al., *Detection of 100 molecules of product formed in a fucosyltransferase reaction.* Glycobiology, 1994. **4**(2): p. 239-242.

65. Poola, I., *Molecular assay to generate expression profile of eight estrogen receptor alpha isoform mRNA copy numbers in picogram amounts of total RNA from breast cancer tissues.* Anal. Biochem., 2003. **314**(2): p. 217-226.

66. Okhonin, V., S.M. Krylova, and S.N. Krylov, *Nonequilibrium capillary electrophoresis of equilibrium mixtures, mathematical model.* Anal. Chem., 2004. **76**(5): p. 1507-1512.

67. Berezovski, M. and S.N. Krylov, *Using DNA-binding proteins as an analytical tool.* J. Am. Chem. Soc., 2003. **44**(125): p. 13451-13454.

68. Berezovski, M., et al., *Affinity analysis of a protein-aptamer complex using nonequilibrium capillary electrophoresis of equilibrium mixtures.* Anal. Chem., 2003. **75**(6): p. 1382-1386.

69. Krylova, S.M., et al., *Tau protein binds both double-stranded and single-stranded DNA - the proof obtained with nonequilbrium capillary electrophoresis of equilibrium mixtures.* FEBS Letters, 2005. **579**: p. 1371-1375.

70. Yang, P., et al., *Capillary Electrophoresis and Fluorescence Anisotropy for Quantitative Analysis of Peptide-Protein Interactions Using JAK2 and SH2-Bb as a Model System.* Anal. Chem., 2005. **in press**.

71. Fang, N. and D.D.Y. Chen, *General Approach to High-Efficiency Simulation of Affinity Capillary Electrophoresis.* Anal. Chem., 2005. **77**(3): p. 840-847.

72. Ma, H., Zou, Y., *Thermodynamic Characterization of the Interaction of Mutant UvrB Protein with Damaged DNA.* Biochemistry, 2004. **43**(14): p. 4206-4211.

73. Schubert, F., Zettl, H., Haefner, W., Krauss, G., Krausch, G., *Comparative thermodynamic analysis of DNA-protein interactions using surface plasmon resonance and fluorescence correlation spectroscopy.* Biochemistry, 2003. **42**(34): p. 10288-10294.

74. Galletto, R., Bujalowski, W., *Kinetics of the E. Coli Replication Factor DnaC Protein-Nucleotide Interactions. II. Fluorescence Anisotropy and Transient, Dynamic Quenching Stopped-Flow Studies of the Reaction Intermediates.* Biochemistry, 2002. **41**(28): p. 8921-8934.

75. Mosig, G., Gewin, J., Luder, A., Colowick, N., Vo, D., *Two recombination-dependent DNA replication pathways of bacteriophage T4, and their roles in mutagenesis and horizontal gene transfer.* Proc. Natl. Acad. Sci. USA, 2001. **98**(15): p. 8306-8311.

76. Sutani, T., Yanagida, M., *DNA renaturation activity of the SMC complex implicated in chromosome condensation.* Nature, 1997. **388**(6644): p. 798-801.

77. Savran, C.A., et al., *Micromechanical detection of proteins using aptamer-based receptor molecules.* Anal. Chem., 2004. **76**(11): p. 3194-3198.

78. Dang, C. and S.D. Jayasena, *Oligonucleotide inhibitors of Taq DNA polymerase facilitate detection of low copy number targets by PCR.* J. Mol. Biol., 1996. **264**(2): p. 268-278.

79. Yakimovich, O.Y., Alekseev, Ya. I., Maksimenko, A. V., Voronina, O. L., Lunin, V. G., *Influence of DNA Aptamer Structure on the Specificity of Binding to Taq DNA Polymerase.* Biochemistry (Moscow, Russian Federation), 2003. **68**(2): p. 228-235.

80. Carra, J.H. and P.L. Privalov, *Energetics of folding and DNA binding of the MAT alpha 2 homeodomain.* Biochemistry, 1997. **36**(3): p. 526-535.

81. Knapp, S., et al., *Thermal unfolding of the DNA-binding protein Sso7d from the hyperthermophile Sulfolobus solfataricus.* J. Mol. Biol., 1996. **264**(5): p. 1132-1144.

82. Davis, K.G., et al., *Comparison of Pf1 and Fd Gene 5 Proteins and Their Single-Stranded DNA Complexes by NMR Spectroscopy and Differential Scanning Calorimetry.* Biochemistry, 1995. **34**(1): p. 148-154.

83. Shumaker-Parry, J.S., R. Aebersold, and C.T. Campbell, *Parallel, quantitative measurement of protein binding to a 120-element double-stranded DNA array in real time using surface plasmon resonance microscopy.* Anal. Chem., 2004. **76**(7): p. 2071-2082.

84. Tsoi, P.Y. and M. Yang, *Surface plasmon resonance study of the molecular recognition between polymerase and DNA containing various mismatches and conformational changes of DNA-protein complexes.* Biosens. Bioelectron., 2004. **19**(10): p. 1209-1218.

85. Perales, C., et al., *Enhancement of DNA, cDNA synthesis and fidelity at high temperatures by a dimeric single-stranded DNA-binding protein.* Nucleic Acids Res., 2003. **31**(22): p. 6473-6480.

86. Lacey, M.E., A.G. Webb, and J.V. Sweedler, *Monitoring temperature changes in capillary electrophoresis with nanoliter-volume NMR thermometry.* Anal. Chem., 2000. **72**(20): p. 4991-4998.

87. Swinney, K. and D.J. Bornhop, *Quantification and evaluation of Joule heating in on-chip capillary electrophoresis.* Electrophoresis, 2002. **23**(4): p. 613-620.

88. Liu, J., et al., *Use of affinity capillary electrophoresis for the study of protein and drug interactions.* Analyst, 1998. **123**(7): p. 1455-1459.

89. Chaudhari, A.M., et al., *Transient liquid crystal thermometry of microfabricated PCR vessel arrays.* J. MEMS, 1998. **7**(4): p. 345-355.

90. Mao, H., T. Yang, and P.S. Cremer, *A Microfluidic Device with a Linear Temperature Gradient for Parallel and Combinatorial Measurements.* J. Am. Chem. Soc., 2002. **124**(16): p. 4432-4435.

91. Lou, J., et al., *Fluorescence-based thermometry: principles and applications.* Rev. Anal. Chem, 1999. **18**(4): p. 235-284.

92. Ross, D., M. Gaitan, and L.E. Locascio, *Temperature Measurement in Microfluidic Systems Using a Temperature-Dependent Fluorescent Dye.* Anal. Chem., 2001. **73**(17): p. 4119-4123.

93. Kozlov, A.G. and T.M. Lohman, *Kinetic Mechanism of Direct Transfer of Escherichia coli SSB Tetramers between Single-Stranded DNA Molecules.* Biochemistry, 2002. **41**(39): p. 6032-6044.

94. Noel, A.-J., W. Wende, and A.J. Pingoud, *DNA Recognition by the Homing Endonuclease PI-SceI Involves a Divalent Metal Ion Cofactor-induced Conformational Change.* Biol. Chem., 2004. **279**(8): p. 6794-6804.

95. Zeeb, M. and J. Balbach, *Single-stranded DNA binding of the cold-shock protein CspB from Bacillus subtilis: NMR mapping and mutational characterization.* J. Protein Sci., 2003. **12**(1): p. 112-123.

96. O'Connell, D., et al., *Calcium-dependent oligonucleotide antagonists specific for L-selectin.* Proc. Natl. Acad. Sci. U S A, 1996. **93**(12): p. 5883-5887.

97. Ulrich, H., et al., *In vitro selection of RNA molecules that displace cocaine from the membrane-bound nicotinic acetylcholine receptor.* Proc. Natl. Acad. Sci. U S A, 1998. **95**(24): p. 14051-14056.

98. Burke, D.H., et al., *Bent pseudoknots and novel RNA inhibitors of type 1 human immunodeficiency virus (HIV-1) reverse transcriptase.* J. Mol. Biol., 1996. **264**(4): p. 650-666.

99. Drolet, D.W., et al., *A high throughput platform for systematic evolution of ligands by exponential enrichment (SELEX).* Comb. Chem. High Throughput Screen., 1999. **2**(5): p. 271-278.

100. Beutel, B.A. and L. Gold, *In vitro evolution of intrinsically bent DNA.* J. Mol. Biol., 1992. **228**(3): p. 803-812.

101. Ciesiolka, J., et al., *Affinity selection-amplification from randomized ribooligonucleotide pools.* Methods Enzymol., 1996. **267**: p. 315-335.

102. Stellwagen, N.C., C. Gelfi, and P.G. Righetti, *The free solution mobility of DNA.* Biopolymers, 1997. **42**(6): p. 687–703.

103. Hoagland, D.A., E. Arvanitidou, and C. Welch, *Capillary electrophoresis measurements of the free solution mobility for several model polyelectrolyte systems.* Macromolecules, 1999. **32**(19): p. 6180–6190.

104. Irvine, D., C. Tuerk, and L. Gold, *SELEXION. Systematic evolution of ligands by exponential enrichment with integrated optimization by non-linear analysis.* J. Mol. Biol., 1991. **222**(3): p. 739-61.

105. Vant-Hull, B., et al., *The mathematics of SELEX against complex targets.* J. Mol. Biol., 1998. **278**(3): p. 579-597.

106. Schneider, D., L. Gold, and T. Platt, *Selective enrichment of RNA species for tight binding to Escherichia coli rho factor.* FASEB J., 1993. **7**(1): p. 201-207.

107. Chen, H. and L. Gold, *Selection of high-affinity RNA ligands to reverse transcriptase: inhibition of cDNA synthesis and RNase H activity.* Biochemistry, 1994. **33**(29): p. 8746-8756.

108. Tian, Y., et al., *Dissecting protein: protein interactions between transcription factors with an RNA aptamer.* RNA, 1995. **1**(3): p. 317-326.

109. Iki, N., Y. Kim, and E.S. Yeung, *Electrostatic and hydrodynamic separation of DNA fragments in capillary tubes.* Anal. Chem., 1996. **68**(24): p. 4321-4325.

110. Park, H.W., et al., *Crystal structure of protein farnesyltransferase at 2.25 angstrom resolution.* Science, 1997. **275**(5307): p. 1800-1804.

111. Berezovski, M., et al., *Measuring the activity of farnesyltransferase by capillary electrophoresis with laser-induced fluorescence detection.* Electrophoresis, 2002. **23**(19): p. 3398-3403.

112. Jitkova, J., et al., *Monitoring the three enzymatic activities involved in posttranslational modifications of Ras proteins.* Anal. Chim. Acta, 2004. **521**(1): p. 1-7.

113. Arkhipov, S.N., et al., *Chemical cytometry for monitoring metabolism of a ras-mimicking substrate in single cells.* Cytometry, 2005. **63A**(1): p. 41-47.

114. Mendonsa, S.D. and M.T. Bowser, *In vitro evolution of functional DNA using capillary electrophoresis.* J. Am. Chem. Soc., 2004. **126**(1): p. 20-21.

115. Hughes, D.E. and B.L. Karger, *Screening natural samples for new therapeutic and diagnostic compounds using capillary electrophoresis.* PCT Int. Appl., 1997: p. 49.

CURRICULUM VITAE

MAXIM BEREZOVSKI

Education

- M.S. in Biochemistry

Novosibirsk State University, Department of Chemistry, Novosibirsk, Russia, 1994.
Master's thesis: "Investigation of interaction of arylized derivatives of nucleic acids with amino acid residuals of proteins".
Supervisor: Prof. Dmitry G. Knorre, Director of Institute of Bioorganic Chemistry.

Specialization

- New methods for selection of target-binding molecules from complex mixtures (libraries).
- Applications of aptamers as artificial antibodies.
- Kinetics and thermodynamics of DNA-Protein, Protein-Protein, Drug-DNA, and Drug-Protein interactions.
- Posttranslational modification of RAS proteins (farnesylation, endoproteolysis, methylation).
- Single cell analysis by capillary electrophoresis and confocal microscopy (chemical cytometry).
- Chemistry of nucleic acids: synthesis of nucleotide triphosphates, oligonucleotides, and their derivatives for molecular biological and gene-engineering experiments, the sequence-specific photo modification of DNA and RNA.

Technical skills

- Capillary electrophoresis: P/ACE MDQ, PA 800 apparatuses (Beckman Coulter) equipped with absorption and fluorescent detectors; Single, two-capillary CE-LIF based chemical cytometers for single cell analysis.
- Microscopy: inverted, fluorescent, and confocal (Olympus).
- Separation techniques: HPLC (RP, IE, size exclusion, affinity); gels (SDS-PAGE, agarose); TLC.
- PCR (Eppendorf) and Real-time PCR (Stratagen, Bio-Rad, Applied Biosystems).
- Molecular biology techniques: cloning, plasmid isolation and sequencing; GFP fused proteins and mRNA expression and purification.
- Enzymology: measuring concentration and activity of enzymes in vitro and in vivo, screening of inhibitors.
- Cell culture technique.
- Organic and bioorganic synthesis.

Employment

- 2001-present: Research and Teaching Assistant (General Chemistry CHEM 1000, Organic Chemistry CHEM 2020 and CHEM 3020), York University, Toronto, Canada.
- 2000-2001: Analytical Chemist, PANCAP (Pharmaceutical Company), Toronto, Canada.
- 1995-2000: CEO, Pharmacia of Siberia (Retail Drugstore Company), Russia
- 1994-1995: Research Associate, Institute of Bioorganic Chemistry, Novosibirsk, Russia.

Awards and Honors

- 2004-2005, Ontario Graduate Scholarship, Toronto, Canada.
- 2001-2002, York Scholarship, York University, Toronto, Canada.

Articles in refereed journals

1. Berezovski, M.; Drabovich, A.; Krylova, S.M.; Musheev, M.; Okhonin, V.; Petrov, A.; Krylov, S.N. (2005) Nonequilibrium capillary electrophoresis of equilibrium mixtures (NECEEM) – a universal tool for selection of aptamers. *Journal of the American Chemical Society*, 127: 3165-3171. (Ph.D. work)
2. Berezovski, M.; Krylov, S.N. (2005) Thermochemistry of Protein-DNA Interaction Studied with Temperature-Controlled Nonequilibrium Capillary Electrophoresis of Equilibrium Mixtures. *Analytical Chemistry*, 77: 1526-1529. (Ph.D. work)
3. Berezovski, M.; Krylov, S.N. (2005) A non-spectroscopic method for the determination of temperature in capillary electrophoresis. *Analytical Chemistry,* 76: 7114-7117. (Ph.D. work)
4. Arkhipov, S.N., Berezovski, M.; Jitkova, J.; Krylov, S.N. (2005) Chemical cytometry for monitoring metabolism of a Ras-mimicking substrate in single cells. *Cytometry,* 63A: 41-47. (Ph.D. work)
5. Okhonin, V.; Berezovski, M.; Krylov, S.N. (2004) Sweeping capillary electrophoresis – a non-stopped-flow method for measuring bimolecular rate constant of complex formation between protein and DNA. *Journal of the American Chemical Society,* 126: 7166-7167. (Ph.D. work)
6. Berezovski, M.; Krylov, S.N. (2003) Using DNA-binding proteins as an analytical tool. *Journal of the American Chemical Societ*y, 125: 13451-13454. (Ph.D. work)
7. Krylov, S. N.; Berezovski, M. (2003) Non-equilibrium capillary electrophoresis of equilibrium mixtures - appreciation of kinetics in capillary electrophoresis. *Analyst,* 128: 571-575. (Ph.D. work)
8. Berezovski, M.; Nutiu, R.; Li, Y.; Krylov, S.N. (2003) Affinity analysis of a protein-aptamer complex using non-equilibrium capillary electrophoresis of equilibrium mixtures. *Analytical Chemistry,* 75: 1382-1386. (Ph.D. work)
9. Berezovski, M.; Krylov, S.N. (2002) Non-equilibrium capillary electrophoresis of equilibrium mixtures - a single experiment reveals equilibrium and kinetic parameters of protein-DNA interactions. *Journal of the American Chemical Society,* 124: 13674-13675. (Ph.D. work)

10. Berezovski, M.; Li, W.-P.; Poulter, C.D.; Krylov, S.N. (2002) Measuring the activity of farnesyltransferase by capillary electrophoresis with laser-induced fluorescence detection. *Electrophoresis* 23: 3398-3403. (Ph.D. work)
11. Godovikova, T. S.; Berezovskii, M. V.; Knorre, D. G. (1995) Photoaffinity modification of amino acid derivatives of oligonucleotides in complementary complex. *Bioorg. Khim*., 21: 858-867. (M.Sc. work)
12. Levina, A. S.; Berezovskii, M. V.; Venjaminova, A. G.; Dobrikov, M. I.; Repkova, M. N.; Zarytova, V. F. (1993) Photomodification of RNA and DNA fragments by oligonucleotide reagents bearing arylazide groups. *Biochimie*. 75: 25-27. (M.Sc. work)

Patents

- Krylov, Sergey; Krylova, Svetlana; Berezovski, Maxim (2005) Non-equilibrium capillary electrophoresis of equilibrium mixtures (NECEEM) - based methods for drug and diagnostic development. U.S. Pat. Appl. Publ., US 2005003362 A1 20050106.

Participation in Conferences

• Poster Presentations

1. Scientific conference "18th International Symposium on MicroScale Bioseparations (MSB 2005)", New Orleans, USA, February 2004. Poster: "Sweeping Capillary Electrophoresis: A Non-Stopped-Flow Method for Measuring Bimolecular Rate Constant of Complex Formation between Protein and DNA*"*.
2. Scientific conference "87th Canadian Chemistry Conference and Exhibition organized by The Canadian Society for Chemistry (CSC 2004)", London, Canada, May 2004. Poster: "NECEEM-based methods for aptamer discovery and diagnostic development".
3. Scientific conference "17th International Symposium on Microscale Separations and Capillary Electrophoresis (HPCE 2004)", Salzburg, Austria, February 2004. Poster: "Measuring Thermodynamic Parameters with *NECEEM"*.
4. Scientific conference "16th International Symposium on Microscale Separations and Analysis Including Mini-Symposia on Genomics, Proteomics and Metabolomics (HPCE 2003)", San Diego, California USA, January 2003. Poster: "Non-Equilibrium Capillary Electrophoresis of Equilibrium Mixtures. Application to Protein Analysis using Nucleotide Aptamers".

• Oral presentations

1. Scientific conference "Students and scientific progress", Novosibirsk, Russia, March 1994. Talk: "Photoaffinity modification of amino acid derivatives of oligonucleotides in complementary complex".
2. Scientific conference "Students and scientific progress", Novosibirsk, Russia, March, 1993. Talk: "Synthesis of photoactive nucleotide triphosphates".
3. Scientific conference "Students and scientific progress", Novosibirsk, Russia, March 1992. Talk: "Photomodification of RNA and DNA fragments by oligonucleotide reagents".

Invited Lectures

Lecture title: "Kinetic Capillary Electrophoresis and Its Applications". *Invited by*: University of California, Irvine, CA USA. *Date*: March 16, 2005.

Lecture title: "NECEEM – Swiss Army Knife for Selection Aptamers". *Invited by*: University of Washington, Seattle, WA USA. *Date*: May 17, 2005.